Targeting the Triple-Negative Breast Cancer Kinome with Chemical Proteomics

Martin Charles Whittle

A dissertation submitted to the faculty of the University of North Carolina at Chapel Hill in partial fulfillment of the requirements for the degree of Doctor of Philosophy in the Department of Pharmacology.

Chapel Hill
2013

Approved by:

Gary L. Johnson, Ph.D.

Lee M. Graves, Ph.D.

H. Shelton Earp, III, MD

Stephen V. Frye, Ph.D.

Jian Jin, Ph.D.

ABSTRACT

MARTIN WHITTLE: Targeting the Triple-Negative Breast Cancer Kinome with Chemical Proteomics
(Under the direction of Dr. Gary Johnson)

Kinases are members of a large dynamic and cooperative signaling network, which senses inhibition of key nodal kinases and induces compensatory responses that offset pharmacological intervention. Combination therapies that target multiple growth- and survival promoting kinases are proving to be a better strategy for successful cancer therapy. What is lacking is the ability to measure whole kinome activity and to assess kinome adaptation and resistance to targeted therapies. We have developed a chemical proteomics approach that couples kinase affinity capture with quantitative mass spectrometry, providing a systems biology platform to profile global kinome activity in cancer cells, GEMM tumors and patient biopsies. Our chemical proteomic approach captures the majority of the expressed kinome estimated by RNA-seq and detects altered kinome activity profiles in response to stimulus or kinase inhibitors. Kinases from all major kinome subfamilies are captured with a large percentage representing the understudied kinome. Applying this technology, we discovered previously undefined activation of tyrosine and serine/threonine kinases in breast cancer cell lines in response to targeted inhibitors against MEK or EGFR that are currently undergoing clinical trials. Combined kinome activity assessment using chemical proteomics and RNAi synthetic lethal screens predicted a specific kinase inhibitor combination therapy. The combination therapy gave apoptosis and tumor regression in a breast cancer GEMM, where single agents were largely ineffective. The relevance of kinome reprogramming to patient

triple-negative breast cancer was confirmed by the investigation of MEK inhibitor-treated patient samples from a window trial established in conjunction with GlaxoSmithKline. However, differential kinome responses were observed across intrinsic breast cancer subtypes, suggesting that broader approaches to targeting or preventing kinome reprogramming may be necessary to avert resistance to kinase inhibitor therapies. The findings presented here define a novel approach to determining kinome-based mechanisms of resistance to targeted therapies to suggest novel inhibitor combinations and strategies that may more effectively treat triple-negative breast cancer.

TABLE OF CONTENTS

LIST OF TABLES vii

LIST OF FIGURES viii

LIST OF ABBREVIATIONS x

CHAPTERS

I. INTRODUCTION 1

Breast cancer presentation and treatment 1

TNBC and intrinsic breast cancer subtypes 2

Targeting kinases for cancer therapy 4

Targeting the RAF-MEK-ERK pathway in breast cancer 7

Kinome resilience and adaptation to targeted inhibition 10

Application of chemical proteomics to study the kinome 15

Objectives of this project 18

II. MATERIALS AND METHODS 23

Chapter III 23

Chapter IV 33

Chapter V 35

III. Dynamic reprogramming of the kinome in response to targeted MEK inhibition in claudin-low triple negative breast cancer 42

Introduction 42

Results 43

Kinome profiling of TNBC 43

Reprogramming the kinome in response to MEK inhibition 46

MEK inhibition deregulates transcription, expression and activation of RTKs 48

MEK-ERK inhibition induces c-MYC degradation leading to RTK reprogramming 50

RTK reprogramming rescues cells from AZD6244-induced growth arrest 52

AZD6244 in combination with RTK inhibitors 53

Kinome reprogramming in the C3Tag TNBC GEMM 54

Profiling kinome response to targeted combination therapies in the C3Tag mouse model of TNBC 54

AZD6244 plus sorafenib causes tumor regression 55

Discussion 56

IV. Investigating resistance to EGFR/HER2 inhibition in basal-like and other breast cancer subtypes 74

Introduction 71

Results 76

Defining EGFR expression and activity in TNBC 76

MIB/MS defines kinome response to EGFR inhibition 77

Mechanisms of reprogramming to EGFR inhibition 78

Targeting lapatinib-induced RTKs 80

Discussion 82

V. Triple-negative breast cancer exhibits subtype-specific kinome Reprogramming to targeted MEK inhibition 89

Introduction 89

Results 90

Differential kinome reprogramming in response to MEK inhibition defines TNBC subtypes 90

Kinome profiling of TNBC MEKi treatment selects for reprogrammed CL cells from heterogeneous cell line 93

Enrichment of tumors with CL characteristics in response to targeted kinase inhibition in C3Tag TNBC GEMM 94

The diversity of kinome reprogramming promotes escape from MEKi/sorafenib combination therapies 96

Targeted BRD4 inhibition blocks kinome reprogramming in BL and CL TNBC cells 97

Combination of JQ1 and GSK212 maintains growth inhibition and blocks MEKi-mediated selection of CL-reprogrammed cells 99

Discussion 100

VI. Significance and future directions 114

REFERENCES 119

LIST OF TABLES

TABLE

3.1: MIB-based phosphoproteomics of RAF-MEK-ERK pathway 64

3.2: Top 40 kinases expressed in patient claudin-low tumor..... 66

LIST OF FIGURES

FIGURE

1.1: MEK/ERK signaling pathway 20

1.2: Mechanisms of resistance to kinase inhibitors 21

1.3: Chemical structures of MEK and EGFR inhibitors 22

2.1: Structures of bead-conjugated kinase inhibitors 41

3.1: Kinase capture of inhibitor beads 60

3.2: Strategy and characterization of MIBs 61

3.3: RAF-MEK-ERK pathway activation in TNBC 62

3.4: Profiling MEKi response in claudin-low TNBC 63

3.5: Defining a signature of kinome response to MEKi in claudin-low TNBC 65

3.6: Characterization of CL RTK response 67

3.7: Induced kinases are target-specific to MEKi 68

3.8: Defining mechanisms of MEKi response 69

3.9: Effects of drug removal or prolonged treatment on c-MYC and RTK reprogramming 70

3.10: Targeting induced RTKs 71

3.11: Kinome reprogramming in C3Tag GEMM 72

3.12: AZD6244/sorafenib combination produces synergistic effects in C3Tag mice 73

4.1: Characterization of pEGFR in TNBC 85

4.2: MIB/MS defines kinome response to EGFR inhibition 86

4.3: Investigating mechanisms of kinome reprogramming in HCC1806 87

4.4: Targeting lapatinib-induced RTKs in HCC1806 88

5.1: Differential kinome reprogramming in BL and CL TNBC following MEKi 104

5.2: Kinome reprogramming in patient window trial for TNBC 105

5.3: Distinct responses within heterogeneous cell populations 106

5.4: Prolonged MEKi treatment of BL/CL heterogeneous cell line selects for CL reprogrammed cells 107

5.5: Treatment of C3Tag mice with MEK inhibitor enriches tumors with claudin-low characteristics 108

5.6: Diversity of kinase activation in response to MEKi protects C3Tag tumors from dual agent combination therapies 109

5.7: Inability of TKIs to prevent MEK/ERK reactivation 110

5.8: Targeted BRD4 inhibition prevents MEKi mediated kinome reprogramming in BL and CL TNBC 111

5.9: Combination of GSK212 and JQ1 promotes stable growth inhibition and prevents selection of CL cells 112

5.10: Strategies to target kinome reprogramming..... 113

6.1: The dilemma of kinome reprogramming 118

LIST OF ABBREVIATIONS

ATP: Adenosine triphosphate

BL: Basal-like

CL: Claudin-low

CML: Chronic myeloid leukemia

EGFR: Epidermal growth factor receptor

EMT: Epithelial to mesenchymal transition

ER: Estrogen receptor

FDA: Food and drug administration

GBM: Glioblastoma multiforma

GEMM: Genetically engineered mouse model

LC: Liquid chromatography

MALDI: Matrix-assisted laser desorption ionization

MAP2K: Mitogen activated protein kinase kinase

MAP3K: Mitogen activated protein kinase kinase kinase

MAPK: Mitogen activated protein kinase

MEK: MAPK/ERK kinase

MEKi: MEK inhibitor

MIB/MS: MIBs and mass spectrometry

MIBs: Multiplexed inhibitor beads

MRM: Multiple reaction monitoring

MS: Mass spectrometry

mTORC1: Mammalian target of rapamycin complex 1

NSCLC: Non-small cell lung cancer

pCR: pathological complete response

PR: Progesterone receptor

qRT-PCR: Quantitative real-time polymerase chain reaction

RNA: Ribonucleic acid

RNAi: RNA interference

RTK: Receptor tyrosine kinase

SFK: Src-family kinase

TK: Tyrosine kinase

TKI: Tyrosine kinase inhibitor

TNBC: Triple-negative breast cancer

TOF: Time of flight

TUNEL: Terminal deoxynucleotidyl transferase dUTP nick end labeling

I. INTRODUCTION

Breast cancer presentation and treatment

Breast cancer is a global health concern that accounts for approximately 29% of cancer diagnoses and 14% of cancer deaths in women each year, and is the most prevalent and second deadliest form of cancer in women[1]. Greater than 40,000 breast cancer-related deaths in the United States are expected during the year 2013 alone, despite improvements in early detection and treatment options contributing to a steady decline in US breast cancer mortality rates since 1989. Not surprisingly, the largest factor contributing to long-term survival of breast cancer patients is the tumor stage at diagnosis. Patients presenting with localized disease have a 5-year survival rate of 99%, compared to a 23% 5-year survival of patients presenting with distant metastases[2]. The majority (60%) of patients are diagnosed with localized diseased, 33% show regional cancer cell invasion, and 5% of patients present with metastatic disease (2% are unstaged). Treatment options vary depending on stage at presentation and tumor subtypes, but a combination of surgery and adjuvant chemotherapy and/or radiation therapy is common as a first line for breast cancer treatment[3]. Targeted systemic therapies that inhibit specific growth- and survival-promoting molecular targets provide another course of therapy where surgery/chemotherapy is unlikely to succeed.

Several targeted therapies have been approved by the Food and Drug Administration (FDA) for use in the treatment of breast cancer, most of which target either HER2, estrogen receptorα/β (ER), or aromatase (which is responsible for estrogen synthesis). These targeted therapies are indicated for breast cancers which exhibit high

expression of HER2 or hormone receptor (ER/progesterone receptor (PR)). Triple-negative breast cancers (TNBC), which comprise approximately 15% of all breast cancers, are ER-negative, PR-negative, and lack HER2 overexpression, and thus do not respond to HER2-targeted or hormonal therapy[4–6]. While TNBCs are often initially sensitive to chemotherapy, tumors almost invariably reappear with a more aggressive phenotype that is resistant to further treatment[7]. A poor understanding of the oncogenic drivers and resistance mechanisms in TNBC has hindered the development and approval of molecularly targeted therapies in this setting, leaving few options to combat TNBC after the failure of chemotherapy.

TNBC and intrinsic breast cancer subtypes

While the term "triple-negative" is clinically convenient, a more accurate classification of breast cancer is provided by gene expression analysis, which shows a clear demarcation of five intrinsic subtypes of breast cancer across a large array of patient tumors[8]. HER2-enrichment defines one subtype, and hormone receptor positive breast cancers are predominantly classified into the luminal A and luminal B subtypes. The vast majority of TNBCs cluster distinctly into either the basal-like (BL) or claudin-low (CL) subtypes, which comprise 11-23% and 7-11% of breast cancers, respectively[8]. Despite sharing negativity for HER2, PR, and ER, distinct genetic signatures discriminate basal-like cancers from claudin-low. Particular differences can be observed in the expression of cell signaling mediators, such as kinases and their regulators, suggesting an intrinsic divergence in growth and survival signaling. For instance, expression of the receptor tyrosine kinases (RTKs) VEGFR2, PDGFRβ, DDR2 or AXL are significantly associated with claudin-low cell lines and tumors as compared to basal-like TNBC[8].

Analysis of subtype-specific gene signatures proposes a hierarchy of breast

cancer differentiation that parallels normal mammary development, where claudin-low cancers precede basal-like cancers as the least differentiated of breast cancer subtypes[9]. Overall, claudin-low tumors and cell lines exhibit mesenchymal and stem-like gene expression patterns, whereas basal-like breast cancers are more differentiated and express epithelial markers[8,9]. The claudin-low subtype is also highly enriched for breast cancers having the $CD44^{+}/CD24^{-/low}$ gene signature that is characteristic of drug-resistant tumor-initiating cells[10]. The acquisition of claudin-low mesenchymal characteristics may result from an epithelial to mesenchymal transition (EMT), an important developmental process which can be reactivated in cancer cells to promote cell invasiveness, motility, stemness, and drug resistance[11]. With increased drug resistance provided by the claudin-low phenotype, treatment of patient tumors with hormone therapy or chemotherapy can select for claudin-low cancer cells from a heterogeneous tumor environment, leading to the outgrowth of aggressive claudin-low cancers from previously basal, luminal, or HER2-amplified breast cancers[10,12].

Taken together, the divergence of basal-like and claudin-low gene expression patterns and differentiation hierarchies, coupled with associated differences in cell signaling and drug responsiveness, underscore the importance of distinguishing between basal-like and claudin-low cancers when designing pre-clinical studies or clinical trials for TNBC. Unique targeted therapies will likely be needed to treat these distinct breast cancer subtypes when chemotherapy/surgery fails. Perhaps the most tractable gene family for the development of targeted inhibitors is the kinome, due to the established role of kinases in mediating oncogenic signaling and the relative ease of targeting kinases with small molecule and antibody inhibitors. Understanding kinase signaling in the distinct contexts of basal-like and claudin-low breast cancers will be important for defining effective targeted therapies for TNBC[13].

Targeting kinases for cancer therapy

The human kinome consists of 518 protein kinases that mediate cellular signal transduction by catalyzing reversible and site-specific phosphorylation of diverse protein substrates. As one of the largest enzyme classes, encompassing 1.7% of the human genome, kinases collectively phosphorylate an estimated one-third of all proteins[14,15]. Phosphorylation on serine, threonine, or tyrosine residues can cause a shift in substrate conformation, often triggering biochemical changes to such properties as localization, protein interactions, or activity of the substrate. This process is reversed by protein phosphatases, which catalyze the hydrolysis of phosphoryl groups from amino acid residues. The kinase domain, which is well-conserved across distinct kinase families, is folded into an N-terminal and C-terminal lobe. ATP binds with varying affinities (K_m^{ATP} ranging from ~1-1000 nM for different kinases) in a pocket between the two lobes, and is coordinated by several highly conserved residues. Among these, a glutamate residue (Glu91 for PKA) that lies on the so-called α-C helix (within the N-lobe) functions as an ion pair with a critical N-lobe lysine (PKA Lys72) that coordinates the α and β phosphates of ATP[16]. Conformational changes to the α-C helix can affect ATP binding and thus kinase activity. For many kinases, enzymatic activity is largely contingent upon the phosphorylation state of a conserved activation segment that runs across the cleft between the lobes, termed the activation loop[17]. Phosphorylation on this loop, by autocatalysis or a separate regulatory kinase, can increase kinase activity through conformational shifts that augment substrate and/or ATP binding[18–20]. When the activation loop is properly oriented to allow substrate and ATP binding, transfer of the γ-phosphate of ATP to the substrate serine, threonine, or tyrosine residue is stabilized by divalent cations (themselves coordinated by several conserved asparagine and aspartate residues) that serve as cofactors in the phosphoryl transfer reaction.

Targeting kinases for cancer therapy has been a driving force in the development

of new treatment strategies across a wide range of cancer types. Greater than 15 small molecule and antibody inhibitors against kinases have been approved by the FDA for cancer therapy, with many more in the developmental pipeline. The majority of these approved inhibitors target RTKs due to the common occurrence of aberrant RTK signaling in many cancers. Most small molecule kinase inhibitors compete with ATP for the conserved ATP-binding cleft between lobes of the kinase domain. ATP-competitive kinase inhibitors that preferentially bind the activated kinase conformation are classified as type I kinase inhibitors, which are usually identified by functional assays using activated kinases and mimic ATP by interacting with similar residues within the kinase domain[13]. Type II kinase inhibitors, such as the HER2/EGFR inhibitor lapatinib, additionally bind to a hydrophobic pocket adjacent to the ATP-binding cleft and are indirectly competitive with ATP in that they bind and stabilize an inactive kinase conformation (DFG-out) that has a lower affinity for ATP[21]. Kinase inhibitors can also bind allosterically, at sites distant from the ATP-binding pocket, inducing conformational changes and/or blocking oligomerization to render the kinase inactive. Allosteric inhibitors are classified as type III, and are usually highly specific because they bind outside the conserved kinase ATP-binding pocket and at regions that may be more unique to the targeted kinase, although few examples exist. The MEK1/2 inhibitor AZD6244 is an example of a type III kinase inhibitor.

Distinct cellular processes, including growth, metabolism, stress response, movement, and apoptosis are regulated by protein phosphorylation, and tight control of kinase activity is required for proper function of these cellular programs. Aberrant kinase signaling, whether by kinase overexpression, mutation, or dysregulation, has been shown to be central to the proliferation and survival of many cancer types. Constitutive kinase activity can drive cancer progression through hyperactivation of growth signaling pathways, suppression of apoptosis, angiogenesis, and other mechanisms. In such

instances where cancer cell growth and survival hinges upon constitutive kinase activity, small molecule inhibition of the activated kinase is often an effective course of therapy. For instance, targeting the BCR-ABL fusion protein that characterizes chronic myelogenous leukemia (CML) with small molecule inhibitors (i.e. imatinib, nilotinib) strongly suppresses cancer cell proliferation and leads to remission in a majority of CML patients[22]. Additionally, targeting HER2 with lapatinib and/or trastuzumab has increased disease-free and overall survival in the setting of HER2-amplified breast cancer[23]. Despite the critical role of kinases in mediating cancer signal transduction, much of the kinome is virtually unstudied and many kinases lack targeted inhibitors[24].

Oncogenic growth signaling often begins with aberrant expression and/or activation of RTKs at the cell surface. RTKs are generally composed of an extracellular ligand-binding domain with specificity towards external growth factors and cytokines, a transmembrane domain and intracellular tyrosine kinase domain. Ligand binding commonly induces homodimerization or heterodimerization of the receptor, whereupon conformational shifts allow transphosphorylation of receptors at multiple tyrosine residues, often including the activation loop. Phosphotyrosine residues on RTKs are subsequently recognized by a wide array of proteins with conserved phosphotyrosine-binding domains (such as the SH2 domain) that directly mediate intracellular signaling or serve as adaptors for other signaling effectors. Specificity of the recruited proteins depends upon the protein sequence on the C-terminal side of the tyrosine phosphorylation, thus providing distinction to the signaling pathways activated by each phosphorylation site and receptor[25]. For example, activation of the RTK EGFR begins by binding of its cognate ligands (EGF, TGFα or amphiregulin), followed by homodimerization or heterodimerization with related paralogs HER2, HER3, or HER4. While dimerization leads to transphosphorylation in each case, dimerization with different partners elicits unique effects due to the phosphorylation of diverse tyrosine

residues on each receptor. Phosphorylation of EGFR on Y1068 leads to recruitment of GRB2, which serves as an adaptor to recruit the Ras guanine nucleotide exchange factor SOS to the membrane. SOS subsequently interacts with membrane-bound Ras to promote GTP binding and Ras activation. Similarly, phosphorylation of HER3 at Y1289 recruits the p85 subunit of PI3K, bringing along the catalytic p110 subunit to the membrane and in close proximity to its phosphoinositol substrates. In cancer, constitutive activation of EGFR and/or other RTKs causes hyperactivation of these and other growth signaling pathways.

Targeting the RAF-MEK-ERK pathway in breast cancer

Oncogenic tyrosine kinases (TKs) and RTKs often feature as drivers of tumorigenesis and tumor progression, but the prominent role of activated ERK signaling in cancer cell growth and survival has made the RAF-MEK-ERK axis a major focus for targeted cancer therapies downstream of RTKs. This pathway is a canonical mitogen-activated protein kinase (MAPK) pathway that relays proliferation signals from upstream RTKs/Ras to the nucleus, where ERK1/2 (the terminal MAPKs) act on a wide array of transcription factors to promote proliferation and survival (Figure 1.1). The RAF-MEK-ERK pathway is hyperactivated in most cancers, often occurring through mutation/overexpression of diverse RTKs or oncogenic mutations in Ras or RAF. There are three RAF proteins (ARAF, BRAF and CRAF) that operate as MAP3Ks in this module. RAFs are serine/threonine kinases that are recruited by activated Ras to the plasma membrane, where they become active by dimerization and association with scaffolding proteins. Once activated, RAFs phosphorylate the MAP2Ks MEK1 and MEK2 on two conserved activation loop serines to induce conformational shifts leading to MEK activation. MEK1/2 subsequently phosphorylate the terminal MAPKs, ERK1/2, on threonine and tyrosine residues within their activation loops. Activated ERK1/2 can

dimerize to phosphorylate cytoplasmic substrates or translocate to the nucleus as monomers to phosphorylate nuclear targets[26]. While the substrates of MEK1/2 are essentially confined to ERK1/2, over 160 substrates (predominantly nuclear) have been identified for ERK1/2, including several well-known oncogenes (such as c-MYC) and tumor suppressors (such as BIM) that are phosphorylated by ERK1/2 to alter protein stability and/or function[27]. In the context of cancer cells, activated ERK1/2 promote cell cycle progression and evasion of apoptosis by acting on such substrates, although in the context of untransformed primary cells hyperactivation of ERK1/2 can lead to oncogene-induced senescence through ERK1/2-mediated activation of p38 MAPK[28]. Very little is known about the unique substrates and roles of MEK and ERK paralogs, largely due to high homology and the lack of reagents to discern between their phosphorylation and/or activity.

An array of targeted therapeutics has been developed against RAF-MEK-ERK pathway components. Vemurafenib and dabrafenib, ATP-competitive inhibitors targeting mutant BRAF(V600E), yield a striking regression of metastatic melanoma harboring mutant BRAF before an invariable resistance and tumor reemergence[29–31]. Targeting wildtype RAF with small molecule inhibitors leads to paradoxical activation of RAF due to drug-induced dimerization, causing concern for the applicability of RAF inhibitors to treat diverse cancer types. In this light, MEK is considered a more broadly targetable component of the RAF/MEK/ERK pathway, and several allosteric MEK1/2 inhibitors (MEKi), including GSK1120212, AZD6244, U0126, CI-1040 and PD0325901, have reached various stages of clinical development. These inhibitors generally exhibit very high selectivity due to the targeting of a MEK-specific allosteric site adjacent to the ATP-binding pocket. Binding at this site stabilizes MEK1 in an inactive conformation while still allowing ATP to bind in the catalytic pocket[32]. Interestingly, phosphorylation of the MEK1/2 activation loop reduces the affinity of GSK1120212 for MEK1/2 by 12- to 20-

fold, suggesting that activated upstream signaling may promote resistance to MEK1/2 inhibitors by reducing drug potency[33]. Other allosteric MEK1/2 inhibitors have recapitulated such phosphorylation-dependent affinity for MEK[34]. A highly selective ATP-competitive ERK1/2 inhibitor, SCH772984, is also under development at Merck that shows promise for the treatment of melanoma and colorectal cancer cell lines with acquired resistance to RAF and/or MEK inhibitors[35]. The ability to target multiple kinases in this pathway may be important to prevent reactivation of RAF/MEK/ERK signaling and drug resistance[36].

Many studies have highlighted the importance of the RAF-MEK-ERK pathway in cell proliferation and survival of breast cancer. Expression and activation of MAPK pathway components are significantly higher in breast tumor samples compared to matched normal tissue, validating this pathway as a target in breast cancer[37–39]. *In vitro* studies have shown that treatment of various breast cancer cell lines with the MEKi U0126 slows proliferation, increases apoptosis and sensitizes cells to anoikis[40,41]. Interestingly, basal-like TNBC cell lines generally exhibit greater sensitivity to MEKi compared to luminal or HER2-amplified breast cancer lines (claudin-low not considered), possibly due to greater activation of RAS/RAF/MEK pathway signaling in this subtype[42–44]. Expression of the ERK phosphatase DUSP6 also contributes strongly to MEKi sensitivity, and expression of a related ERK phosphatase, DUSP4, leads to reduced ERK activity and improved outcomes after neoadjuvant chemotherapy in basal-like breast cancer patients[43,45]. Studies by Balko, et al. and MacKeigan, et al. have further revealed that the addition of MEKi to taxol-based chemotherapeutics causes synergistic induction of apoptosis in breast cancer cell lines and tumors[45,46].

Despite the apparent importance of RAF/MEK/ERK activity in breast cancer, clinical trials with single-agent MEK inhibitors have so far yielded disappointing results[47,48]. Mutations to MEK that prevent inhibitor binding have been described, but it

is likely that tumor cells also develop resistance to MEK inhibitors through other mechanisms of pathway reactivation[49,50]. Phosphorylation of MEK1/2 by upstream kinases leading to reduced MEKi affinity could theoretically contribute to intrinsic MEKi resistance, leading to reduced efficacy of single-agent MEKi treatments. Thus, activation of alternative kinases, both upstream and/or parallel to the RAF/MEK/ERK pathway, may sustain cancer cell growth/survival in the presence of MEKi. In support of this, combination therapies with MEK inhibitors have shown promise in preclinical cancer models[51]. These studies make it clear that greater understanding of the mechanisms behind MEKi resistance is needed for the development of efficacious MEKi-based therapies to treat breast and other cancers.

Kinome resilience and adaptation to targeted inhibition

Though kinases are often studied singularly or as members of linear pathways, kinases integrate into convoluted signaling cascades and networks that relay and integrate diverse cell signals. RAF-MEK-ERK signaling exemplifies this plasticity, where pathway activity is modified by diverse upstream kinases, phosphatases responsive to pathway activity, and internal feedback phosphorylation on RAF and MEK1 (from MEK and ERK, respectively). Unfortunately, this resiliency of the kinome has made single-agent kinase inhibitor cancer treatment extremely difficult. Mutation at a conserved "gatekeeper" residue in the ATP binding pocket (such as T790M in EGFR) can provide drug resistance by sterically hindering drug binding, making the mutant kinase insensitive to previously effective drug doses[52]. Cancer cells can circumvent targeted kinase inhibition to reactivate growth signaling through such mutations and/or amplification of the targeted kinase, activation of alternative pathways, or pathway reactivation through other methods (Figure 1.2)[53]. Such diverse mechanisms of adaptive resistance to kinase inhibitors have been described in a variety of cancer types.

A prominent example of kinase inhibitor resistance is seen in malignant melanomas, where oncogenic mutation in the kinase BRAF are common[54]. The most frequent BRAF mutation in melanoma is the V600E mutation and this primarily results in chronic activation of the MEK/ERK pathway to promote cell growth. Consequently, small molecule inhibitors of mutant RAF are attractive therapeutics for the treatment of melanoma and other RAF-driven cancers[55]. Interestingly, multiple studies uncovered a surprising paradoxical resistance of RAF kinase signaling to select RAF inhibitors[56–58]. RAF kinase inhibitors (PLX4720, sorafenib and 885-A), while highly effective at inhibiting mutant BRAF, activated wild-type RAF through inhibitor-mediated dimerization[57]. This compensatory activation is dependent on inhibitor binding to the ATP site of one RAF molecule, which stimulates dimerization and activation of the drug-free RAF protomer. Thus, despite efficacy at inhibiting mutant BRAF in tumors, RAF inhibitors pose a risk of enhancing Ras-dependent tumors through activation of wild-type RAF. Moreover, N-Ras mutation or up-regulated PDGFRβ expression were also shown to accompany the resistance of cells to PLX4032[54]. As suggested from these findings, strategies to co-target both RAF and MEK simultaneously have demonstrated improved growth inhibition and suppression of RAF-MEK-ERK pathway activation and prolonged disease-free survival in patients[49,59–61]. Other groups have shown that combining MEK and/or PI3K/mTOR prevented the acquired resistance to the BRAF inhibitor GSK2118436, suggesting that co-targeting these two pathways is also a viable strategy[62,63]. While such studies provide an important cautionary example of the unexpected changes in the kinome in response to single kinase inhibitors, they also illustrate the importance of elucidating kinome responses to select inhibitors.

Another example of kinome feedback adaptation has been gleaned from studies on PI3K and AKT inhibitors. Of central importance is the role of feedback regulation of the mTOR pathway[64]. Rapamycin-dependent inhibition of mTOR complex 1 (mTORC1)

relieves feedback regulation of IGF1R, thereby triggering a compensatory activation of IGF1R and AKT targets such as the transcription factor FOXO[65,66]. Furthermore, Chandarlapaty et al. showed that inhibition of PI3K/AKT relieved feedback inhibition and increased the expression of a unique set of receptor tyrosine kinases including HER3, IGF1R and INSR[67]. In addition to expression, the phosphorylation of multiple RTKs was also stimulated by AKT inhibition. Treatment of cells with AKT inhibitors resulted in up-regulation of RTK transcripts in a FOXO-dependent manner. Given the significance of this RTK response, the authors tested the combination of HER kinase inhibitors (lapatinib and Iressa) with AKT inhibitors in xenograft models and showed that the combination of these inhibitors was highly effective at inhibiting tumor growth. Chakrabarty et al. also showed that inhibition of PI3K with the small molecule inhibitor XL147 upregulated the expression and activation of multiple RTKs, including HER3, in a manner dependent on HER2[68]. Again, co-targeting the RTK response with trastuzumab or lapatinib was synergistic at inhibiting growth, compared with the action of these inhibitors alone. These studies exemplify the importance of elucidating the kinome feedback mechanisms and understanding their implications for successful therapeutic applications.

Activation or mutation of the EGFR and downstream kinase pathways is common in glioblastoma multiforma (GBM), colorectal cancer, non-small-cell lung carcinoma (NSCLC) and TNBC[69]. This is often a result of EGFR mutations or overexpression, hence EGFR inhibitors have been investigated as possible therapeutics in these settings, with limited success[70,71]. Studies now demonstrate the difficulty of targeting this RTK is due to either secondary gatekeeper mutations (T790M) that prevent EGFR inhibition or from activation of alternative RTKs following loss of EGFR activity. In particular, several studies in EGFR-mutant NSCLC identify MET amplification and activation as a mechanism for resistance to EGFR inhibitors, where MET amplification is

observed in 15–22% of NSCLC patient's tumors that were resistant to EGFR inhibitors[72,73]. Multiple lines of evidence suggest that activated MET can compensate for EGFR inhibition by partially protecting against loss of phospho-EGFR and contributing to sustained activation of downstream growth signaling through ERK and AKT. A direct association between EGFR and MET has been observed, although it is unclear how this heterodimerization contributes to EGFR inhibitor resistance[74]. In such cases where MET is induced as a mechanism of EGFR inhibitor resistance, cotreatment with EGFR and MET inhibitors synergistically inhibited proliferation of cell lines, prevented tumor growth, and induced apoptosis in cell and tumor models. Similar studies demonstrate the remarkable plasticity of MET signaling in response to expression of EFGR mutations (de2-7 EGFR) in GBM[75]. While it has been shown that EGFR inhibitor treatment can select for cells with pre-existing MET amplification, it is also evident that loss of EGFR activity can rapidly induce compensatory expression/activation of MET and other tyrosine kinases, including FGFR2 and Src-family kinases (SFKs)[76–79]. This induced kinase activity is independent of genetic mutation or amplification, and likely results, in part, from loss of negative-feedback regulation of suppressed kinases. Additionally, acute loss of upstream kinase signaling can trigger changes in transcription factor stability and/or activity that lead to induced expression of RTKs and their ligands. This was exemplified by Ware et al., who defined loss of ERK activity downstream of EGFR inhibition as causal in de-repression of FGFR2/3 expression in NSCLC cell lines[77].

Some examples of kinome adaptation to targeted inhibitors in breast cancer have also been described. In HER2-amplified breast cancers, inhibition of HER2 with the monoclonal antibody trastuzumab yields a small but significant benefit in disease-free and overall survival, whereas treatment with the HER2-targeted small molecule inhibitor lapatinib provides only marginal improvement to disease-free survival[80–82]. Combination of trastuzumab and lapatinib, which have differing mechanisms of inhibition, gives a

synergistic tumor inhibition in preclinical models and doubles the pathological complete response rate (pCR) to approximately 40% prior to surgery[83]. However, this translates to only a 5-month improvement to median overall survival, sparking several studies to understand why near-complete inhibition of HER2, considered to be the major driver in these cancers, yields only a modest tumor response *in* vivo[84]. One major mechanism of HER2-inhibitor resistance that has been characterized is upregulated expression and activation of other HER-family members such as EGFR and HER3[85,86]. Increases in HER3 mRNA transcript, protein abundance and protein phosphorylation can be observed within 48h of lapatinib treatment of HER2-amplified SKBR3 cells[87]. This resulted from loss of AKT-mediated negative feedback regulation, and constitutively active AKT prevented HER3 upregulation following HER2 inhibition. Increased expression of HER3, which is widely considered to be catalytically inactive, was proposed to enhance HER2-HER3 dimerization to mediate allosteric activation of HER2 and subsequent reactivation of ERK and AKT. This mechanism suggests that minimal residual HER2 activity may be sufficient to allow escape from inhibition to redrive growth signaling pathways, especially where dose-limiting toxicities prevent absolute inhibition. These studies have led to the development of the monoclonal antibody pertuzumab, which binds the dimerization domain of HER2 to prevent receptor dimerization (unlike trastuzumab, which binds to prevent ligand-independent mitogenic signaling). Combination of trastuzumab and pertuzumab was shown to synergistically inhibit tumor growth in preclinical models and provide a significant benefit for overall and disease-free survival in clinical trials[88,89]. The importance of HER-family reprogramming as a mechanism of resistance to HER2-targeted therapies is clear, however, multiple groups have also revealed contributions of EPHA2, AXL, MET and IGF1R towards intrinsic and/or acquired resistance to targeted therapies in HER2-driven breast cancer[90–93]. These studies suggest that multiple mechanisms of kinome adaptation may

simultaneously contribute to resistance to targeted inhibitors, highlighting the need to understand exactly how targeted inhibitors influence kinome signaling.

Such examples of kinome adaptation demonstrate the diverse mechanisms of plasticity and resistance in the kinome of tumor cells under the selective pressure of targeted kinase inhibitors. With most oncogenic RTKs driving cell growth through conserved kinase signaling pathways, there is a high potential for cancer cells to circumvent targeted kinase inhibition by induced expression or activity of alternative kinases. The high plasticity and resiliency of the kinome suggests that drug combinations targeting multiple kinase signaling pathways or nodes may be a more effective strategy to treat cancers driven by aberrant kinase signaling[94]. Anticipating the mechanisms of drug response in cancer cells will help to prevent the persistence and selection of resistant populations from a heterogeneous tumor environment[95]. Taken together, these studies highlight the need for standard methods to study kinome network signaling in the context of drug response and resistance.

Application of chemical proteomics to study the kinome

The philosophy of studying the kinome as a network of kinases or 'kinomics' was first proposed by Johnson and Hunter in 2005[96]. Initial efforts to study the kinome focused on identifying kinase substrates through large-scale phosphoproteomic analyses[97]. However, because of the massive complexity of the phosphoproteome, these studies have provided only a partial insight into the detailed regulation of the kinome[98]. Some studies have attempted to characterize the kinome through kinase activity assays[99]. However, a limitation to this approach is the considerable assay development required to profile large-scale changes in kinase activity. Recently, advances in proteomics and genomics technologies have revolutionized the analysis of the human kinome itself as an entity. RNA-seq analysis revealed that approximately

70% of the total kinome (370/518) is expressed in typical breast cancer cell lines[100,101]. Other studies performed extensive profiling of expressed kinases in a large numbers of tissues or specific cancers[102,103].

Despite this information, important questions remain. For instance, how many of these kinases are active and how does the activity of the kinome change in response to different stimuli or inhibitors? Moreover, how does one study the untargeted or understudied members of the kinome where well-characterized reagents are lacking? Increasing evidence of kinome plasticity as a mechanism of drug resistance has made understanding kinome network signaling a priority for cancer research. Fortunately, advances in kinase enrichment and proteomics have greatly facilitated the ability to study the kinome at the protein level[104]. On the basis of the original method of Haystead et al. using γ-phosphoryl-linked ATP affinity columns to capture kinases, Knockaert et al. were the first to demonstrate the utility of immobilized kinase inhibitors[105–107]. Daub and co-workers refined this approach by using a broad range of immobilized kinase inhibitors coupled to Sepharose beads[108]. An inherent advantage of the latter approach is the nanomolar affinity binding of kinases to the inhibitor beads, thereby permitting efficient capture of a large fraction of the kinome. In addition, by increasing the variety of the coupled inhibitors, a greater diversity of kinases could be captured[109].

Initially this technology was used to profile kinase inhibitor selectivity and identify new cellular targets for select kinase inhibitors such as SB203580, gefitinib, SU6668 and others[110–113]. Termed ‘kino-beads’, this method was commercialized (Axxima, Cellzome, Ambit) and broadly applied to assess kinase inhibitor specificity across the kinome [109,114–117]. For example, Bantscheff et al. performed quantitative analysis of the kinase targets for imatinib, dasatinib and bosutinib in K562 leukemia cells[116]. Similar studies have compared the selectivity of nilotinib and second-generation dual ABL/SFK (SRC family kinase) inhibitors[118,119]. Others used this technology to compare the binding

affinity of 38 kinase inhibitors across a panel of 317 kinases[117]. Importantly these papers marked some of the first studies to evaluate the specificity of structurally distinct inhibitors against large numbers of kinases. The results of these and other studies demonstrated exquisite specificity for some inhibitors (lapatinib), whereas others (staurosporine, sunitinib, lestaurtanib and dasatinib) lacked specificity and bound many kinases from various kinase families[117,120]. More recent studies expanded this technology to profile changes in the kinome itself. Multiple investigators have used this strategy to demonstrate cell-type-specific sets of expressed kinomes using the immobilized inhibitors combined with LC (liquid chromatography)-MS/MS (tandem MS), phosphoproteomics analysis and quantitative MS[115,121,122]. In an interesting application, Daub et al. used this approach to profile the change in the kinome from S- and M-phase-arrested cells[123]. Specifically, the authors quantified over 219 kinases, detecting over 1000 phosphorylation sites (including activation loops) and identifying multiple kinases not previously associated with mitotic progression. It has further been shown that activated kinases bind with higher affinity to type I inhibitor beads (compared to analogous inactive conformations), likely due to greater accessibility of the ATP-binding pocket in the active conformation and the use of activated kinases in the development of type I kinase inhibitors[116]. Taken together, these data suggest that immobilized kinase inhibitors may be used as a platform to profile kinome expression and activity.

Importantly, these recently developed technologies for kinome enrichment and characterization could be applied as a discovery mechanism to define the dynamic activity of the kinome in response to inhibitors. Typically studies of kinome adaptation have relied on immunoblotting of select kinases or the use of phosphoantibody arrays to assess kinome changes[124]. However, these methods are limited by phosphoantibody availability and specificity, and therefore limit the scale of analysis. Affinity chromatography with immobilized pan-kinase inhibitors followed by quantitative mass

spectrometry allows for a more unbiased assessment of changes in kinase expression and activity after drug treatment. A major application of this technique would be to define mechanisms of adaptive resistance from the kinome reprogramming response, providing a method for the rational design of inhibitor combinations with greater efficacy for cancer treatment.

Objectives for this project

Currently, there are no standard methods for the rational design of targeted inhibitor combinations for cancer treatment. Our first goal for this project was to design a method to systematically measure the kinome response to small molecule inhibitors (kinome reprogramming) in triple-negative breast cancer. A precedent for the use of chemical proteomics for kinase enrichment and analysis of drug specificity or kinase expression has been established, but these techniques have not been applied to define drug-induced changes in kinome expression/activity. We hypothesized that a chemical proteomic approach using immobilized kinase inhibitors can define novel kinase targets that are induced by the treatment of small-molecule inhibitors to MEK1/2 or HER2/EGFR (Figures 1.3A,B), which represent potentially important kinase targets in TNBC. Characterization of our multiplexed inhibitor-bead (MIB) strategy with mass spectrometry revealed substantial coverage of the expressed kinome across diverse kinase families. Basal-like and claudin-low TNBC subtypes were assessed individually, as the differential gene expression patterns indicated the likelihood of distinct kinome responses to targeted inhibitors. The kinome reprogramming to diverse inhibitors was measured in order to define target-specific reprogramming events. We also sought to define the mechanisms behind induced drug-induced kinase expression and activity.

We further posited that induced kinases may be supporting cancer cell proliferation and/or survival in the presence of inhibitor, and that targeting induced

kinases with additional small molecule inhibitors may attenuate drug resistance. Our ultimate goal was the rational design of small molecule inhibitor combinations that exhibit greater efficacy for the treatment of triple-negative breast cancer patients. To this end, kinases responding to targeted MEK or EGFR/HER2 inhibitors were targeted with RNAi or small molecule inhibitor combinations and assessed in cell growth assays to define those kinases contributing to growth/survival after MEK or EGFR/HER2 inhibition.

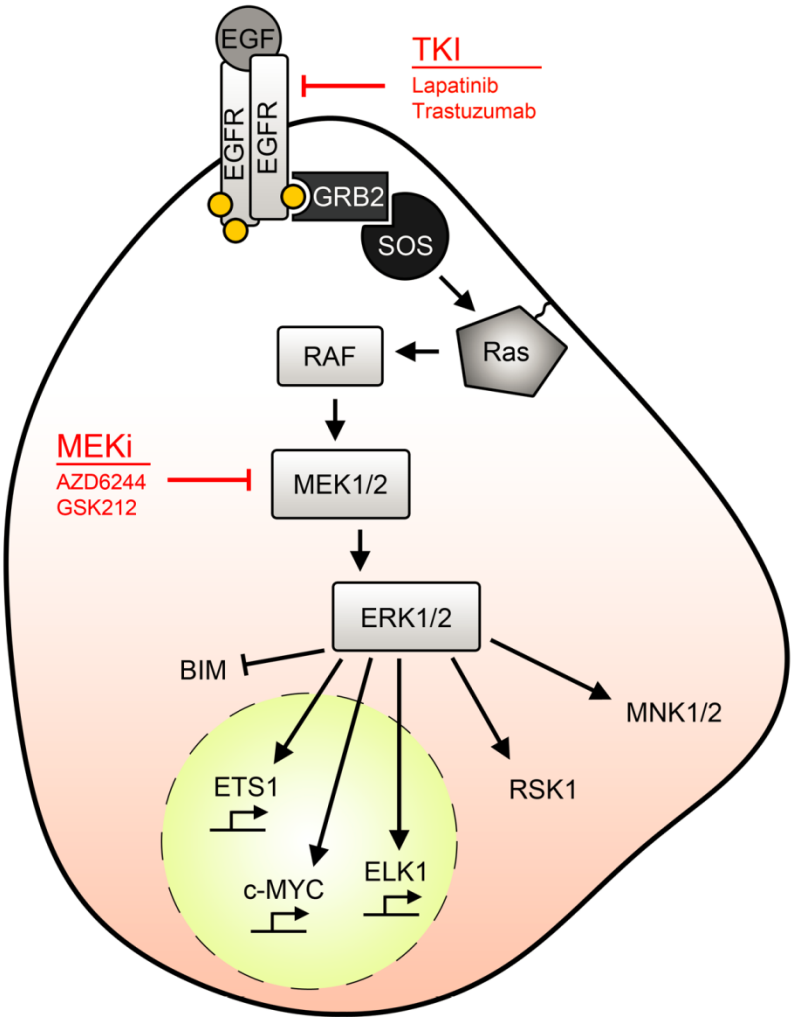

Figure 1.1 MEK/ERK signaling pathway. Canonical ERK pathway signaling is shown. Activated RTKs (such as EGFR shown here) recruit factors leading to the activation of Ras at the plasma membrane. Ras induces activity of the MAP3K RAF, leading to MEK and ERK activation. ERK phosphorylates numerous substrates in the nucleus and cytoplasm to regulate transcription and growth/survival signaling. Targeted inhibitors to MEK and EGFR (exemplified in red) are applied in this study.

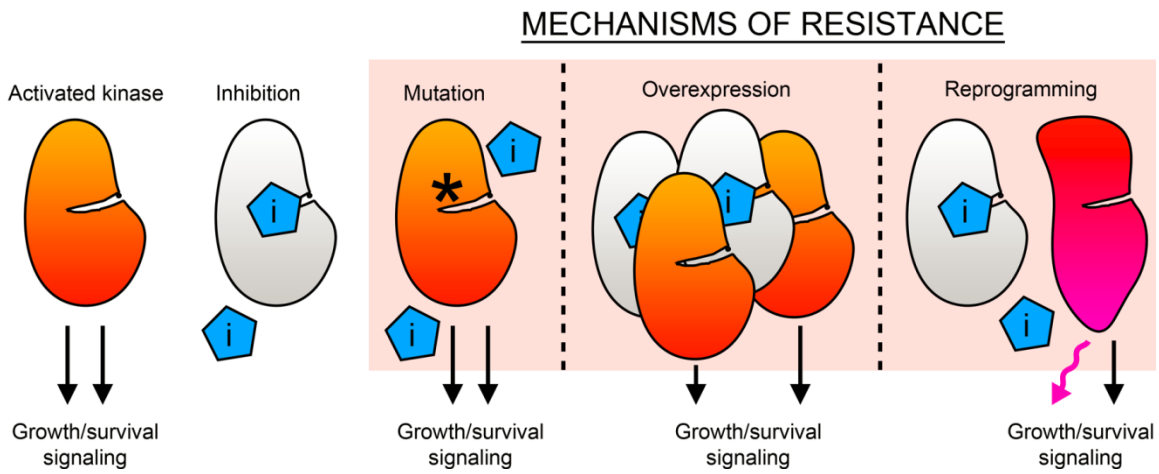

Figure 1.2 Mechanisms of resistance to kinase inhibitors. Demonstration of diverse mechanisms of resistance to kinase inhibitors is shown. Kinase inhibitors (shown in blue) can be bypassed by mutation of gatekeeper and other residues, overexpression/amplification of the targeted kinase, or by activation of alternative growth signaling pathways through reprogramming.

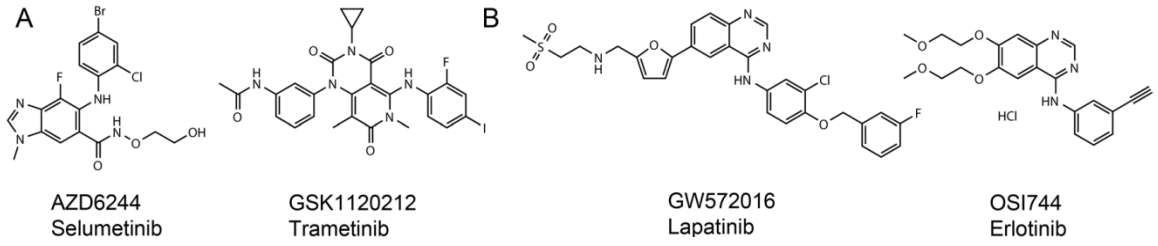

Figure 1.3 Chemical structures of MEK and EGFR inhibitors. A) Chemical structures of MEKi used in this study are shown. B) Chemical structures of EGFR inhibitors used in this study are shown.

II. MATERIALS AND METHODS

Chapter III

Cell culture

HuMEC cells were grown in 5% FBS with HuMEC supplements. MDA-MB-231 and T2-C3Tag cells were grown in DMEM/F12 supplemented with 10% FBS. SUM159 cells were grown in DMEM/F12 supplemented with 5% FBS, 1 µg/ml hydrocortisone and 5 µg/ml insulin. MYL CML cells were cultured in RPMI 1640 medium supplemented with 10% fetal bovine serum and 1% antibiotic/antimycotic. SUM159-R cells were continually grown in the presence of 5 µM AZD6244. For SILAC labeling, cells were grown for five doublings in arginine- and lysine-depleted media (as above) supplemented with either unlabeled L-arginine (42 mg/L) and L-lysine (71 mg/L) or equimolar amounts of [$^{13}C_6$,$^{15}N_4$]arginine (Arg10) and [$^{13}C_6$]lysine (Lys6) (Cambridge Isotope Laboratories). Proliferation was quantified by Cell-Titer Glo Luminescent Cell Viability Assay (Promega). Media containing kinase inhibitors was replaced daily.

Multiplexed inhibitor bead affinity chromatography

Cells were lysed on ice for 20 minutes in lysis buffer containing 50 mM HEPES (pH 7.5), 0.5% Triton X-100, 150 mM NaCl, 1 mM EDTA, 1 mM EGTA, 10 mM sodium fluoride, 2.5 mM sodium orthovanadate, 1X protease inhibitor cocktail (Roche), and 1% each of phosphatase inhibitor cocktails 2 and 3 (Sigma). Cell lysate was sonicated (3x10s) on ice and centrifuged for 15 min (13,000 rpm) at 4°C and the supernatant was collected and syringe-filtered through a 0.2 µM SFCA membrane. The filtered lysate

(approximately 20-40 mg of protein per experiment) was brought to 1M NaCl and pre-cleared by flowing over 500 µl of blocked and washed NHS-activated Sepharose 4 Fast Flow beads (GE Healthcare). The flow-through was collected and passed through a column of layered inhibitor-conjugated beads (Bisindoylmaleimide-X (50 µl), SB203580 (50 µl), lapatinib (100 µl), dasatinib (100 µl), purvalanol B (100 µl), VI16832 (100 µl), PP58 (100 µl)) to isolate protein kinases from the lysates. Kinase-bound inhibitor beads were washed with 20 ml of high-salt buffer and 10 ml of low-salt buffer, each containing 50 mM HEPES (pH 7.5), 0.5% Triton X-100, 1 mM EDTA, 1 mM EGTA, and 10 mM sodium fluoride, and 1M NaCl or 150 mM NaCl, respectively. A final wash of 1 ml 0.1% SDS was applied to the columns before elution in 1 ml of a 0.5% SDS solution in high heat. Elutions from all columns were combined and cysteines were alkylated by sequential incubations with DTT (final concentration 5 mM) for 20 min at 60° C and iodoacetamide (final concentration 20 mM) for 30 min at room temperature in the dark. The elution was spin-concentrated to 100 µl and detergents were removed by a chloroform/methanol extraction. Briefly, 400 µl of HPLC-grade methanol, 100 µl HPLC-grade chloroform, and 300 µl HPLC-grade water was added to the 100 µl concentrated elution, with vortexing and centrifugation at 13,000 rpm between each addition. After a final mixing, the sample was centrifuged for 5 min to pellet the protein at the interface and the upper phase was removed with care to leave the protein pellet intact. The protein pellet and lower phase were resuspended in 300 µl of methanol, and the sample was again vortexed and centrifuged for 5 min to pellet the protein at the bottom of the tube. The supernatant was removed and one or more methanol washes were performed to ensure the removal of detergents, resuspended in 50 mM ammonium bicarbonate (pH 8) or 50 mM HEPES (pH 8) for SILAC or iTRAQ respectively. Samples were digested overnight at 37°C with sequencing grade modified trypsin (Promega). iTRAQ labeling of digested peptides was carried out using iTRAQ 4-plex reagent (AB SCIEX) for 2h at

room temperature in the dark. Peptides were fractionated with Mini SCX Spin Columns and cleaned with PepClean C18 Spin Columns (Thermo Scientific) before separation by a Tempo LC MALDI Spotting System.

MS analysis

MS and MS/MS data were acquired with a MALDI TOF/TOF 5800 (ABSCIEX) and analyzed by ProteinPilot Software Version 3.0 (ABSCIEX) with a UniProtKB/Swiss-Prot database. Proteins were accepted when ≥1 unique peptide was identified at 99% confidence. Peptide quantitation by ProteinPilot was performed using the Pro Group Algorithm and quant ratios are bias-corrected. MIB/MS analysis with cell lines was done in 2-3 independent experiments. A set of 3 independent experiments using SILAC labeled SUM159 cells treated with AZD6244 or DMSO was used to assess statistical significance and reproducibility of MIB/MS.

qRT-PCR

RNA was isolated from cell lines or murine tumors using the RNeasy® Plus Mini Kit (Qiagen). qRT-PCR was performed on diluted cDNA with the Applied Biosystems 7500 Fast Real-Time PCR System and inventoried TaqMan® Gene Expression Assays.

In vivo tumorigenesis experiments

Animal handling and procedures were approved by the UNC Institutional Animal Care and Use Committee and followed the NIH guidelines. Male C3Tag mice were bred with wildtype females to produce experimental offspring. Treatment began the same day a palpable mass was found. Drugs were incorporated into chow and food was provided ab libitum. Tumor size was assessed twice weekly by caliper measurements of tumor areas ((width)2 × length))/2 for 21d. Percent change of tumor volume was

calculated using (Final volume – Initial Volume)/Initial Volume and graphed using R (http://www.r-project.org/). Tumors at harvest were halved and either snap-frozen in liquid nitrogen and stored at -80°C or placed in neutral buffered 10% formalin solution.

Human breast tissue procurement

All human breast tissue was obtained from the Tissue Procurement Facility in compliance with the laws and institutional guidelines as approved by the UNC IRB committee. Clinical specimens were phenotyped by gene expression analysis in the lab of Chuck Perou.

Generation of immortalized T2-C3Tag cell line from a C3Tag tumor

An autochthonous tumor from a C3Tag mouse was excised and dissociated in a sterile fashion in the presence of 0.25% trypsin (Gibco). Cells were then passed through a 40 micron cell strainer and grown in the presence of DMEM + 10% FBS. Cells were isolated and expression of SV40T antigen verified by immunoblotting with antibodies specific to SV40 large T (EMD Biosciences, monoclonal, clone PAb416).

Compounds

Sorafenib and U0126 were purchased from LC Labs. BEZ235 was purchased from Selleck; bisindoylmaleimide-X was from Alexis and purvalanol B was from Tocris. GSK3 Inhibitor X was obtained from Calbiochem. Foretinib and AZD6244 were synthesized according to the procedures described in two patent applications (WO2005030140A2, WO2007002157A2). PP58, VI16832, dasatinib, lapatinib, SB203580, PLX4720 and SB590885 were custom synthesized according to previously described methods by The Center for Combinatorial Chemistry and Drug Discovery, Jilin University, P.R. China[123,125–128].

RNA sequencing

Polyadenylated (poly-A) mRNA was isolated from 10 µg total RNA using Dynal oligo(dT) beads (Invitrogen). Poly-A mRNA was fragmented for five minutes at 70°C using Fragmentation buffer from Ambion. First strand cDNA synthesis used random hexamer primers and SuperScriptII (Invitrogen). Second strand cDNA synthesis was performed using DNApolI (Invitrogen) and was purified using QIAquick PCR spin columns (Qiagen). Library preparation was performed according to manufacturer's instructions (Illumina).

RNA-seq alignment and transcript expression analysis

76-bp Illumina RNA-seq reads for a claudin-low tumor (3 lanes), SUM159 (4 lanes), and MDA-MB-231 (3 lanes) were obtained from the TCGA and aligned to the UCSC human knownGene mRNA from NCBI build 37 (hg19) using Bowtie[129]. The alignment was performed allowing just one mismatch in each read and only the best resulting alignment was reported for each aligned read. Duplicate reads were removed using Picard (http://picard.sourceforge.net) and in-house scripts were used to obtain read counts for protein kinases. Read counts were summed for all isoforms of each kinase gene. The raw kinase transcript read counts were then normalized with a calculation of reads per kilobase of exon model per million mapped reads (RPKM)[130]. The value of "N" (total number of mappable reads) in the RPKM formula was defined as the total number of aligned reads minus the duplicate reads. Additionally, the mean isoform length for each gene was used in the RPKM calculations.

Western blotting

Proteins from cell lysates were separated by SDS-PAGE chromatography, transferred to nitrocellulose membranes, and probed with the indicated primary

antibodies. Antibodies recognizing pAKT (S473), pAKT (T308), pAXL (Y702), AXL, c-MYC, DDR1, EGFR, pERK1/2 (T202/Y204), pHER3 (Y1197), MAX, pMEK1/2 (S217/S221), MEK1/2, MKP3, pP70S6K (T389), pPDGFRβ (Y751), pPDGFRβ (Y1009), pPDGFRβ (Y857), PDGFRβ, pRAF (S338), pRSK1 (T359/S363), pVEGFR2 (Y1175), VEGFR2 were obtained from Cell Signaling Technology. Antibodies for c-MYC (C-terminal), Cyclin A2, Cyclin B1, Cyclin D1, ERK2, MEK2 and RAF were obtained from Santa Cruz Biotechnology. The antibody recognizing BIM was obtained from Chemicon. The antibody recognizing p-c-MYC (S62) was obtained from Abcam. Secondary HRP-anti-rabbit, HRP-anti-mouse and HRP-anti-goat secondary antibodies were from Jackson Immunoresearch Laboratories, GE Healthcare and Santa Cruz Biotechnology, respectively. Western blots were visualized by incubation with SuperSignal West Pico Chemiluminescent Substrate (Thermo Scientific).

RTK arrays

Cells were harvested in RTK array lysis buffer containing 20 mM Tris-HCl (pH 8.0), 1% NP-40, 10% glycerol, 137 mM NaCl, 2 mM EDTA, 1X EDTA-free protease inhibitor cocktail (Roche), and 1% each of phosphatase inhibitor cocktails 1 and 2 (Sigma). After incubating on ice for 20 minutes, cell debris was pelleted at 4°C. Lysates (500 µg protein) were applied to R&D Systems Proteome Profiler™ Human Phospho-RTK antibody arrays. Washing and secondary antibody steps were performed according to the manufacturer's instructions. RTK arrays were visualized by SuperSignal West Pico Chemiluminescent Substrate (Thermo Scientific).

Generation of c-MYC(T58A) SUM159 and T2-C3Tag Cells

Phoenix cells were transfected with either pMSCV MYC(T58A) puro (Addgene Plasmid 18773) or empty vector pMSCV. Retrovirus-containing media was filtered 48h

post-infection after addition of polybrene (6 µg/ml), and placed on SUM159 and T2 cells for 36h. After an additional 4d in fresh media, cells were selected in either 3 µg/ml (SUM159) or 6 µg/ml puromycin (T2-C3Tag) for one week. Selected cell populations were used in subsequent experiments.

ChIP-PCR

Cells were fixed for 10 min in 1% formaldehyde, sonicated (VCX130 Ultrasonicator), and immunoprecipitated with 5 µg anti-c-MYC and protein A dynabeads (Invitrogen). Crosslinking was reversed by overnight incubation at 65°C, and DNA was purified with the MinElute PCR purification kit (QIAGEN). ChIP assay was quantified by real-time PCR using Absolute Blue SYBR green PCR mix (Thermoscientific). Fold enrichment was determined by the 2^-ΔCT method using the following PCR primers designed to amplify 75-100 bp fragments from genomic DNA: forward 5'-GGCTTTGAGACGTGAAAAGGA-3' and reverse 5'-GGTCATCCAGCACAGATTGGA-3'; forward 5'-TGGGCCTTGGTTTGTCCTT-3' and reverse 5'-CATGGAGGAGATGGAAAGATCCT-3'.

Inhibitor-conjugated bead preparation

Inhibitor beads were prepared via carbodiimide coupling of appropriately derivatized kinase inhibitors to ECH Sepharose 4B (Lapatinib, Bisindoylmaleimide-X, SB203580, Dasatinib, PP58 and VI16832) or EAH Sepharose 4B (Purvalanol B) (GE Healthcare). Briefly, ECH-Sepharose and EAH-Sepharose beads were washed with 50% DMF/EtOH followed by incubation with kinase inhibitors in 50% DMF/EtOH and 0.1M EDC (Sigma) at pH 5-6 overnight at 4°C in the dark. Following coupling, excess remaining groups were blocked with 0.1M N-ethyl-N'-(3-dimethylaminopropyl) carbodiimide hydrochloride (EDC) in 50% DMF/EtOH 1M ethanolamine (ECH-

Sepharose) or 20 mM HAc in 50% DMF/EtOH (EAH-Sepharose). Subsequently, beads were washed with 50% DMF/EtOH and alternating washes of 0.1 M Tris-HCl (pH 8.3) and 0.1 M acetate (pH 4.0) buffers, each containing 0.5 M NaCl. Inhibitor beads were stored in 20% ethanol at 4°C in the dark. See Figure 2.1 for structures of inhibitor-bead conjugates.

MIB statistical analysis

Data obtained from the MALDI TOF/TOF was processed with the ProteinPilot software to identify proteins from database searches and quantify changes in binding of kinases to MIBs using the Paragon Algorithm. The search results are further processed by the Pro Group Algorithm to determine the smallest justifiable set of detectable proteins and relative protein levels. We performed three replicates of SILAC labeled SUM159 cells treated with AZD6244 (2 'heavy', 1 'light') or DMSO to assess the reproducibility of MIB kinase affinity capture. A total of 113 unique kinases are identified. For each kinase, we computed the pool protein ratio and p-value across the three replicates as follows. Let y_{ij} denote the log2 protein ratio for kinase i, i=1, …,113 in replicate j, j=1,2,3. The pool protein ratio for kinase i is defined as $2\hat{}y_i$, where $y_i=(\Sigma^3_{j=1}y_{ij})/3$. To avoid directional conflict, we convert the two-sided p-value reported in ProteinPilot to one-sided p-value and denote it as p_{ij}. We apply Stouffer's z-score method to combine the p-values. Let $z_{ij}=\Phi^{-1}(1-p_{ij})$, where Φ is the standard Gaussian cumulative distribution function. Define the combined Z-score as $z_i=(\Sigma^3_{j=1}z_{ij})/\sqrt{3}$. The combined two-sided p-value for kinase i is given as $p_i = 2(1-\Phi(|z_i|))$. We also assessed the overlap/concordance between the kinases ranked by p-values for any two pairs of replicates. For each replicate, we identified kinases which exhibit statistically significant changes in expression based on Benjamini-Hochberg adjusted p-values at FDR of 0.05

to account for multiple comparisons. 24, 13 and 10 kinases are identified to be statistically significant for replicate 1, 2 and 3, respectively. 24 kinases are identified to be statistically significant in the pooled p-values.

Cell viability assays using siRNA knockdown of protein kinases

siGENOME pooled siRNAs for the genes of interest were obtained from Dharmacon, Thermo Scientific. RNAi assays were performed in either 96- or 384-well clear bottom plates. Prior to the assay, transfection conditions were optimized for SUM159 or MDA-MB-231 cells using Dharmafect transfection reagent and siRNAs for GAPDH (negative control), and UBB (lethality control). A 40 µl mixture of Dharmafect and siRNA was plated into each well by a multi-channel pipette and then followed by adding 160 µl cell suspension using a microplate dispenser. The final assay volume was 200 µl with a dose of 25 nM siRNA. Drug or vehicle solvent was added to the cell suspension before plating the cells. The assay was performed in triplicate and each plate had quadruple positive (UBB) and negative (GAPDH) controls. After 96h incubation at 37°C with 5% CO2, the number of viable cells in each well was determined by a luminescence viability assay with a Pherastar microplate reader. The % activity was calculated against the averages of positive and negative controls (% activity = 100 x (1 - [raw value - σp]/[σn - σp], where σp and σn are averages of raw values for the positive and negative controls, respectively. Each median in triplicate was used as a representative of % activity in the figures. Two-to-three independent experiments were performed with each cell line and siRNA.

Phosphoproteomics analysis of MIBs

Phosphopeptides were enriched from MIB elution digests using TiO2 beads as previously described[131]. Tryptic peptides were separated by reverse phase nano-HPLC

using a nanoAquity UPLC system (Waters Inc). Peptides were first trapped in a 2 cm trapping column (75 µm ID, C18 beads of 2.5µm particle size, 200 Å pore size) and then separated on a self-packed 25 cm column (75 µm ID, C18 beads of 2.5µm particle size, 100 Å pore size) at room temperature. The identity and phosphorylation status of the eluted peptides was determined with a Velos-Orbitrap mass spectrometer (Thermo-Scientific). Specifically, following a FT full scan, MS2 spectral data were acquired by one of three dissociative methods on the 9 most intense ions from the full scan, taking into account dynamic exclusions. For ion dissociation, collision induced dissociation (CID), high energy collision induced dissociation (HCD) or a CID/HCD toggle was employed. The polysiloxane lock mass of 445.120030 was used throughout. All raw data were converted to mzXML format and then searched using Sequest on a Sorcerer 2.0 platform (Sage N Research, Milpitas, CA). The search was semi-tryptic on the human IPI database (10/3/2010) appended with reversed sequences as decoys. Dynamic modifications for phosphorylated serines, threonines, and tyrosines were used, as well as a static modification for carbamidomethylated cysteines. Another search was also performed with the SpectraST algorithm provided in the Transproteomic Pipeline (TPP) version 4.4.1 using the NIST human ion trap database (1/14/2010). Results from the Sequest and SpectraST searches were analyzed using TPP's PeptideProphet and then combined using IProphet[132]. SILAC ratios were calculated with the XPRESS algorithm within TPP. XPRESS parameters were heavy arginines' with a mass difference of 10 and heavy lysines' with a mass difference of 6. Protein identifications were output by TPP's ProteinProphet.

Immunofluorescence and TUNEL assays

Tumors were snap frozen, cryosectioned at 6 µm and fixed in 4% paraformaldehyde for 15 min. Sections mounted on glass slides were incubated

overnight with PDGFRβ rabbit antibody (Cell Signaling #3169) at 1:1000 dilution. Secondary antibody was Alexa 555 goat-anti rabbit. Protocol provided by Cell Signaling for staining of cryosections was followed. TUNEL assays were performed using the In Situ Death Detection Kit per manufacturers protocol (Roche, #12156792).

Chapter IV

Cell culture

MDA-MB-231 were grown in DMEM/F12 supplemented with 10% FBS. SUM159 and SUM229 cells were grown in DMEM/F12 supplemented with 5% FBS, 1 µg/ml hydrocortisone and 5 µg/ml insulin. BT474, SKBR3, and HCC1806 cells were grown in RPMI with 10% FBS. Media containing kinase inhibitors was replaced daily.

Multiplexed inhibitor bead affinity chromatography

Performed as in Chapter III.

MS analysis

Performed as in Chapter III.

Human breast tissue procurement

All human breast tissue was obtained from the Tissue Procurement Facility in compliance with the laws and institutional guidelines as approved by the UNC IRB committee.

Compounds and reagents

Lapatinib, dasatinib and erlotinib were purchased from LC Labs. BEZ235, BGJ398, MK2206 and XL184 were purchased from Selleck. Foretinib and AZD6244

were synthesized according to the procedures described in two patent applications (WO2005030140A2, WO2007002157A2). Compounds for MIBs were acquired/synthesized as in Chapter III. siGENOME siRNAs for the genes of interest and Dharmafect transfection reagent were obtained from Dharmacon, Thermo Scientific.

RNA sequencing, alignment and transcript expression analysis

Performed as in Chapter III.

Western blotting

Proteins from cell lysates were separated by SDS-PAGE chromatography, transferred to nitrocellulose membranes, and probed with the indicated primary antibodies. Antibodies recognizing pAKT (S473), pAKT (T308), DDR1, EGFR, pEGFR (Y1045), pEGFR (Y1068), pEGFR (Y1173), EpCAM, pERK1/2 (T202/Y204), HER2, KIT, pMET (S1234/S1235) and vimentin were obtained from Cell Signaling Technology. Antibodies for cyclin B1, ERK2 and FGFR2 were obtained from Santa Cruz Biotechnology, and the E-cadherin antibody was from Upstate. Secondary HRP-anti-rabbit, HRP-anti-mouse and HRP-anti-goat secondary antibodies were from Jackson Immunoresearch Laboratories, GE Healthcare and Santa Cruz Biotechnology, respectively. Western blots were visualized by incubation with SuperSignal West Pico Chemiluminescent Substrate (Thermo Scientific).

Cell viability assays

Cells were plated in 96-well plates at low density (200-2000 cells per well) and grown in the presence of drug for 72h, with daily replacement of drug and media. For luminescence viability assays, 50 µL of Cell Titer-Glo (Promega) was added to each well containing 100 µL of media. Plates were incubated at room temperature for 10 minutes

and luminescence was measured by a Pherastar microplate reader. For cell counting assays, nuclei were stained with Hoechst 33342 (Invitrogen, 1:4000) and counted with a Cellomics ArrayScan VTI (Thermo).

Chapter V

Compounds

Selumetinib, sorafenib, BEZ235, and compounds for MIBs were acquired or synthesized as previously described[100]. Trametinib for *in vitro* experiments was purchased from Selleck. Conjugation of inhibitors to beads was performed by carbodiimide coupling to ECH Sepharose 4B (bisindoylmaleimide-X, SB203580, lapatinib, dasatinib, VI16832 and PP58) or EAH Sepharose 4B (purvalanol B) (GE Healthcare).

The MEK inhibitors trametinib and selumetinib gave similar kinome reprogramming responses in preclinical models as shown previously[1]. Similarly, in cultured cell systems trametinib, selumetinib and U0126 were similar in regulating MEK1 and MEK2, induction of kinome reprogramming and inhibition of proliferation. This is consistent with the different MEK inhibitors binding to a common allosteric regulatory site and having the same mechanism of action.

Cell culture

SUM159, SUM229, MDA231, T11, WHIM12 and Hs578t cell lines were grown in DMEM/F12 supplemented with 5% FBS, 1% penicillin/streptomycin, 1 µg/ml hydrocortisone and 5 µg/ml insulin. HCC1806, MDA-MB-468, 2225, and HCC1937, were grown in RPMI with 10% FBS and 1% penicillin/streptomycin. All cells were incubated at 37°C with 5% CO_2. Media and drug was replaced daily for experiments longer than 24h.

Western blotting

Cell lysates were subjected to SDS-PAGE chromatography and transferred to nitrocellulose membranes before western blotting with primary antibodies. Antibodies against pAKT (T308), pAKT (S473), pAXL (Y702), AXL, BIM, c-MYC, DDR1, DDR2, EpCAM, pERK1/2 (T202/Y204), pFOXO3(T32), HER2, HER3, KIT, pMEK1/2 (S217/S221), pPKC(pan), pPDGFRβ (Y751), PDGFRβ, pRAF(S289), pRAF (S338), SNAIL, pSRC (Y416), VEGFR2 and Vimentin were obtained from Cell Signaling Technology. Antibodies for Cyclin A, Cyclin B1, Cyclin D1, ERK2 and FGFR2 were obtained from Santa Cruz Biotechnology. Antibodies against Aurora A, BRD4 and E-Cadherin were from Upstate, Active Motif and BD Transduction Laboratories, respectively. Secondary HRP-anti-rabbit and HRP-anti-mouse were obtained from Jackson Immunoresearch Laboratories. SuperSignal West Pico Chemiluminescent Substrate (Thermo Scientific) was used to visualize blots.

qRT-PCR

Performed as in Chapter III.

MIB/MS analysis

Performed as in Chapter III.

Cell viability assays using siRNA knockdown of protein kinases

Performed as in Chapter III.

RTK arrays

Performed as in Chapter III.

Kinome clustering and visualization

Two-way complete linkage unsupervised hierarchical clustering was utilized to visualize the activity pattern of the top 100 most variable kinases by median absolute deviation across the tumors. The analysis was carried out on logarithm transformed kinase quant ratios in R (http://www.r-project.org/).

Proliferation assays

For short-term growth assays, 200-2000 cells were plated per well in 96-well plates and allowed to adhere and equilibrate overnight. Drug was added the following morning and replaced daily. After 72 hrs of drug treatment, cells were stained with Hoechst 33342 (Invitrogen, 1:4000) for 30 minutes at 37°C, washed with PBS and counted with a Cellomics ArrayScan VTI (Thermo) using Cellomics Scan software v7.6.2.1 (Thermo). For colony formation assays, cells were plated in 6-well dishes (200-1000 cells per well) and incubated overnight before continuous drug treatment for 30 days, with drug and media replaced twice weekly. At the end of treatment, cells were rinsed with PBS and fixed with chilled methanol for 10 min at -20°C. Methanol was removed by aspiration and cells were stained with 0.5% crystal violet in 20% methanol for 20 min at room temperature, washed with distilled water, and scanned. For quantitative analysis, crystal violet was solubilized from stained cells with 30% acetic acid and analyzed at λ=590 for relative quantitation of staining. Error bars represent standard deviation.

Cell sorting

SUM229 cells were trypsinized and resuspended in Hank's Balanced Salt Solution containing 2% fetal bovine serum (HF media). For analytical flow cytometry, cells were fixed with 3% paraformaldehyde. Cells were stained for 30 minutes at 4°C with the

fluorescently-labeled primary antibodies EpCAM-FITC (Stem Cell Technologies) and CD49f-PE-Cy5 (BD Biosciences), washed twice with HF media and filtered with a 0.2 µm filter. Fixed cells were analyzed using a Beckman-Coulter CyAn Cytometer, and live cells were sorted using a Sony iCyt Reflection Cytometer. Sorting was analyzed with FlowJo v7.6.5 software.

In vivo tumorigenesis experiments

The UNC Institutional Animal Care and Use Committee approved all mouse protocols. Drug treatment was administered through chow, provided ad libitum upon discovery of a palpable tumor. Tumors were harvested by snap-freezing in liquid nitrogen and stored at -80°C.

Human breast tissue procurement

Human breast tissue was acquired from the Tissue Procurement Facility in full compliance with the laws and institutional guidelines as approved by the UNC IRB committee. Gene expression analysis was used to define subtypes of clinical specimens.

Window trial

Eligible women included those with stage I-IV newly diagnosed and previously untreated triple negative breast cancer that was accessible for biopsy and surgery; stage I-IIIc subjects could not be candidates for therapeutic neoadjuvant treatment. Triple negative status was based upon the clinical assays and defined by ASCO/CAP criteria including estrogen receptor (ER) and progesterone receptor (PR) <1% staining by immunohistochemistry (IHC) and HER2-negative by IHC or fluorescence in situ hybridization. Study subjects provided written informed consent that included details of

the nontherapeutic nature of the trial, and the study was approved by the UNC Office of Human Research Ethics. After enrollment, study subjects underwent core biopsy of the breast tumor, and then received trametinib for the 7 consecutive days prior to the scheduled surgery date. The last dose of trametinib was taken $\leq$ 24 hours before surgery. At surgery a post trametinib tumor specimen was reserved for research. Patients were monitored for toxicity during and up to several weeks after treatment, until any evidence of toxicity had resolved. The dosing schedule of trametinib was determined by the surgery date; delays in standard therapy for trial purposes were not permitted. Given the nontherapeutic nature of the trial, the dose was deliberately set low at 1.5 mg orally daily under fasting conditions; this dose was increased per protocol to 2 mg daily after interim analysis of pharmacodynamic endpoints in the pre- and post-treatment tumor samples from, and toxicity assessment of, the first 3 patients enrolled.

Biopsy and surgical specimens were immediately placed into liquid nitrogen. Both pre- and post- trametinib tumor tissue was analyzed for baseline kinome profile and for the dynamic effects of MEK inhibition on the whole kinome. Frozen tissue intrinsic subtyping was performed by gene expression profiling using Agilent DNA microarrays and the PAM50 algorithm[133]; claudin-low subtyping used a centroid-based predictor[8].

Statistical analysis of patient tumor peptides

Kinome response to trametinib in patient tumors was determined by MIB/MS using quantitative iTRAQ labeling on a MALDI TOF-TOF 5800 (ABSCIEX). A breast cancer cell line mix consisting of HER2amp (BT474 and SKBR3), luminal (MCF7), basal-like (HCC1806, SUM229, MDA-MB-468 and SUM149) and claudin-low (SUM159, MDA-MB-231, HS578T and WHIM12) cell lines was used as a reference sample. Five untreated snap-frozen basal-like TNBC patient tumors obtained from UNC Tissue Procurement

Facility and two patient (Pt.1. and Pt. 2) 7d-tramatinib treated tumors from the window trial were used in the analysis. Endogenous protein kinases from tumors and the breast cancer cell mix were isolated using MIBs and iTRAQ-labeled for quantitative comparison of peptides. MEK1 and MEK2 peptide abundance from each tumor was quantitatively determined as an iTRAQ ratio of tumor/breast cancer cell line mix. Differences in MIB-binding of MEK1 and MEK2 relative to control between trametinib treated tumors and the five untreated tumors was analyzed using non-parametric Mann Whitney tests to compare the peptide abundance between control and MEKi treated patients for MEK1 and MEK2. False discovery rate (FDR) control was used to adjust for multiple testings.

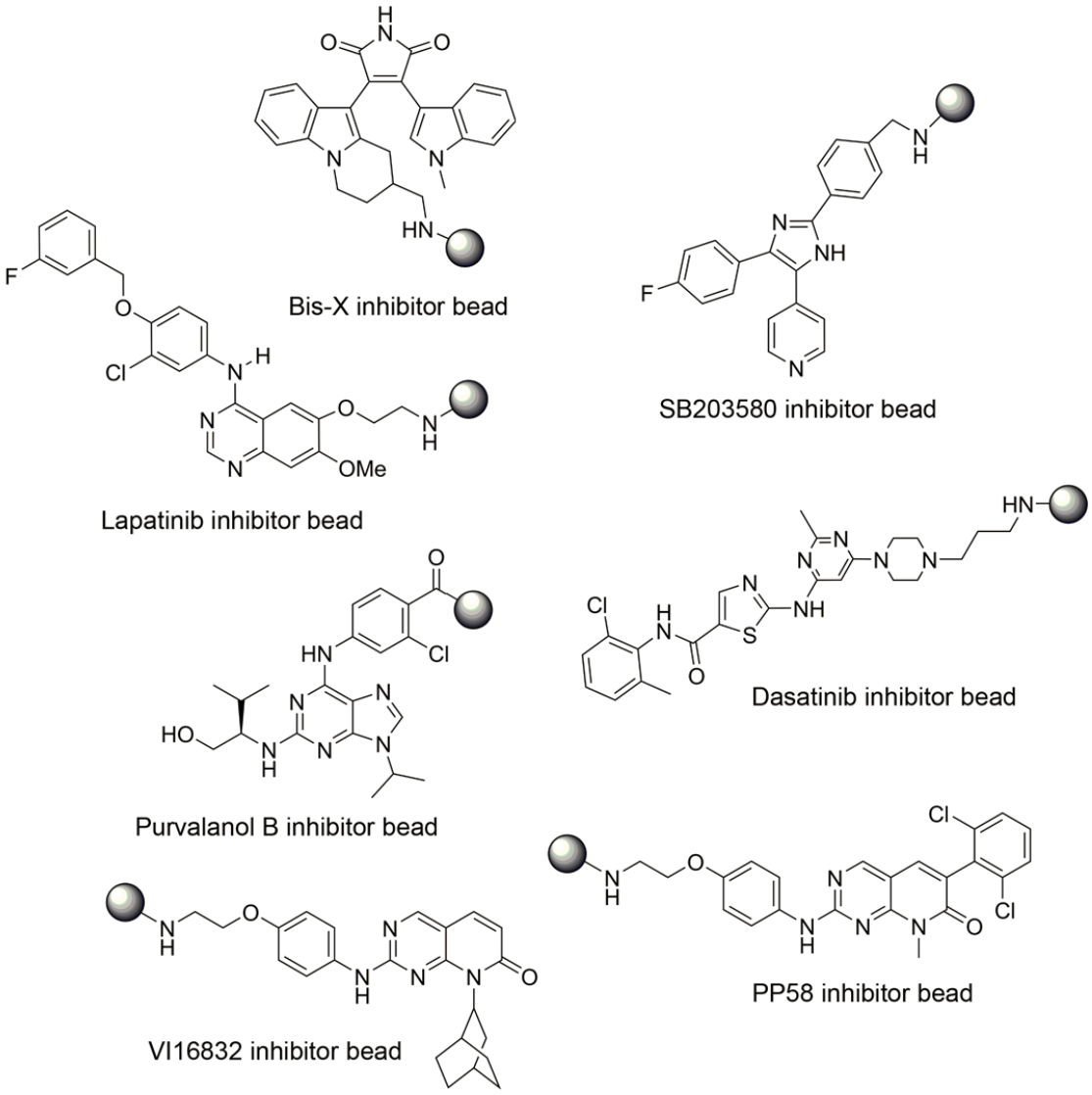

Figure 2.1 Structures of bead-conjugated kinase inhibitors. A) Bead-inhibitor conjugates are shown for specific and pan-kinase inhibitors used for MIB-based isolation of protein kinases.

III. DYNAMIC REPROGRAMMING OF THE KINOME IN RESPONSE TO TARGETED MEK INHIBITION IN CLAUDIN-LOW TRIPLE NEGATIVE BREAST CANCER

Introduction

Kinase-targeted cancer therapies can fail when tumor cells circumvent the action of a single agent, facilitating therapeutic resistance. Acquired or selected mutations can decrease affinity for kinase inhibitors, but resistance also develops through alternate routes of kinase pathway activation. For example, RTK upregulation has been observed following targeted inhibition of selective kinases; this kinome reprogramming circumvents inhibition of proto-oncogenic kinases[54,63,67,134]. Alternatively, genomic loss of PTPN12 phosphatase expression similarly causes activation of multiple tyrosine kinases[135]. Thus, dynamic and system-wide changes in multiple kinases can occur in tumor cells following pharmacological or progressive genetic perturbations. An understanding of these kinome responses and the mechanisms by which they occur will be crucial for determining how to abrogate therapeutic resistance. With over 130 kinase-specific inhibitors currently in Phase 1-3 clinical trials, developing combination therapies relevant for molecularly-defined cancer subtypes is a highly tractable goal. However, rational design of kinase inhibitor combinations requires an overall knowledge of kinome activity and response, not just a simple measure of an inhibitor's effect on one or two kinase pathway components. Currently, there is no optimal discovery mechanism to define the entire kinome and its dynamic activity. Such a technique could globally assess tumor kinome response to small molecule inhibitors and suggest more effective combination therapies.

To meet this challenge, we developed a chemical proteomics approach using multiplexed kinase inhibitor beads and mass spectrometry (MIB/MS) to define and quantitate the activity and drug responsiveness of a significant percentage (50-60%) of the expressed kinome. We applied this technique to triple negative breast cancer cell lines, pre-clinical tumor models and human tumors. Analysis of patient TNBC showed activated RAF-MEK1/2-ERK1/2 signaling, supporting MEK as a target in TNBC. Pharmacologic MEK inhibition in TNBC cell lines and genetically engineered mouse model (GEMM) tumors resulted in rapid kinome reprogramming through the induced expression and activation of multiple tyrosine and serine/threonine kinases that bypassed the initial MEK-ERK inhibition. Alterations in virtually every tyrosine and serine/threonine kinase family were observed. The mechanism of this kinome reprogramming involved the proteolytic degradation of c-MYC following MEK1 and MEK2 inhibition which resulted in increased expression and activity of RTKs. MIB/MS analysis showed that reprogrammed kinase activation overcame MEK2 (but not MEK1) inhibition leading to therapeutic resistance. The MEK inhibitor kinome response signature allowed us to predict and test the efficacy of a novel small molecule kinase inhibitor combination. The combination synergistically inhibited TNBC cell line proliferation and caused apoptosis and tumor regression in the C3Tag GEMM of basal-like/claudin-low TNBC.

Results

Kinome profiling of TNBC

We built upon previous chemical proteomic work to develop methods for isolating the endogenous kinome from whole cell lysates and interrogating kinase expression and activity dynamics through mass spectrometry (MIB/MS)[122]. Ten different kinase inhibitor beads were generated and tested for the distribution and number of kinases captured

(Figure 3.1A,B). As expected, some kinase inhibitor beads were fairly specific for kinases captured, such as lapatinib (with high binding of EGFR) and bisindoylmaleimide-X (which bound mostly GSK3α/β and PKC isoforms), while others, like purvalanol B, PP58, and VI16832, were promiscuous. Multiplexing beads within a single column enhanced the number of kinases captured and provided the greatest assessment of kinome expression and activity. Kinase capture with inhibitor beads is reproducible and is a function of the affinity of kinases for the immobilized inhibitors, kinase expression, and the activation state of the kinase[116]. Using MIB/MS, we have observed that different cell types and model systems exhibit partially overlapping but unique signatures of kinome expression and activity[100,136]. Across all cell line and tumor models tested, approximately 360 protein kinases and 24 metabolic kinases were observed above a cutoff of 90% confidence.

TNBC clinical trials of single kinase inhibitors have largely failed, consistent with drug-induced activation of alternative survival signaling pathways. Figure 3.2A outlines our strategy to interrogate kinome dynamics with the goal of defining endpoints leading to rational design of combination therapies. RNA-seq defined the transcript-level expressed kinome and affinity capture of endogenous kinases followed by quantitative mass spectrometry measured kinome activity profiles in tumors and cells. The proteomic assessment was used to define the kinome response to targeted inhibition of kinases. RNAi tested growth and survival functions of the kinases activated in response to inhibitors, and the cumulative results were used to rationally predict kinase inhibitor combinations to test in models of TNBC.

The kinome transcript expression profile of a patient's claudin-low breast tumor and two claudin-low TNBC lines, SUM159 and MDA-MB-231, was determined by RNA-seq. Greater than 400 of the 518 human protein kinases were expressed in the claudin-low human TNBC tumor and cell lines (Figure 3.2B). Approximately 10% of the kinases

expressed in the claudin-low patient tumor were unique compared to the claudin-low cell lines, undoubtedly due to the tumor's complex cellular composition. The majority of expressed kinases are common between tumor and claudin-low cell lines, suggesting that interrogating the cellular kinome response to inhibitors will be relevant to patient tumors.

Profiling kinase activity in tumors and cell lines was carried out using multiplexed inhibitor beads (MIBs), consisting of a subset of the immobilized, linker adapted, kinase inhibitors (bisindoylmaleimide-X, SB203580, dasatinib, lapatinib, VI16832, purvalanol B, and PP58)[123]. Acute changes in activation-dependent binding were demonstrated by the increased binding of MAPK pathway kinases in EGF-stimulated cells and the increased retention of tyrosine kinases from cells treated with the tyrosine phosphatase inhibitor pervanadate (Figures 3.2C,D). Our data showed that MIBs capture the majority of the expressed kinome estimated by RNA-seq and detect altered kinome activity profiles in response to stimulus or clinical kinase inhibitors.

Using MIBs and mass spectrometry, we have cumulatively sequence identified more than 320 kinases from cell lines and tumors. MIB/MS profiling of an invasive ductal carcinoma breast tumor and two claudin-low cell lines identified approximately 50-60% of the expressed kinome (Figures 3.2E-G). Kinases from all major kinome subfamilies were captured, with a large percentage representing the untargeted kinome[24]. iTRAQ labeling of digested MIB elutions allowed quantitative profiling of kinases in patient invasive ductal carcinoma compared to adjacent uninvolved mammary tissue (Figure 3.3A). Of the kinases detected, there was a general increase in MIB binding of tumor kinases, suggesting escalated kinome activity in the tumor compared to uninvolved mammary tissue. For example, the RAF-MEK-ERK pathway is increased in MIB binding in the tumor relative to control tissue, consistent with ERK activity being a driver for TNBC proliferation. Immunoblots confirmed the activation of RAF-MEK-ERK

signaling in the patient invasive ductal carcinoma (Figure 3.3B). RTK arrays further revealed tyrosine phosphorylated RTKs in two human tumors, which showed phosphorylation of EGFR, HER2, PDGFRβ, CSF1R, RON and EPHB2 (Figure 3.3C). Although our data pointed to the potential importance of tyrosine phosphorylated EGFR and PDGFRβ in patient TNBC, clinical trials targeting these RTKs have largely failed[137,138]. The failure of single agent RTK inhibitors in TNBC is consistent with drug-induced activation of multiple kinases or compensatory tumor kinome responses. Since many expressed RTKs drive ERK activation, we profiled claudin-low breast cancer cells after MEK inhibition (e.g. AZD6244 currently in clinical trials), to determine if dynamic kinome reprogramming occurs. Our goal was to define kinome alterations that would suggest a more effective, rationally designed combination therapy.

Reprogramming the kinome in response to MEK inhibition

MEK inhibitors AZD6244 or U0126 inhibited growth of SUM159 (Figure 3.4A) and MDA-MB-231 cells (Figure 3.4B). ERK remained inhibited after 4h of MEK inhibitor treatment, while MEK phosphorylation was enhanced (Figure 3.4C). Inhibitor treatment for 24h resulted in reactivation of ERK, demonstrating both lines overcame the initial MEK inhibition (Figures 3.4C,D). Phosphoproteomic analysis revealed loss of ERK-mediated feedback regulation of both BRAF and MEK1 (Table 3.1). Reduced phosphorylation of negative feedback sites on BRAF and MEK1 indicate escape from the suppressive feedback regulation on the ERK pathway[139]. Analysis of MIB isolated protein kinases identified 52 peptides with decreased and 59 peptides with increased phosphorylation, while the phosphorylation status of 365 phosphopeptides was unchanged after MEK inhibition. The majority of these phosphorylation sites were serine, threonine and proline-directed serine/threonine sites, but phosphotyrosine changes were also included, suggesting a broad change in kinome activity in response

to AZD6244.

We next used MIB/MS to profile the SUM159 kinome response after exposure to AZD6244 (Figure 3.4E). MEK inhibition resulted in time-dependent MIB binding changes for more than 140 kinases, including cell cycle regulatory kinases, MAPK pathway kinases, RTKs, cytosolic TKs and other serine/threonine kinases. Figure 3.4F highlights the MIB binding dynamics for MAPK component kinases during the time course of MEK inhibitor response in SUM159 cells. At 4h of AZD6244 treatment both MEK1 and MEK2 are inhibited, as measured by loss of MIB binding. However, while MEK1 binding remains largely inhibited, MEK2 binding to MIBs increases at 12h of treatment and by 24h was similar to control cells, indicating a return of MEK2 activity. In parallel to restored MEK2 binding to MIBs, RAF1 and ERK1 binding to MIBs increased over the time course of AZD6244 treatment, correlating with activation of these kinases. We used RNAi for each kinase in the MAPK pathway to determine if knockdown had a differential growth affect in response to MEK inhibition (Figure 3.4G). RNAi knockdown showed that loss of MEK2 and ERK1 inhibited SUM159 cell growth in the presence of MEK inhibitor, whereas MEK1 knockdown did not enhance growth inhibition. Taken together, these data indicate that MEK2 and ERK1 can escape from inhibition by AZD6244, suggesting a critical role for MEK2/ERK1 in SUM159 growth and survival during AZD6244 treatment.

Figures 3.5A and B present a 21-kinase signature defining a reprogrammed kinome in response to MEK inhibitors. This signature shows a loss of cyclin-dependent kinases, consistent with growth inhibition, and increased ERK binding to MIBs indicating escape from MEK inhibition. RTKs including AXL, DDR1 and PDGFRβ, cytosolic tyrosine kinases FAK2 and JAK1, and the serine kinase ACVR1 all showed increased MIB binding. While MDA-MB-231 cells have a somewhat less robust kinome response to AZD6244, they displayed a significant kinome reprogramming that included a strong

increase in PDGFRβ binding to MIBs (data not shown).

RTK arrays confirm the increased tyrosine phosphorylation of multiple RTKs, including PDGFRβ and AXL in response to MEK inhibition (Figure 3.5C). In SUM159 cells AZD6244 also significantly increased tyrosine phosphorylation of VEGFR2 and RET. The AZD6244 response of SUM159 cells is dose-dependent (Figure 3.5D), as PDGFRβ and VEGFR2 show increased RTK phosphorylation and expression with increasing AZD6244. These results demonstrate that a significant number of kinases were induced in response to MEK inhibition. Relevant to the changes in the kinome to MEK inhibition, Table 3.2 lists the 40 highest expressed kinase transcripts of a patient claudin-low tumor. Of these 40 kinases, 14 (24%) were dynamically regulated in SUM159 and/or MDA-MB-231 cells in response to AZD6244, suggesting patient tumors could have a similar kinome reprogramming in response to targeted kinase inhibition.

MEK inhibition deregulates transcription, expression and activation of RTKs

Figure 3.6A defines the time course of kinome reprogramming to AZD6244 in SUM159 cells. MEK and ERK were rapidly inhibited, allowing accumulation of MKP3, the MAPK phosphatase that inactivates ERK[140]. Increased MKP3 expression combined with AZD6244 to strongly suppress ERK activity, but MKP3 protein was lost as MAPK pathway activity returned. Over time, VEGFR2, PDGFRβ and DDR1 expression was increased with AZD6244 treatment, as was the phosphorylation of HER3 and AXL. qRT-PCR analysis of SUM159 cells treated with AZD6244 demonstrated elevated RNA levels for several of these RTKs (Figure 3.6B), including DDR1/2, PDGFRβ, VEGFR2 (SUM159 only) and HER2/3. Analysis of cytokine RNA expression showed EGF, Gas6, PDGFB and PDGFD induction, indicating the establishment of autocrine/paracrine loops for RTK activation (Figure 3.6C). RTK arrays further showed a time dependent increase in tyrosine phosphorylation of PDGFRβ, VEGFR2 and HER2/3 (DDR1/2 are not on the

array) (Figure 3.6D). PDGFRβ whose RNA and protein expression was induced in response to AZD6244, was phosphorylated at tyrosines 751, 857 and 1009; sites required for PDGFRβ activation and recruitment of PI3K and PLCγ (Figure 3.6E).

After 30d of continuous exposure to AZD6244, SUM159 cells have become significantly resistant to MEK inhibitor-induced growth arrest (Figure 3.6F). Expression of cyclins A2 and B1 have recovered, consistent with increased proliferation (Figure 3.6G). The AZD6244-resistant cells (SUM159-R; grown continuously in 5 μM AZD6244) continue to have a reprogrammed kinome where PDGFRβ and VEGFR2 exhibited both increased expression and tyrosine phosphorylation, and AXL showed increased tyrosine phosphorylation (Figures 3.6D,H). Activation of these RTKs was accompanied by increases in phosphorylated AKT, RAF, p70 S6 kinase, MEK, ERK and RSK1, showing that the cells overcame MEK inhibition by RTK activation of the ERK, AKT and mTOR pathways (Figure 3.6H).

These findings indicate that targeted MEK inhibition significantly alters the activity of multiple kinases. It was therefore important to determine if the changes in kinase activity were specific for MEK inhibition or a function of growth arrest. BEZ235 is a dual PI3K/mTOR inhibitor that strongly inhibits SUM159 cell growth (Figure 3.7A). BEZ235 inhibited p70 S6 kinase activity consistent with mTOR inhibition but had no effect on the ERK pathway (Figure 3.7B). We compared the SUM159 kinome responses to BEZ235 and AZD6244 to determine if kinome reprogramming was target-specific or a function of growth arrest. Whereas AZD6244 induced PDGFRβ, VEGFR2 and AXL phosphorylation, BEZ235 treatment did not change the RTK phosphorylation profile except for increased phosphorylation of INSR, IGF1R and AXL (Figure 3.7C). MIB/MS confirmed that AZD6244 altered the kinome differently from BEZ235, indicating that drug-induced kinome reprogramming is target-specific (Figure 3.7D).

MEK-ERK inhibition induces c-MYC degradation leading to RTK reprogramming

ERK phosphorylates the transcription factor c-MYC at Ser62 and stabilizes c-MYC protein by preventing its proteasomal degradation[141]. Treatment of both SUM159 and MDA-MB-231 cells with AZD6244 caused rapid loss of c-MYC protein and mRNA (Figures 3.8A,B). This AZD6244-mediated repression of c-MYC protein and transcript, along with reduced phosphorylation of c-MYC at Ser62, resulted in decreased MYC-MAX heterodimerization that is required for c-MYC transcriptional regulation (Figure 3.8C)[142,143]. Despite partial recovery of MEK-ERK activation after 24-72h, total c-MYC expression remained repressed in the continued presence of AZD6244.

c-MYC binds the promoter of human PDGFRβ to repress PDGFRβ expression[144]. To define the role of c-MYC loss in the AZD6244 reprogramming response, we applied RNAi to knockdown expression of c-MYC; the effect was analogous to the reprogrammed RTK and cytokine response seen with AZD6244 treatment (Figures 3.8D-F). Similar to the AZD6244 response, knockdown of c-MYC induced expression of PDGFRβ, VEGFR2 and PDGFB, and increased tyrosine phosphorylation of PDGFRβ, VEGFR2, HER3 and AXL. RNAi knockdown of ERK1/2 confirmed that ERK inhibition was the primary signal inducing loss of c-MYC mRNA expression in the AZD6244 reprogramming of the kinome. Dual ERK1/2 knockdown resulted in reduced c-MYC and increased PDGFRβ expression (Figure 3.8G). Thus, reprogramming of RTKs in response to AZD6244 occurs by loss of ERK-mediated stabilization of c-MYC and the subsequent transcriptional derepression of RTKs and cytokines that are negatively regulated by c-MYC. BEZ235 inhibition of mTOR and PI3K inhibited cell growth but did not change ERK activity, c-MYC expression or RTK reprogramming, confirming the specificity of MEK-ERK in controlling c-MYC levels (data not shown).

Proteasomal degradation of c-MYC lacking Ser62 phosphorylation triggers

AZD6244-induced kinome reprogramming. Expression of a non-degradable c-MYC(T58A) mutant in SUM159 cells significantly blocked AZD6244-mediated induction of PDGFRβ, DDR1 and VEGFR2 (Figures 3.8H,I). GSK3β promotes c-MYC degradation, and inhibition of GSK3β stabilized c-MYC protein to repress the induction of PDGFRβ (data not shown). Similarly, treatment of SUM159 or SUM159-R cells with the proteasome inhibitor bortezomib prevented AZD6244-mediated c-MYC degradation, blocked c-MYC mRNA repression, and inhibited the induction of PDGFRβ, DDR1 and VEGFR2 (Figure 3.8J, data not shown). Washout of AZD6244 from SUM159 or SUM159-R cells led to increased ERK activity, stabilization of c-MYC expression and subsequent loss of RTK reprogramming (Figures 3.9A,B). Thus, stabilizing c-MYC protein levels prevented the onset of RTK reprogramming to AZD6244 and reversed the reprogramming in SUM159-R cells. Taken together, these findings show that AZD6244-induced c-MYC proteasomal degradation is responsible for kinome reprogramming and RTK upregulation.

In SUM159-R cells c-MYC protein, mRNA levels and MYC-MAX heterodimers have partially returned due to reactivated ERK stabilizing c-MYC (Figure 3.9C-E). This correlates with SUM159-R cells having an increased growth rate compared to cells acutely treated with MEK inhibitor (Figure 3.6F). The level of c-MYC protein, however, is insufficient to completely repress RTK expression, which remains elevated compared to control cells but at lower levels than cells treated with AZD6244 for 4-72h (Figures 3.9D,F). A 5-fold increase in AZD6244 concentration inhibited ERK activation in SUM159-R cells (Figure 3.9G) because the higher dose of MEK inhibitor more effectively prevented RTK-stimulated reactivation of MEK-ERK signaling. As expected, the resulting loss of phospho-c-MYC S62 and total c-MYC protein led to a corresponding increase in RTK expression in SUM159-R cells. Notably, the return of phospho-ERK in the continued presence of AZD6244 was insufficient to completely reverse RTK

reprogramming, suggesting ERK may not be fully reactivated. This was shown by measuring the phosphorylation of two ERK substrates, RSK1 and c-MYC, after only 1h of AZD6244 washout from SUM159-R cells (Figure 3.9H). Phosphorylation of both substrates and phospho-ERK was increased, demonstrating further activation of ERK shortly after the removal of MEK inhibitor. Thus, the combination of persistent c-MYC transcriptional repression and partial MEK-ERK reactivation allows the maintenance of RTK reprogramming, leading to MEK inhibitor resistance.

RTK reprogramming rescues cells from AZD6244-induced growth arrest

RNAi knockdown of PDGFRβ in SUM159 cells enhanced growth inhibition by AZD6244 (Figure 3.10A), indicating the induction of RTK signaling was critical for growth and survival of cells inhibited by AZD6244. To test the role of additional RTKs in the rescue response of cells to MEK inhibition, we performed siRNA knockdown of RTKs found to be transcriptionally induced and/or tyrosine phosphorylated in response to U0126 in SUM159 (Figure 3.10B) and MDA-MB-231 cells (data not shown). As controls we used siRNA to knockdown BRAF, RAF1 and ERK1/2; knockdown of each pathway member enhanced growth arrest observed with MEK inhibition. Knockdown of PI3K and AKT produced a greater growth arrest response in SUM159 than MDA-MB-231 cells, consistent with mutant PI3K being a driver in SUM159 cells. siRNA knockdown of LYN and EPHA2 had no effect on the growth of either cell type in the presence or absence of MEK inhibitor (LYN and EPHA2 show no change or loss of MIB binding in response to MEK inhibitor). While knockdown of HER2 or HER3 had little effect in SUM159 and MDA-MB-231 cells, knockdown of AXL, DDR1, DDR2, PDGFRβ and VEGFR2 each resulted in a strong synthetic lethal-like effect in the presence of U0126. Thus, loss of MEK-ERK signaling causes induction of multiple RTKs, each contributing to the subversion of MEK inhibition.

AZD6244 in combination with RTK inhibitors

Our results suggested RTK inhibitors in combination with AZD6244 could block the growth-promoting activity of the reprogrammed kinome. Given the repertoire of AZD6244-activated RTKs, we tested sorafenib and foretinib alone or in combination with AZD6244 for their ability to inhibit cell growth (Figures 3.10C,D). Whereas the two RTK inhibitors were ineffective as single agents, both were synergistic in inhibiting cell growth in combination with AZD6244, with sorafenib being most effective. Cell counting assays reinforced the strong synergistic growth arrest of SUM159 cells with the AZD6244/sorafenib combination (Figure 3.10E); RTK arrays validated that sorafenib inhibited tyrosine phosphorylation of multiple RTKs induced by AZD6244 (Figure 3.10F). The combination of AZD6244/sorafenib enhanced the inhibition of ERK1/2, decreased cyclin D1 levels and increased expression of the pro-apoptotic BIM protein compared to AZD6244 alone, indicating the cells were primed for apoptosis (Figure 3.10G).

Sorafenib inhibits PDGFRα and β, VEGFR2 and DDR1/2, but is also an inhibitor of BRAF and RAF. Therefore, we assayed the action of different RAF inhibitors in combination with AZD6244 to determine if the effect of sorafenib could be mimicked by other BRAF/RAF inhibitors (Figure 3.10H). RAF inhibitors, but not sorafenib, in combination with AZD6244 actually stimulated the growth of SUM159 cells, consistent with the known activation of wild-type RAF signaling by both PLX4720 and SB590885. At 250-500 nM, only sorafenib synergistically inhibited growth of SUM159 cells in combination with AZD6244. Thus, sorafenib in combination with AZD6244 inhibits growth of SUM159 cells more effectively than BRAF inhibitors by cotargeting induced RTKs.

SUM159-R cells that have become resistant to AZD6244 rely on RTK-driven reactivation of ERK for drug resistance. If a 10-fold higher dose of AZD6244 is used, ERK activity can be inhibited (Figure 3.10I). At the 5 μM of AZD6244 that was used to

develop SUM159-R cells, the addition of sorafenib inhibited ERK activity and cell growth (Figure 3.10J), confirming that AZD6244-induced activation of upstream RTKs drives ERK reactivation. In SUM159-R cells the combination of low doses of AZD6244 and sorafenib was similarly effective as high dose AZD6244 at inhibiting ERK activation and cell growth (Figures 3.10I,J).

Kinome reprogramming in the C3Tag TNBC GEMM

The genetically engineered C3Tag mouse model has a gene expression signature similar to human TNBC. To define AZD6244-mediated kinome reprogramming *in vivo*, we harvested tumor tissue before or after oral delivery of AZD6244. Figure 3.11A shows increased expression of PDGFRβ in response to AZD6244 in both the tumor cells and stroma of C3Tag tumors, demonstrating *in vivo* induction of PDGFRβ. Rapid degradation of c-MYC protein and induction of PDGFRβ was observed in 2d and 7d AZD6244-treated tumors, consistent with loss of c-MYC repression of RTK expression (Figure 3.11B). A C3Tag-derived breast cancer cell line (T2-C3Tag) isolated from the GEMM tumor responded to AZD6244 with upregulation of PDGFRβ and DDR1, confirming the tumor cell response to MEK inhibitor (Figure 3.11C). Expression of non-degradable c-MYC(T58A) in T2-C3Tag cells prevented the induction of PDGFRβ and DDR1, further indicating that proteasomal degradation of c-MYC is responsible for RTK reprogramming in C3Tag tumor cells (Figure 3.11D).

Profiling kinome response to targeted combination therapies in the C3Tag mouse model of TNBC

MIB/MS was then used to define the kinome response profile of C3Tag tumors from mice treated with AZD6244, sorafenib or the combination of AZD6244 and sorafenib (Figure 3.11E). The MIB/MS signatures of tumors continuously treated with

AZD6244 or sorafenib share some overlap but exhibit significant differences, demonstrating drug selective reprogramming of the kinome. AZD6244-treated tumors have upregulation of RTKs PDGFRβ, DDR2 and CSF1R, as well as a number of tyrosine kinases similar to the AZD6244 response in human TNBC cell lines. Importantly, the escape of MEK2 and ERK1 from AZD6244 inhibition was recapitulated in MIB/MS profiles of AZD6244-treated C3Tag tumors. Sorafenib-treated tumors showed decreased MIB binding of the previously reported sorafenib targets: BRAF, PDGFRβ, CSF1R, DDR1, DDR2, KIT, MLTK and FRK[117]. Both AZD6244- and sorafenib-treated tumors showed increased MIB-binding of cyclin-dependent kinases, indicating the tumors have circumvented the action of the single agents to reenter cell cycle progression. MIB/MS profiling of tumors treated with the combination of AZD6244 and sorafenib showed reduced MIB-binding of kinases activated by AZD6244 treatment (Figure 3.11F). Sorafenib inhibited AZD6244-mediated activation of RTKs PDGFRβ, DDR2 and CSF1R, as well as a number of intracellular tyrosine kinases, including JAK1. RTK-driven activation of MEK2-ERK1 was inhibited by sorafenib in tumors and loss of cyclin-dependent kinase binding to MIBs was also observed, consistent with the combination of AZD6244 and sorafenib arresting tumor growth (Figure 3.11E).

AZD6244 plus sorafenib causes tumor regression

After only 2d of AZD6244 or sorafenib treatment, the expression of VEGFR2 and PDFGRβ was increased along with increased phosphorylation of RAF at Ser338, demonstrating RAF activation (Figure 3.12A). The combination of AZD6244 and sorafenib reduced VEGFR2 and PDGFRβ expression, suppressed RAF activation and synergistically inhibited reactivated ERK. Figure 3.12B shows the combination of AZD6244 and sorafenib blocked ERK activation and induction of PDGFRβ in the T2-C3Tag cell line. Cyclin B1 levels are also reduced by the combination therapy, and a

strong growth arrest was observed in cells cotreated with AZD6244 and sorafenib, indicating that AZD6244 sensitizes cells to sorafenib treatment (Figure 3.12C).

Our findings showed that the combination of AZD6244 and sorafenib was significantly more effective in inhibiting ERK activation in 2d treated C3Tag mice and the C3Tag tumor cell line. Therefore, C3Tag mice were allowed to develop tumors and then treated for 21d with AZD6244 and/or sorafenib (Figures 3.12D,E). Sorafenib treatment alone had no effect on tumor progression, whereas 30% of the AZD6244-treated mice showed some tumor regression. In contrast, 77% of mice treated with AZD6244 and sorafenib had tumor regression, demonstrating a significantly greater effect of the combination therapy versus AZD6244 alone. TUNEL assays of the tumors showed that the combination of AZD6244 and sorafenib induced a strong apoptotic response in only 2d of treatment, in stark contrast with single drug treatment (Figure 3.12F).

Discussion

We describe a novel approach to study the reprogramming of protein kinase networks “en masse”. Our methods allowed the isolation and analysis of protein kinases from cells and tumors with 50-60% of the expressed kinome assayed in a single mass spectrometry run. Profiling MIB binding of kinases is a highly sensitive method to simultaneously monitor activation and inhibition of numerous kinases. This profiling technique allows interrogation of kinases known by sequence but which have been understudied due to lack of biologic or phenotypic knowledge or reagent availability. An example of the latter is the ability to distinguish changes in MEK1 and MEK2.

This technique identified a kinome response signature to the selective MEK1/2 kinase inhibitor AZD6244. The only defined substrates for MEK are ERK1 and 2, yet we observed changes in activity of kinases in every subfamily of the kinome in response to MEK inhibition. Kinome assessment showed a time-dependent reprogramming that

involved an early loss of ERK feedback regulation of RAF and MEK, as well as increased MKP3 protein stability. The increased expression of MKP3 functions to enhance ERK inactivation. In contrast, the loss of RAF and MEK feedback inhibition would allow upstream activation of the pathway. The time-dependent change in MIB binding of specific RTKs such as PDGFRβ and DDR1 was readily detected and provided the critical experimental observation that MEK inhibition was driving the expression and activation of multiple RTKs, each of which are capable of stimulating the RAF-MEK-ERK pathway. Importantly, we identified c-MYC degradation as a key mechanism mediating kinome reprogramming; preventing proteasomal degradation of c-MYC inhibited the reprogramming response. RNAi knockdown of ERK or c-MYC recapitulated the MEK inhibitor-induced expression and tyrosine phosphorylation of several RTKs, demonstrating ERK regulation of c-MYC stability is critical in controlling the expression and activation of specific kinases. The fact that multiple RTKs are activated in response to MEK inhibition demonstrates the difficulty in using single kinase inhibitors to arrest tumor progression.

In addition to c-MYC, inhibition of AKT and mTOR also causes kinome reprogramming in different breast cancer subtypes[67,145]. Whereas c-MYC functions as a repressor of PDGFRβ, DDR1/2 and VEGFR2 expression in claudin-low breast cancer, AKT has been shown to negatively regulate FOXO-dependent expression of HER3, IGF1R and INSR in several breast cancer cell lines. Inhibition of mTOR kinase activity leads to AKT inhibition and subsequent RTK reprogramming[145]. Differential kinome reprogramming is seen not simply with targeting the MEK-ERK and AKT pathways but with tyrosine kinase inhibitors as well. HER3 upregulation was shown to play a major role in lapatinib resistance and in lung cancer MET amplification leads to gefitinib resistance[72,146].

Analysis of the ERK pathway in cells treated with AZD6244 showed a time-

dependent rescue of BRAF/RAF, MEK2, ERK1 and RSK1 binding to MIBs. We demonstrated that MIB binding of these kinases is a function of their activation. The time course of recovery parallels that of AZD6244-induced RTK expression. The C3Tag tumor shows a comparable increase in MEK2 and ERK1 binding after AZD6244 treatment, mimicking the reprogramming response observed in SUM159 cells. Published work with a similar MEK inhibitor, GSK1120212, which binds to the MEK allosteric regulatory site (as does AZD6244) provides insight into how MEK2 escapes inhibition[33]. MEK1 phosphorylated at the activation loop serines has a 20-fold lower affinity for GSK1120212 than nonphosphorylated MEK1, effectively alleviating allosteric site inhibition of MEK. Because ERK activity is increasing over time, MEK1 would be feedback phosphorylated at its negative regulatory site Thr292, preventing MEK1 reactivation even in the setting of RTK reprogramming; MEK2, however, lacks this regulatory site and selectively escapes inhibition. This suggests a unique paradigm of activation of an upstream signaling pathway increasing the IC_{50} of an inhibitor for a target kinase.

In many tumor types tyrosine kinases are molecular drivers of transformation and also play a major role in resistance to therapy. Claudin-low SUM159 cells and the C3Tag breast cancer GEMM were remarkably similar in response to AZD6244, with induction and activation of PDGFRβ, VEGFR2, CSFR1, DDR1/2 and AXL. The claudin-low MDA-MB-231 cell line was somewhat less responsive, but still showed the induction of PDGFRβ, DDR1 and DDR2 and activation of AXL with AZD6244 treatment. RNAi knockdown of the different RTKs indicated that each kinase contributed to the survival response of SUM159 and MDA-MB-231 cells. Given the repertoire of RTKs whose expression and activity is induced with AZD6244 treatment, we predicted that the combination therapy of sorafenib and AZD6244 would “broaden” the kinase targeting sufficiently to produce significant therapeutic benefit. The combination therapy

increased apoptosis and tumor regression significantly compared to either drug alone in the C3Tag TBNC GEMM.

We identified AZD6244-induced RTKs (and serine/threonine kinases) using a combination of MIB/MS and immunoblotting of cell lines and C3Tag tumors. We created a signature of therapeutic resistance allowing a rational prediction of combinatorial therapies in claudin-low breast cancer. This approach can be extended to human tumors using so-called “window trials” in which a patient is treated with a targeted agent prior to surgery and their tumor analyzed at excision for kinome-resistance signatures. Importantly, we have shown that the kinome response is unique for inhibitors targeting different kinases and the response of different tumor types to a common inhibitor may also vary. Thus, this systems kinome approach can be applied to help define patterns of resistance for a variety of drugs and biopsy-accessible tumor types.

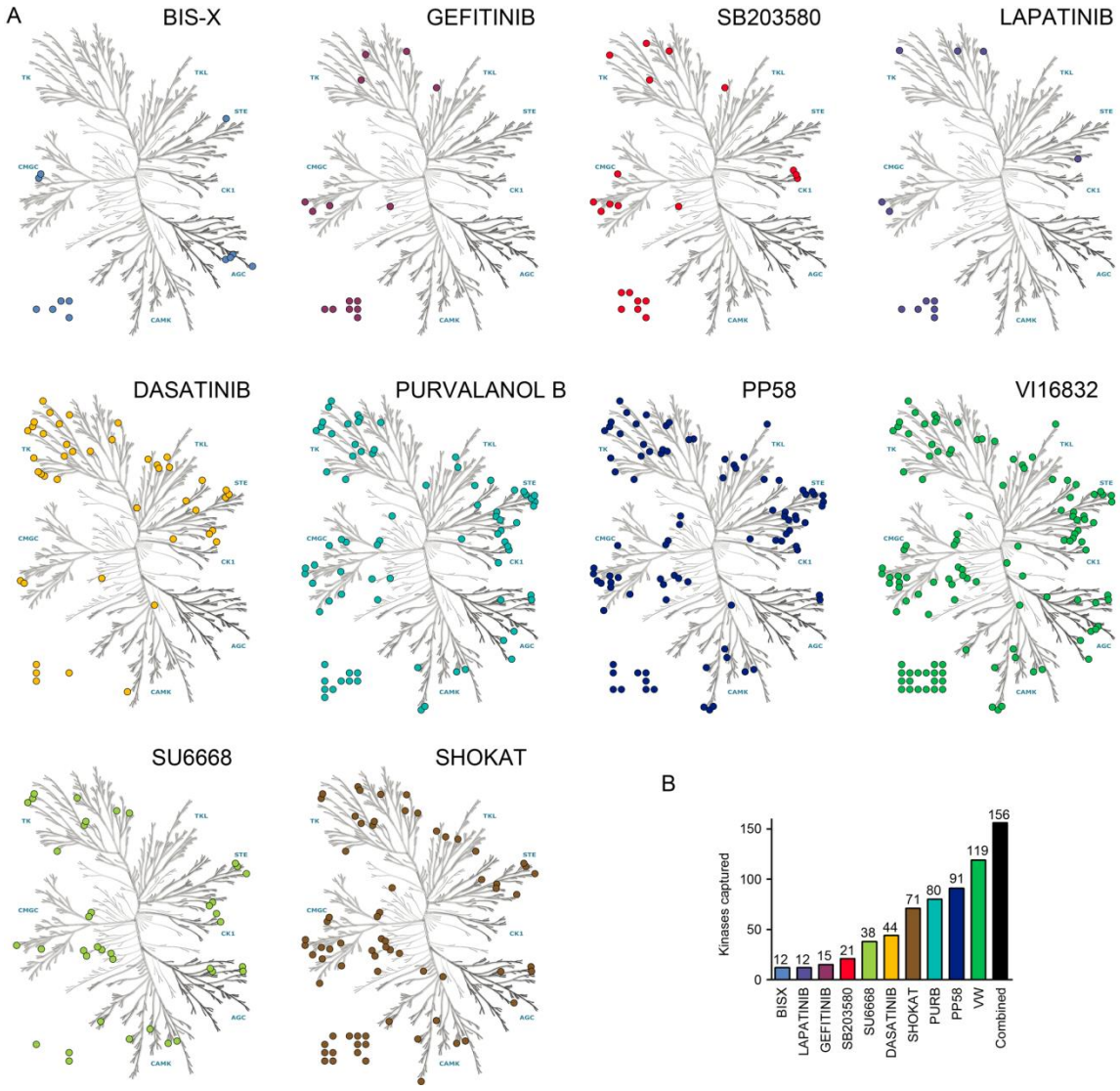

Figure 3.1 Kinase capture of inhibitor beads. A) Distribution of kinases captured using individual inhibitor beads. Binding of atypical or metabolic kinases are represented in lower left corner of kinome trees. B) Number of kinases captured using each inhibitor bead and a combined column of bisindoylmaleimide-X, SB203580, lapatinib, dasatinib, purvalanol B, PP58, and VI16832. For each run, HuMEC lysate containing 5 mg of total protein was applied to the column.

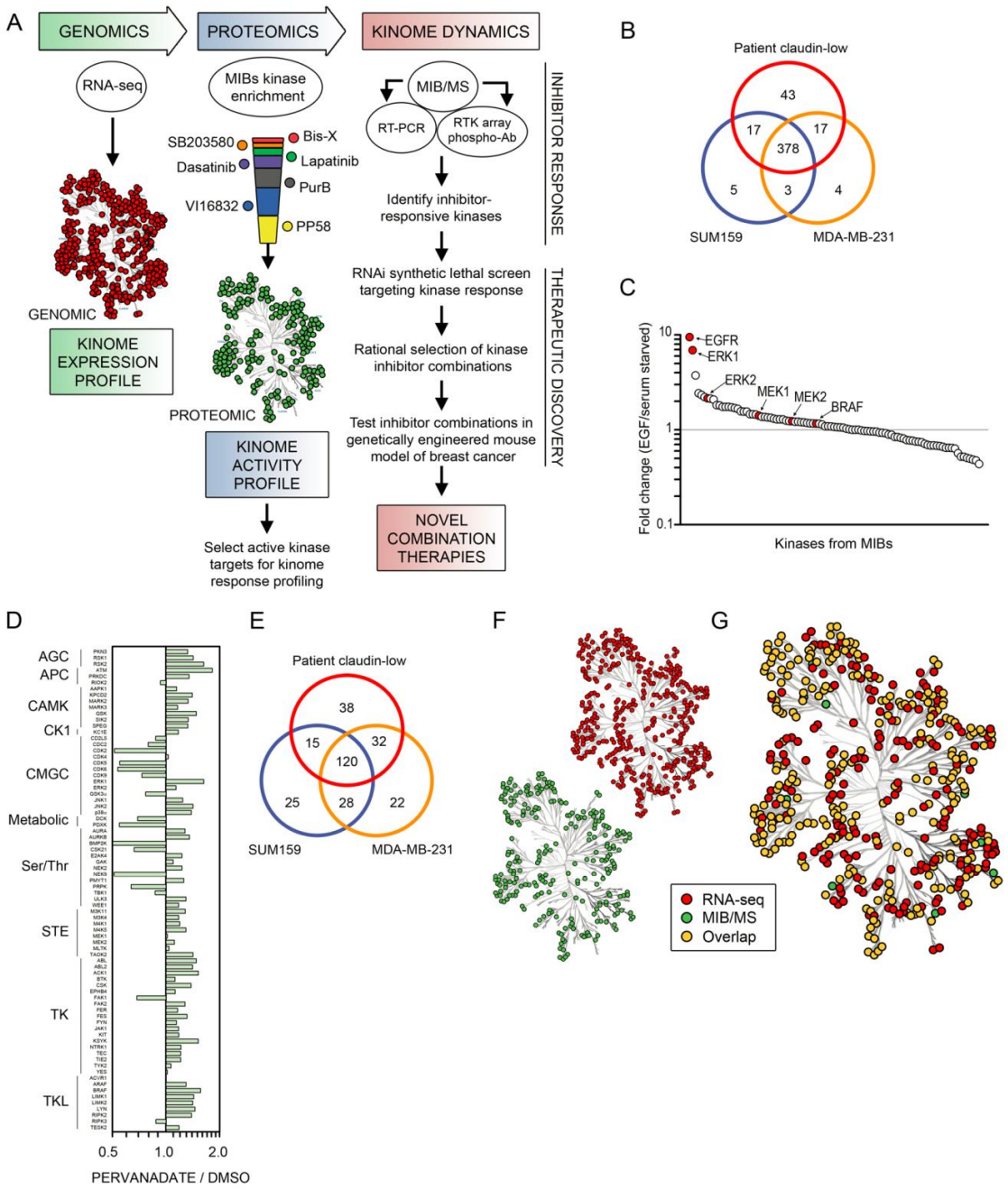

Figure 3.2 Strategy and characterization of MIBs. A) Experimental strategy. B) Venn diagram shows number of expressed kinases defined by RNA-seq across TNBC samples. C) Increased binding of EGFR signaling components following EGF stimulation. SILAC labeled MDA-MB-231 cells were serum starved overnight and stimulated with 30 ng/ml EGF for 15 min, harvested and applied to MIBs. A SILAC-based quantitative comparison of MIB-bound kinases was performed. D) Increased binding of tyrosine kinases to MIBs following pervanadate treatment. SILAC labeled CML cells (MYL) were treated with 100 µM pervanadate for 15 min, harvested and kinome isolated using MIBs. A SILAC-based comparison of MIB-bound kinases in the presence or absence of pervanadate was determined. E) Venn diagram shows number of kinases captured and identified by MIB-based proteomics across TNBC samples. F) Distribution and G) overlap of expressed and MIB-bound kinases across TNBC samples.

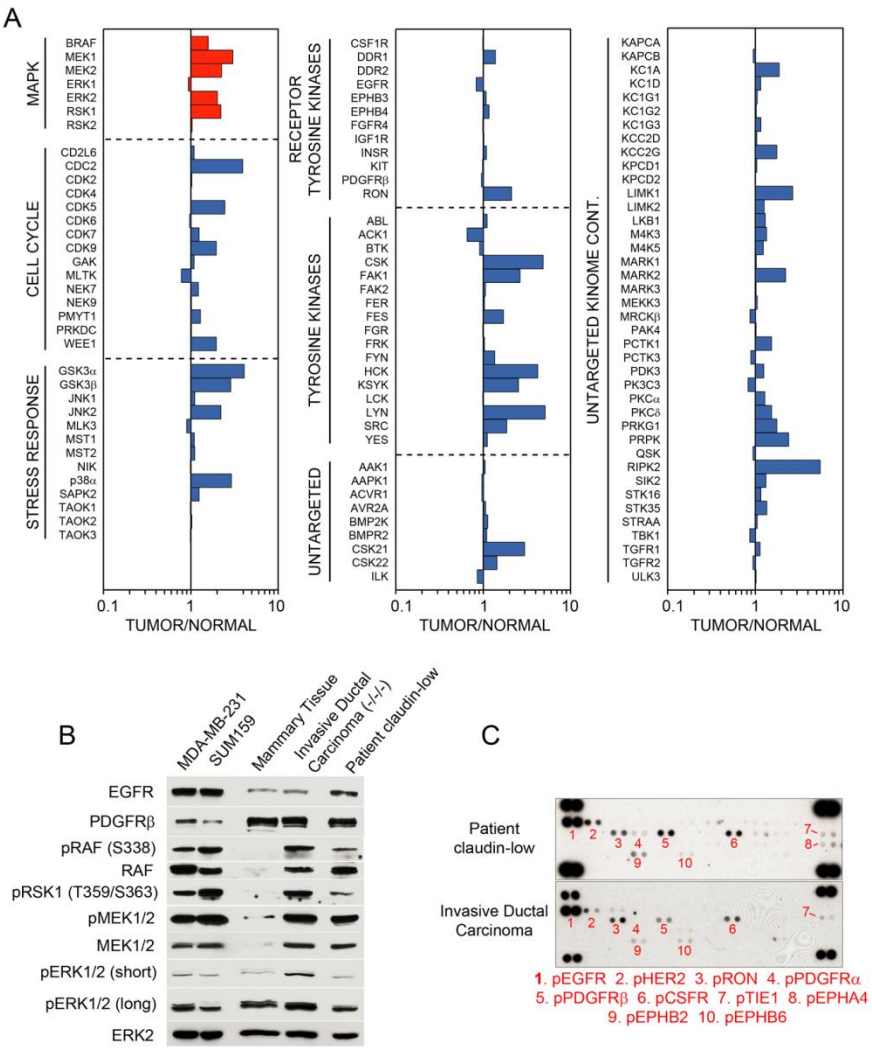

Figure 3.3 RAF-MEK-ERK pathway activation in TNBC. A) RAF-MEK-ERK pathway activated in patient TNBC tumors. Quantitative comparison of patient TNBC to matched uninvolved mammary tissue using MIB/MS. The line graphs show iTRAQ determined quantitative changes in MIB binding as a ratio of tumor/uninvolved. Ratio <1 denotes decreased MIB binding and >1 increased MIB binding of kinase in tumor versus control tissue. B) Immunoblotting confirms an activated RAF-MEK-ERK pathway in TNBC cell lines and TNBC patient samples. C) RTK array analysis of patient TNBC tumors reveals multiple Tyr phosphorylated RTKs, including EGFR and PDGFRβ.

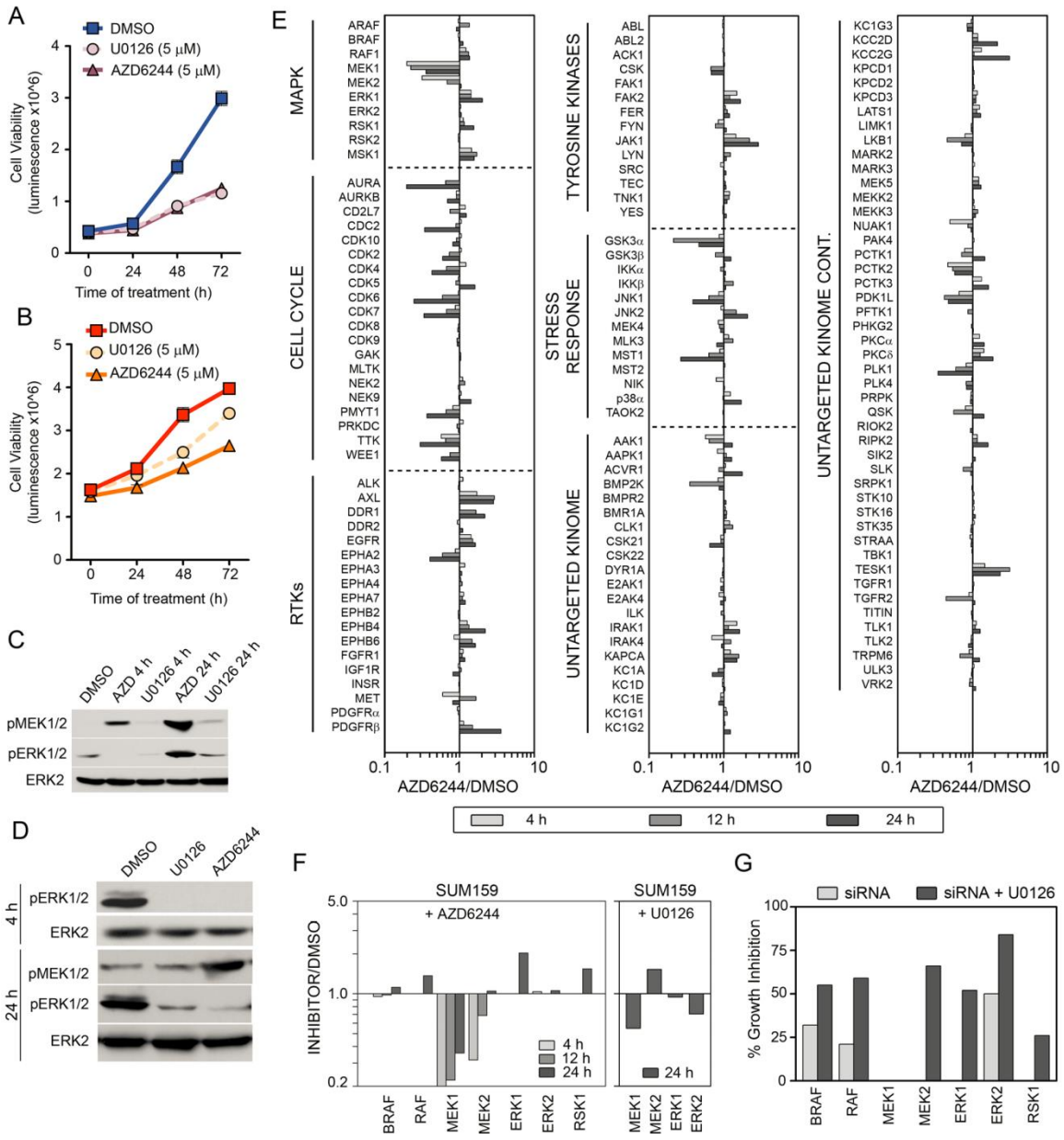

Figure 3.4 Profiling MEKi response in claudin-low TNBC. Growth inhibition of A) SUM159 and B) MDA-MB-231 cells in response to AZD6244 or U0126. Triplicate experiments ± SD. Reactivation of MEK and ERK in the continued presence of 5 μM AZD6244 was shown by western blot in C) SUM159 and D) MDA-MB-231 cells. E) Activation and repression of the kinome in response to 5 μM AZD6244 in SUM159 cells. Line graphs show iTRAQ-determined quantitative changes in MIB binding as a ratio of AZD6244/DMSO. Ratio <1 denotes decreased and >1 denotes increased MIB binding of kinases in treated versus control cells. F) MEK2 and ERK1 escape AZD6244 inhibition. MIB/MS binding profile of RAF-MEK-ERK from SUM159 cells treated with 5 μM AZD6244 for 4, 12 and 24h or 5 μM U0126 for 24h. G) MEK2 and ERK1 promote survival following MEK inhibition. siRNA knockdown of MAPK signaling components in SUM159 cells shows loss of MEK2, but not MEK1, inhibits growth in the presence of U0126.

Kinase	Site	AZD / DMSO	Description
BRAF	S151	0.1	phosphorylated by ERK1/2
BRAF	S365	0.5	phosphorylated by AKT
BRAF	T401	0.5	phosphorylated by ERK1/2
BRAF	S446	1.3	phosphorylated by PAK1
BRAF/RAF1	S465/S357	9.0	unknown
BRAF	T753	0.4	phosphorylated by ERK1/2
MEK1	T286	0.8	phosphorylated by ERK1/2
MEK1	T292	0.2	phosphorylated by ERK1/2
MEK1	S298	1.0	phosphorylated by PAK1
ERK1	T202/Y204	0.3	activation loop
ERK2	T185/Y187	0.2	activation loop
RSK1	S221	1.1	phosphorylated by PDK1
RSK1	S363	0.3	phosphorylated by ERK1/2
RSK1	S732	0.4	autophosphorylated by RSK1
RSK2	S227	0.9	phosphorylated by PDK1
RSK2	S715	0.5	unknown

Table 3.1 MIB-based phosphoproteomics of RAF-MEK-ERK pathway. Loss of ERK regulated feedback of the RAF-MEK-ERK pathway and downstream signaling. SUM159 cells were treated with 5 μM AZD6244 for 12h and kinome phosphorylation analyzed by MIB/MS.

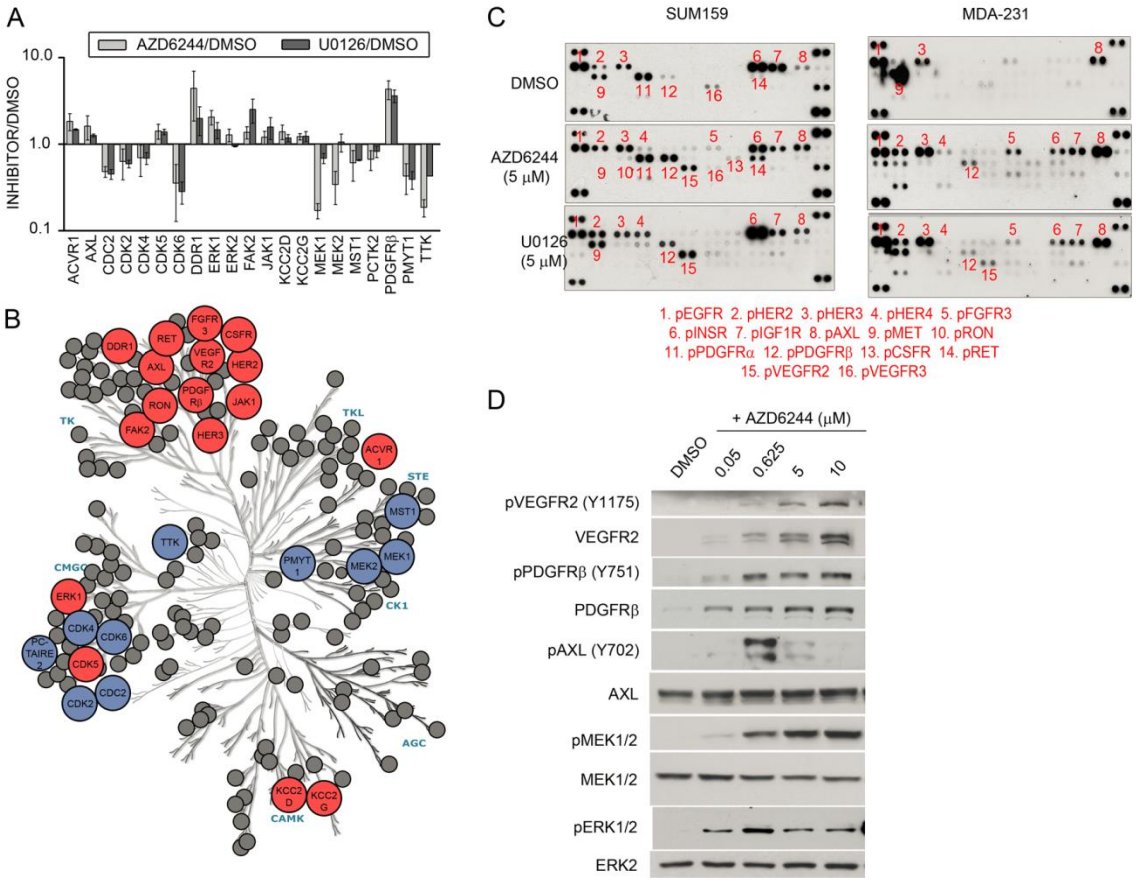

Figure 3.5 Defining a signature of kinome response to MEKi in claudin-low TNBC. A) Kinome response signature for MEK inhibition in SUM159 cells. Triplicate MIB/MS runs of SILAC-labeled SUM159 cells ± 5 μM AZD6244 or U0126 relative to DMSO. Error bars represent mean ± SD where kinases are significant at FDR of 0.05. B) Kinome map of AZD6244 response (blue: inhibited, red: induced) as determined by MIB/MS and RTK arrays. C) Increased tyrosine phosphorylation of RTKs in response to MEK inhibition. SUM159 and MDA-MB-231 cells were treated with 5 μM AZD6244 or U0126 for 24h and analyzed by RTK array. D) Dose-dependent RTK reprogramming in response to AZD6244. Dose-dependent induction of RTK expression and activity in 24h-treated SUM159 cells was determined by western blot.

KINASE	RPKM	KINASE	RPKM
WNK1	119	FYN*	60
AKT1*	93	CSK*	59
TIF1B	86	DYR1A	58
ATM	83	CD11B	55
FGFR2	81	STK25	54
KC1A	79	IRAK1	54
PDGFRα*	77	NRBP	54
ILK	75	SGK1	54
JAK1*	71	FAK2*	53
PDGFRβ*	71	PKCδ*	53
CLK1	70	KCPD2	53
CSF1R*	70	PRP4B	53
KC1D	67	ARBK1	52
ERK2*	65	CDK10	52
KC1E	64	MST1*	52
BRD4	64	JAK3	51
PTK7	63	PKN1	51
M4K4	62	MET*	50
HIPK3	61	KAPCA*	50
LIMK2	60	E2AK1*	50

Table 3.2 Top 40 kinases expressed in patient claudin-low tumor. RPKM values for each kinase determined by RNA-seq. *denotes AZD6244-responsive kinase in SUM159/MDA-MB-231 cell profiling.

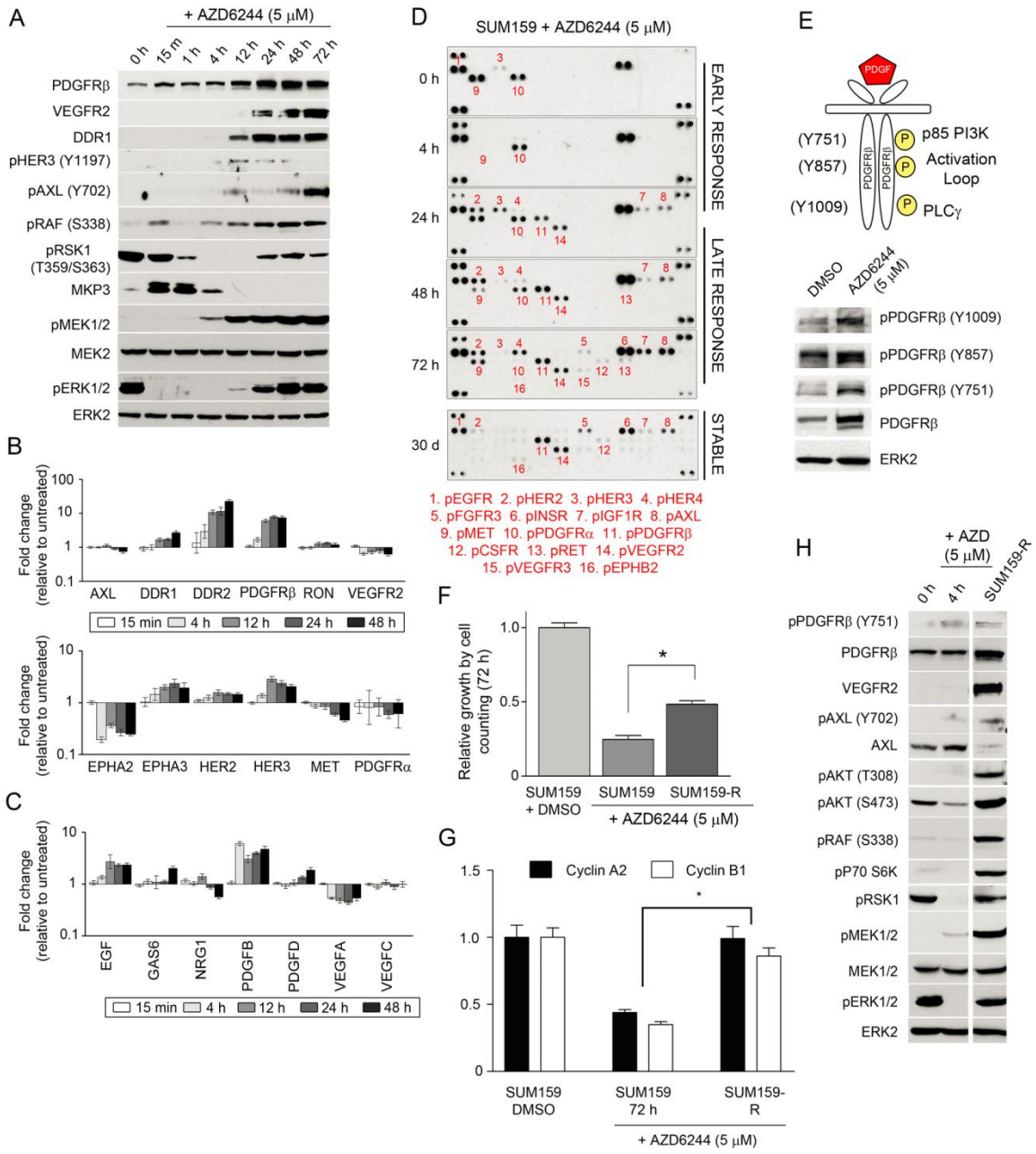

Figure 3.6 Characterization of CL RTK response. A) Western blot of long-term AZD6244 treatment in SUM159 cells. B) Time-dependent increase in RTK and C) cytokine expression in SUM159 cells after AZD6244 treatment, determined by qRT-PCR. D) Prolonged treatment of AZD6244 leads to stable upregulation of RTKs, as shown by RTK arrays. E) Treatment with AZD6244 enhances phosphorylation of PDGFRβ at multiple sites, including the activation loop. F) Increased cell growth of SUM159-R cells compared to SUM159 cells treated with AZD6244 for 72h determined by cell counts (*p-value<0.001). G) Return of cyclin expression in SUM159-R cells compared to SUM159 cells treated with AZD6244, as determined by qRT-PCR. H) Maintenance of RTK reprogramming in SUM159-R cells accompanied by increased survival signaling, as shown by western blot. Error bars represent triplicate ± S.D.

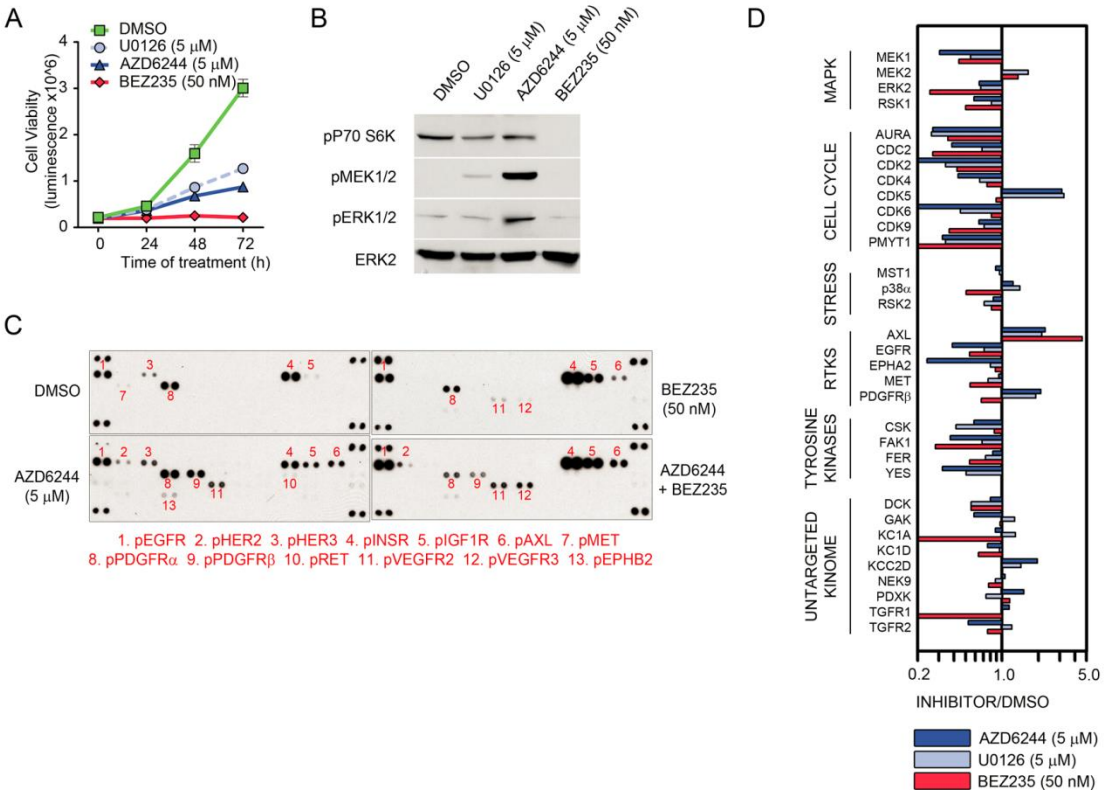

Figure 3.7 Induced kinases are target-specific to MEKi. A) SUM159 cells are growth inhibited by U0126 (5 μM), AZD6244 (5 μM), and BEZ235 (50 nM). B) BEZ235 inhibits p70 S6 kinase activity but not ERK1/2 signaling in SUM159 cells. C) AZD6244 and BEZ235 are target-specific in their reprogramming of kinome response. BEZ235 induces a kinase response different from AZD6244 in SUM159 cells, despite similar growth inhibition. D) Treatment of SUM159 cells with BEZ235 (50 nM) induces a distinct kinome response compared to AZD6244 or U0126 (5 μM), as determined by MIBs/MS using iTRAQ. Drug treatments are standardized to untreated SUM159 cells, and only kinases with statistically significant changes (pvalue<0.1) are shown. Error bars represent triplicate experiments ± SD.

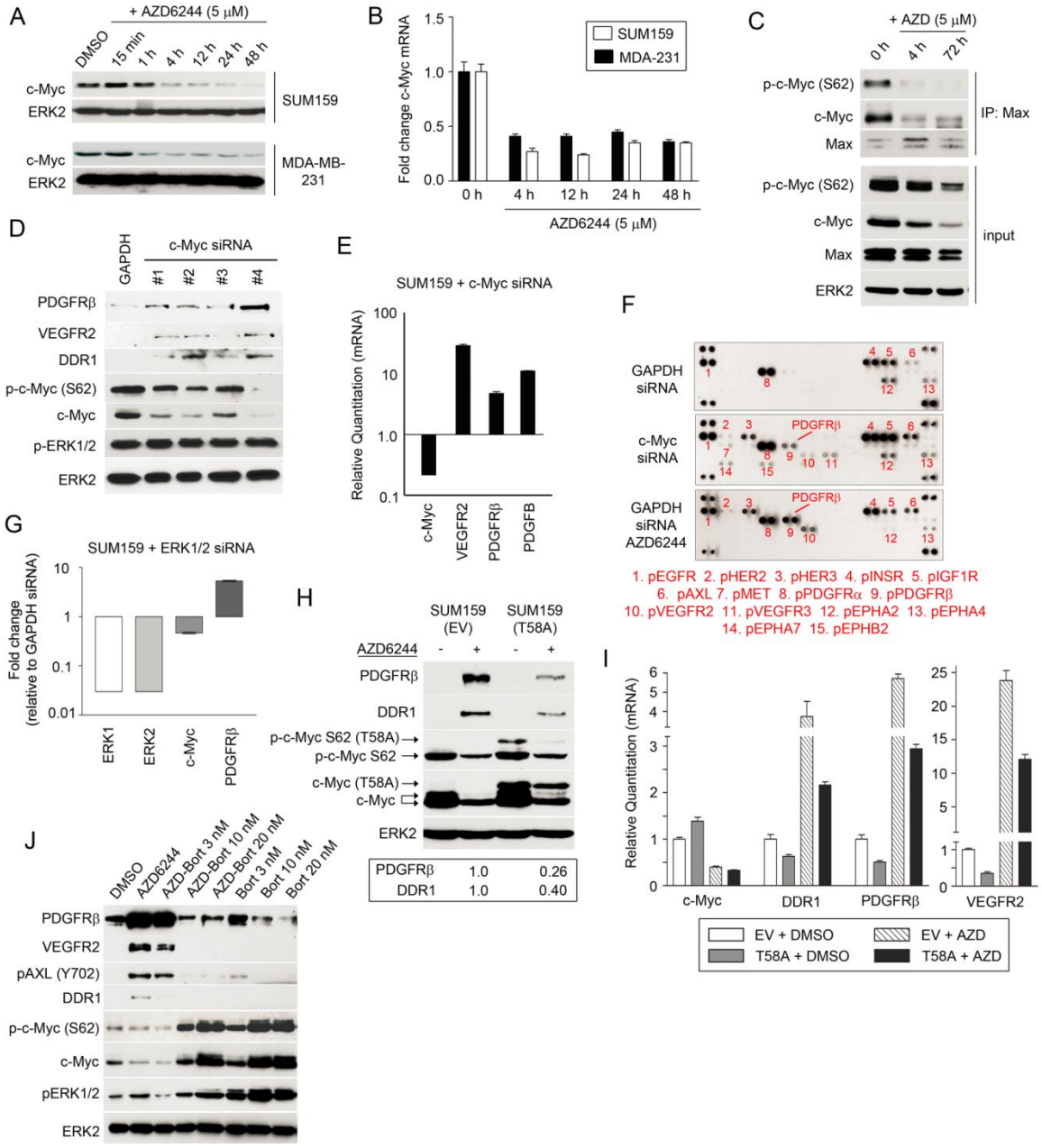

Figure 3.8 Defining mechanisms of MEKi response. Stable suppression of c-MYC A) protein and B) RNA after MEKi treatment. C) Disruption of MYC-MAX complexes after MEKi treatment. Knockdown of c-MYC with D) deconvolved or E) and F) pooled siRNA for 72h in SUM159 cells induced kinase expression and activity. G) siRNA-mediated knockdown of ERK1/2 suppresses c-MYC expression, inducing PDGFRβ transcript, as shown by qRT-PCR. H) Retroviral expression of c-MYC(T58A) in SUM159 cells suppresses RTK induction after 24h of 5 μM AZD6244, as shown by western blot and quantified by densitometry. I) DDR1, PDGFRβ and VEGFR2 transcripts are reduced by expression of c-MYC(T58A) in the presence and absence of 5 μM AZD6244. SUM159 cells were treated for 24h and analyzed by qRT-PCR. J) Stabilization of c-MYC protein levels by bortezomib prevents AZD6244-mediated kinome reprogramming. SUM159 cells were treated with AZD6244 (5 μM) or bortezomib alone or in combination for 24h.

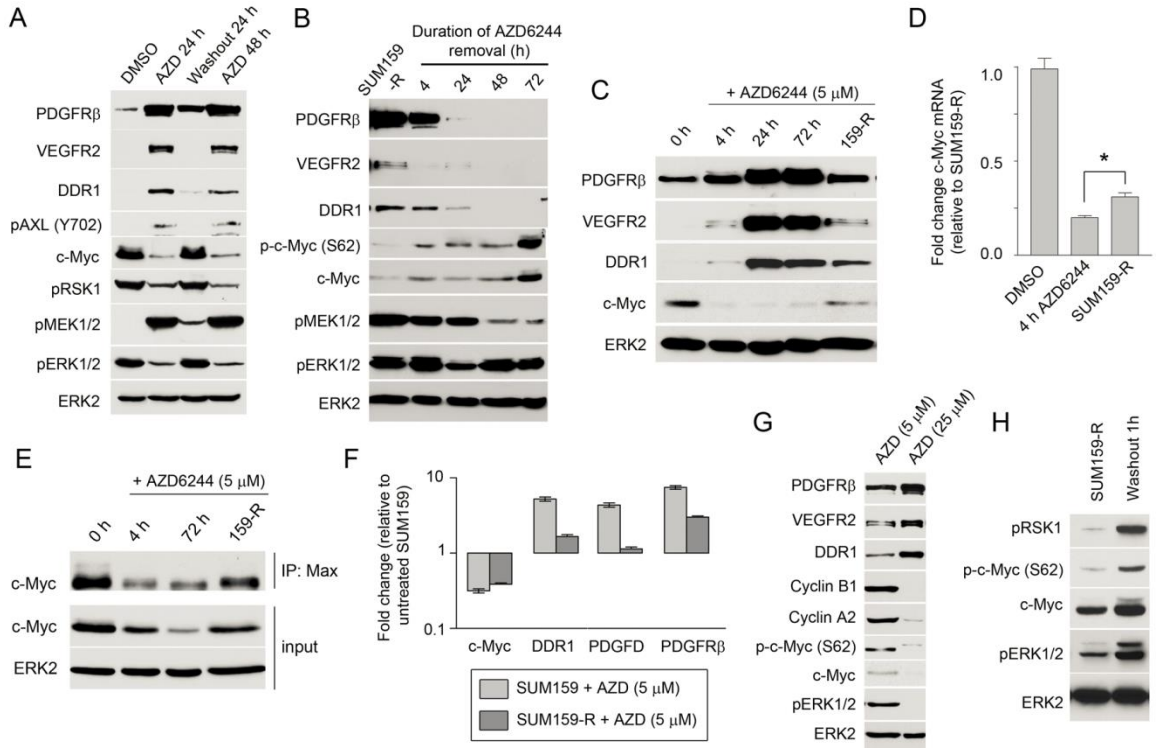

Figure 3.9 Effects of drug removal or prolonged treatment on c-MYC and RTK reprogramming. Removal of AZD6244 results in stabilization of c-MYC protein and reversal of RTK reprogramming. AZD6244 was removed from the media of A) SUM159 cells after 24h of treatment or B) SUM159-R cells. C) c-MYC protein levels partially return in SUM159-R cells, while AZD6244-mediated RTK reprogramming is reduced but still maintained. SUM159 cells were treated with AZD6244 and RTK and c-MYC levels compared to SUM159-R cells by western blot. D) Increased c-MYC RNA levels in SUM159-R cells relative to AZD6244 treated SUM159 cells. SUM159 cells were treated with DMSO or 5 μM AZD6244 for 4h and c-MYC gene expression compared to SUM159-R cells using qRT-PCR (*p-value<0.001). E) Recovery of c-MYC stability and MYC:MAX heterodimers in SUM159-R cells. MAX IP from SUM159 cells shows MYC:MAX heterodimerization is inhibited at 4h and 72h of 5 μM AZD6244 treatment, but not in SUM159-R cells. The recovery of c-MYC transcript and MYC:MAX heterodimerization in SUM159-R correlates to the partial suppression of RTKs in SUM159-R cells compared to SUM159 cells acutely treated with AZD6244. F) AZD6244-induced RTK expression is maintained at reduced levels in SUM159-R cells. qRT-PCR was used to compare gene expression in SUM159 cells treated with AZD6244 for 24h or SUM159-R cells relative to DMSO-treated cells. G) c-MYC stabilized by RTK-mediated ERK activation in SUM159-R cells. RTK reprogramming and c-MYC levels were determined by western blot comparing SUM159-R treated with AZD6244 for 24h. H) RTK-mediated reactivation of ERK is incomplete in the continued presence of AZD6244. AZD6244 (5 μM) was removed from media of SUM159-R cells for 1h and ERK1/2 phosphorylation of c-MYC and RSK1 determined by western blot.
Error bars represent triplicate experiments ± S.D.

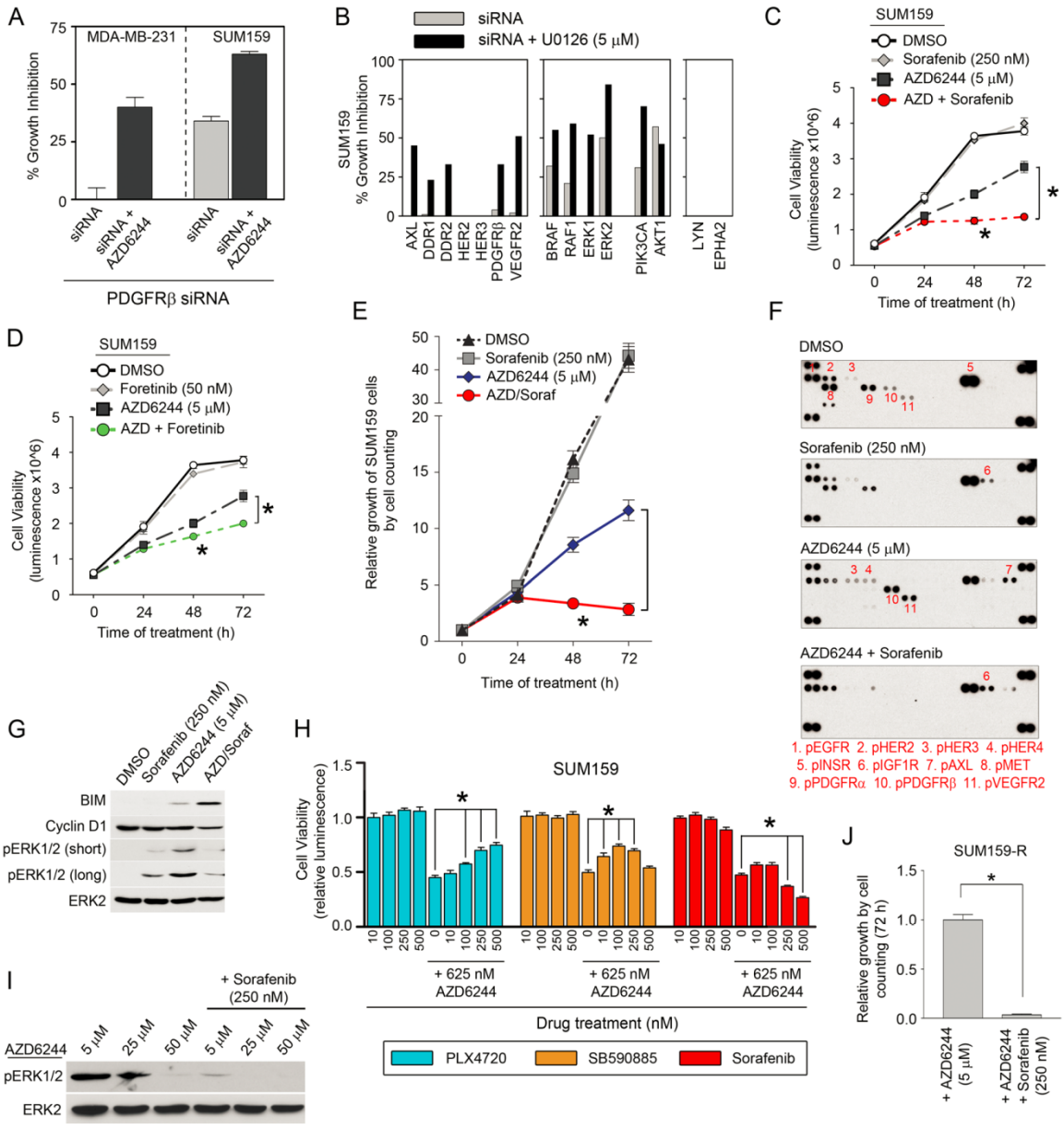

Figure 3.10 Targeting induced RTKs. A) RNAi knockdown of PDGFRβ enhances AZD6244-induced growth arrest. PDGFRβ knockdown with 1.25 μM AZD6244 in SUM159 cells for 96h and cell growth assayed by Cell-Titer Glo. B) Knockdown of MEKi-responsive RTKs in SUM159 cells synergizes with U0126 to inhibit proliferation, as determined at 96h of treatment by Cell-Titer Glo. Cotreatment with AZD6244 and C) sorafenib or D) foretinib synergizes in cell growth inhibition of SUM159 cells, as determined by Cell-Titer Glo. E) Cell counting of AZD6244/sorafenib treated SUM159 cells. F) Sorafenib inhibits AZD6244-mediated activation of RTKs, as shown by RTK arrays. G) Cotreatment of SUM159 cells with AZD6244/sorafenib enhances ERK inhibition and promotes apoptosis. H) AZD6244/sorafenib synergizes to inhibit SUM159 growth better than AZD6244 and targeted RAF inhibitors PLX4720 or SB590885. I) Inhibition of ERK activity in SUM159-R cells occurs after high dose MEKi or cotreatment of MEKi with sorafenib. J) SUM159-R cells require MEKi-induced RTK activity for drug resistance, as shown by cell counting.*p-value<0.001; Triplicate experiments ± S.D.

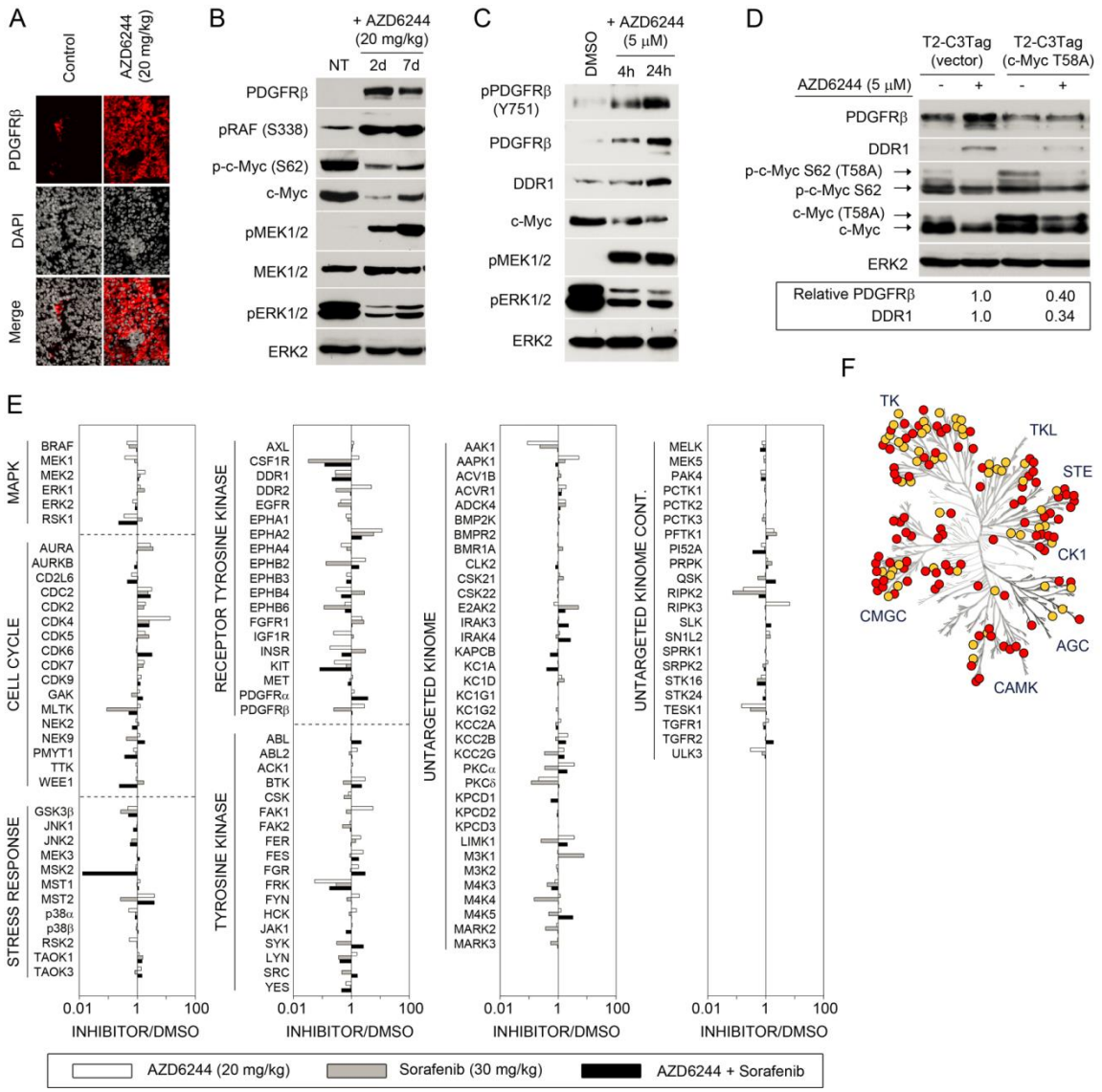

Figure 3.11 Kinome reprogramming in C3Tag GEMM. A) PDGFRβ is induced in C3Tag tumors after 2d AZD6244 treatment, as shown by immunofluorescence. B) AZD6244 treatment of C3Tag mice for 2 and 7d causes c-MYC degradation and induced PDGFRβ expression, as shown by western blot. C) Tumor-derived C3Tag cell line shows AZD6244-mediated c-MYC loss and RTK induction. T2-C3Tag cells were treated with AZD6244 and RTK reprogramming determined by western blot. D) Expression of c-MYC(T58A) in T2-C3Tag cells suppresses AZD6244-mediated RTK reprogramming. T2-C3Tag cells stably expressing vector or human c-MYC(T58A) were treated with AZD6244 for 24h and analyzed by western blot. E) MIB/MS profile of C3Tag tumors in response to AZD6244 for 28d, sorafenib for 26d, or combined AZD6244 and sorafenib for 26d show distinct kinome responses. The line graphs show iTRAQ-determined quantitative changes in MIB binding as a ratio of inhibitor/untreated. Ratio <1 denotes decreased MIB binding and >1 increased MIB binding of kinases in treated versus control tumors. F) AZD6244 plus sorafenib inhibits AZD6244-induced kinome response in C3Tag tumors, as identified by MIB/MS. Changes in MIB binding (>1.5 fold) of AZD6244-responsive kinases following cotreatment with sorafenib are shown in yellow.

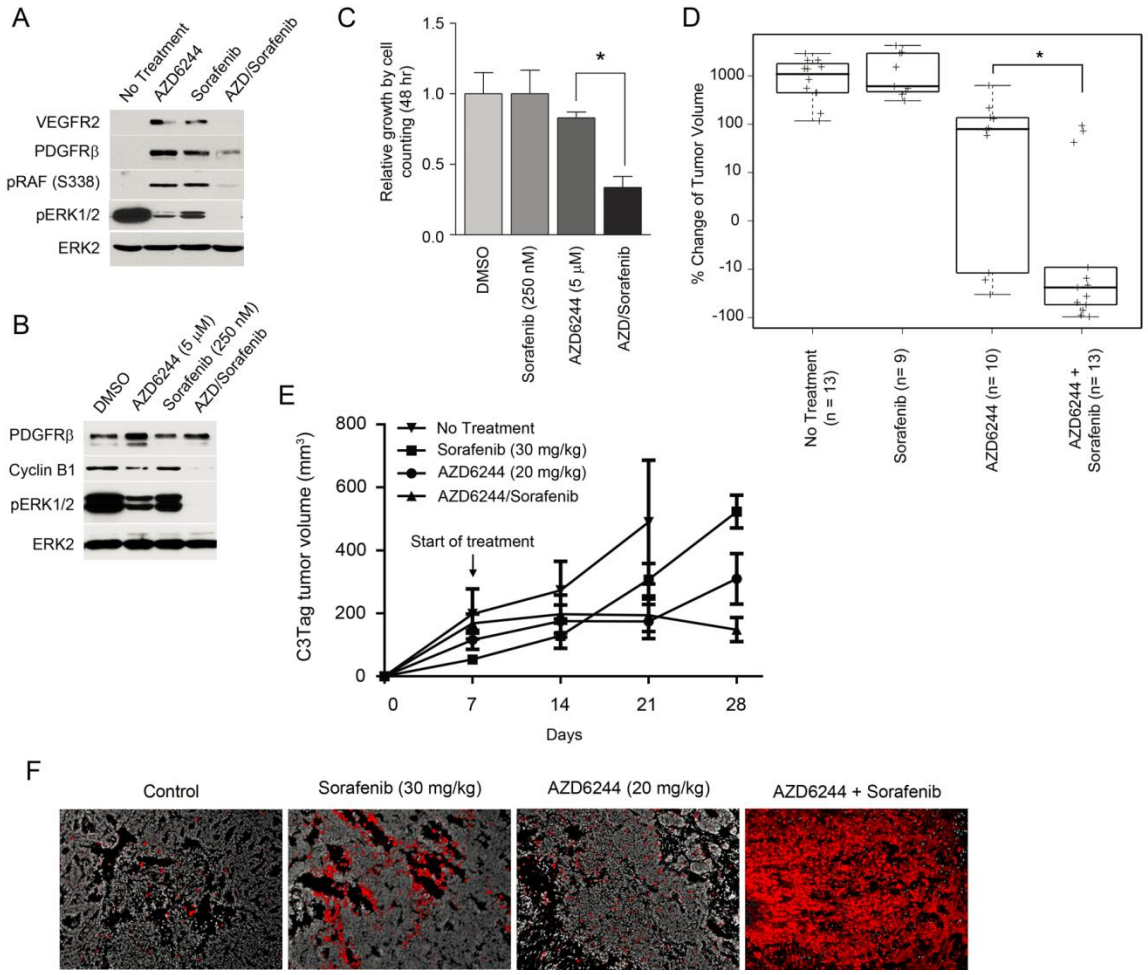

Figure 3.12 AZD6244/sorafenib combination produces synergistic effects in C3Tag mice. A) AZD6244 (20 mg/kg) or sorafenib (30 mg/kg) fed in chow results in ERK activation after 2d of treatment in C3Tag GEMM, while cotreatment with AZD6244 and sorafenib inhibits RTK-mediated ERK activation. RTK reprogramming was monitored in tumors treated with AZD6244 and/or sorafenib relative to untreated tumors by western blot. B) Sorafenib inhibits AZD6244-dependent reactivation of ERK, promoting c-MYC degradation and loss of cyclin B1 expression in T2-C3Tag cells. T2-C3Tag cells were treated for 24h and analyzed by western blot. C) AZD6244 and sorafenib synergize to inhibit cell growth in C3Tag cell line. T2-C3Tag cells were treated with AZD6244 and sorafenib, alone or in combination, and cell growth determined by cell counting (*p-value<0.001; quadruplicate experiments). D) Cotreatment of C3Tag mice with AZD6244 and sorafenib for 21d causes significant tumor regression compared to AZD6244 alone. C3Tag mice were treated with AZD6244 (20 mg/kg), sorafenib (30 mg/kg) or the combination of AZD6244 and sorafenib and compared to untreated tumors. Percent change in tumor volume of drug treated relative to untreated is shown (* Wilcoxon p-value=0.007). E) Tumor volumes of C3Tag breast tumors during a 21d time course of AZD6244 and/or sorafenib treatment. F) Increased apoptosis of C3Tag mouse tumors following cotreatment with AZD6244 and sorafenib. Apoptosis in C3Tag tumors treated for 2d was determined by TUNEL staining (shown in red; DAPI is grayscale).

IV. INVESTIGATING RESISTANCE TO EGFR/HER2 INHIBITION IN BASAL-LIKE AND OTHER BREAST CANCER SUBTYPES

Introduction

The epidermal growth factor receptor (EGFR) has recently emerged as another potential therapeutic target in TNBC[147]. Multiple groups report EGFR to be overexpressed in a significant proportion (40-70%) of basal-like or triple-negative breast cancers, and this high expression of EGFR has been linked by multivariate analysis of patient TNBCs to poorer prognosis for disease-free and overall survival[148,149]. These findings implicate EGFR as contributing to tumor growth and resiliency in EGFR-expressing TNBCs. However, phase II and III clinical trials combining chemotherapeutics with EGFR-targeting agents (i.e. cetuximab or lapatinib) show no improvement in progression-free or overall survival of TNBC patients by the addition of these EGFR inhibitors[138,150]. A possible explanation for this paradox is that targeted inhibition of EGFR in TNBC causes cancer cells to compensate for the loss of EGFR by the upregulation of parallel growth signaling pathways. Indeed, multiple studies have linked EGFR inhibitor resistance in TNBC to the rapid induction of alternative RTKs or SFKs[78,151].

We have previously shown that treating claudin-low TNBC cells with targeted MEKi initiates a rapid reprogramming of the kinome to drive drug resistance. This effect was shown to be target-selective with distinct kinome reprogramming events occurring after MEK1/2 or PI3K/mTOR inhibition, suggesting that EGFR inhibition with lapatinib may induce a unique kinome response. To test this, we applied our MIB/MS strategy

towards defining how breast cancer cells respond to targeted EGFR/HER2 inhibition for basal-like, claudin-low, and HER2-amplified subtypes. Interestingly, a significant disparity in baseline levels of activated EGFR was observed between the two TNBC subtypes, with basal-like cell lines having much higher phosphorylated EGFR than claudin-low cells. The presence of phosphorylated EGFR in patient tumors and basal-like cell lines validates EGFR as a target in basal-like (but not claudin-low) breast cancer. However, the inability of lapatinib to strongly inhibit basal-like cancer cell growth and growth signaling pathways suggests that mechanisms of intrinsic and/or adaptive resistance protect basal-like TNBC cells from EGFR inhibition. Inhibition of EGFR/HER2 with lapatinib caused a robust RTK reprogramming in basal-like and HER2-amplified cell lines, but a minimal response in claudin-low cell lines lacking EGFR phosphorylation. Loss of downstream signaling after EGFR inhibition was shown to cause RTK induction in HCC1806 cells, with reduced activity of ERK and AKT contributing independently to the overall reprogramming. EGFR inhibition was not sufficient to completely inhibit ERK or AKT pathway activation, possibly due to compensatory preexisting or induced RTKs, suggesting that combination therapies will be necessary for inhibiting cell growth. Small molecule inhibitor combinations targeting EGFR and induced RTKs were tested in multiple basal-like cell lines, yielding synergistic growth inhibition.

These data define another unique instance of kinome reprogramming in breast cancer, highlighting the importance of considering kinome adaptation to any targeted kinase inhibitor. Interestingly, while EGFR inhibition provides a distinct strategy to target basal-like TNBC, the downstream inhibition of ERK was the greatest contributor to the transcriptional component of kinome reprogramming, suggesting that any TKI causing ERK inhibition will similarly circumvent growth inhibition through induction of alternative RTKs. The demonstrated benefit of kinase inhibitor combinations that target induced kinases further supports the notion that single-agent kinase inhibitor strategies will

ultimately fail.

Results

Defining EGFR expression and activity in TNBC

The failure of targeting EGFR in TNBC clinical trials, despite high EGFR expression and correlation with poor prognosis, led us to investigate possible causes of insensitivity to EGFR inhibitors in basal-like and claudin-low TNBC. Efforts to target EGFR in TNBC are largely based upon gene expression analysis showing elevated EGFR expression, which may be independent of EGFR activity. To address this, we first probed TNBC patient samples for EGFR phosphorylation to determine whether TNBCs exhibit activated EGFR (Figure 4.1A). Tyrosine phosphorylation at three sites, including two major autophosphorylation sites (Y1068 and Y1173) was observed with varying intensity across seven basal-like TNBC patient tumors, suggesting that EGFR is actively signaling in these tumors. To validate TNBC cell lines as models for studying EGFR inhibition, we blotted a panel of basal-like and claudin-low TNBC cell lines for total and phospho-EGFR. While EGFR expression was fairly consistent between claudin-low and basal-like cell lines, phosphorylated EGFR was found exclusively in basal-like lines (Figure 4.1B). This unexpected result highlights the disparity between expression and activity, a pitfall of gene expression analysis, and reveals subtype-specific EGFR signaling in TNBC. While basal-like TNBC may benefit from EGFR inhibition, it is clear that claudin-low TNBC lacks EGFR activity (despite elevated EGFR expression) and is likely intrinsically resistant to EGFR-targeted therapies. Differential EGFR phosphorylation in non-tumorigenic RMF (mesenchymal, similar to claudin-low) and HuMEC (epithelial, similar to basal-like) cell lines suggest that EGFR activation may depend largely on the differentiation state of the cell.

Treatment of a panel of basal-like and claudin-low cell lines with the EGFR/HER2

inhibitor lapatinib resulted in little to no growth inhibition, whereas HER2-amplified SKBR3 cells were strongly inhibited (Figure 4.1C). Treatment with an alternative EGFR inhibitor, erlotinib, showed a similar lack of efficacy in claudin-low and basal-like cell lines (data not shown). Similarly, lapatinib treatment only partially affected ERK and AKT signaling in basal-like cell lines, whereas downstream signaling was strongly inhibited in SKBR3 cells and unaffected in claudin-low lines (Figure 4.1D). Claudin-low cells were not expected to respond due to the lack of active EGFR, but the insensitivity of basal-like cell lines suggests that these cells are able to evade growth inhibition after loss of activated EGFR.

MIB/MS defines kinome response to EGFR inhibition

In order to define possible mechanisms of resistance to EGFR inhibition, we applied MIB/MS to measure the kinome response to lapatinib in basal-like, claudin-low, and HER2+ cell lines (Figure 4.2A). Two cell lines from each subtype were analyzed, yielding over 260 kinases across the six cell lines. Though inhibition of EGFR and HER2 was evident whenever these kinases were quantified, induction of distinct kinase signatures was observed in each case. HER2+ cell lines responded robustly, with activation of DDR1, FRK, MYLK3, NEK9, and YES in SKBR3 cells and CDK9, CSK, FRK, INSR, LYN, and YES in BT474 cells (FDR cutoff at 0.05). Though most of these are not known to be involved in HER2-inhibitor resistance, SRC-family kinases such as FRK, LYN, and YES have been shown to confer resistance in this setting, confirming the MIB/MS strategy as a method to define resistance mechanisms[78,152]. Claudin-low cell lines were not expected to exhibit a kinome response, and this was the case with MDA-MB-231 cells where no kinases were induced at an FDR of 0.05. Interestingly, induction of ABL1, EPHB4, EPHA2 and KS6A1 was observed in response to lapatinib in SUM159 cells. This may be a result of inhibition of low-level EGFR activity or off-target effects of

lapatinib. Basal-like HCC1806 cells responded robustly to EGFR inhibition, exhibiting activated DDR1, FGFR2, KIT, and MET after lapatinib treatment. Induced expression/activity of these kinases was confirmed by western blotting of a time course and dose-response of lapatinib treatment in HCC1806 (Figure 4.2B,C). The time course of EGFR inhibition shows an initial loss of downstream ERK signaling that returns coincidentally with increased RTK expression. The RTK induction, with the exception of pMET, was sustained after 30 day treatment with lapatinib (HCC1806-R) and phosphorylated ERK neared untreated levels (Figure 4.2D). In contrast, SUM229 cells were unresponsive to lapatinib treatment, with no induced RTKs and only a very transient loss of ERK and AKT signaling (data not shown). However, these cells are known to have abundant and highly activated MET, which may be contributing to an intrinsic immunity to EGFR inhibition in these cells[151].

Mechanisms of reprogramming to EGFR inhibition

To determine whether kinome reprogramming to lapatinib in HCC1806 was occurring at the mRNA level, RNA-seq was used to define transcriptional changes following EGFR inhibition. From more than 20,000 genes sequenced, 1437 genes exhibited a >1.5-fold change in expression, with 79 kinases significantly altered (Figure 4.3A). In concordance with the MIB/MS data, expression levels of DDR1, KIT, and FGFR2 were substantially increased by lapatinib treatment (Figure 4.3B), as well as other kinases not well represented by MIB/MS (including FGFR3, HER2, CIT, RIPK4). Expression of MET was not increased, consistent with MET induction occurring at the level of kinase activation rather than induced expression. Interestingly, expression of MET ligand HGF was low and unresponsive to lapatinib treatment, indicating MET activation may occur through a ligand-independent mechanism. While treatment of HCC1806 with lapatinib caused a transcriptional induction of DDR1, FGFR2, and KIT,

EGF treatment reduced expression of these RTKs and attenuated RTK induction by lapatinib (Figure 4.3C). These data suggest that the RTK reprogramming to EGFR inhibition results from changes to signaling pathways downstream of EGFR affecting transcription factor activity. Because lapatinib treatment prevents EGFR-mediated signaling through the ERK and AKT pathways, targeted MEK1/2 and AKT inhibitors were used to define the relative contributions of these pathways to RTK reprogramming. Whereas inhibition of MEK1/2 with AZD6244 caused induction of KIT, DDR1 and FGFR2, AKT inhibitor MK2206 strongly activated MET (Figure 4.3D). Thus, the RTK reprogramming observed after EGFR inhibition likely results from loss of signaling through both ERK and AKT.

ERK and AKT act upon numerous transcription factors to affect gene transcription, often regulating protein levels of transcription factor substrates through phosphorylation. We have previously shown that RTK reprogramming to MEK inhibition in claudin-low TNBC occurs through loss of negative gene regulation from the transcription factor c-MYC. In an effort to define transcription factors downstream of ERK and AKT that are directly responsible for RTK reprogramming in HCC1806, proteasomal inhibition was used to determine whether stabilizing high-turnover proteins affects the reprogramming response to lapatinib. Inhibition of the proteasome with bortezomib attenuated lapatinib induction of DDR1, FGFR2 and KIT, but did not affect pMET induction (Figure 4.3E). These data are consistent with ERK acting on one or more transcription factors that negatively regulate DDR1, FGFR2, and KIT expression. To provide some insight into which transcription factors may be responsible for RTK induction, the RNA-seq data was analyzed for alterations in transcription factor expression following lapatinib treatment (Figure 4.3F). More than 60 transcription factors were reduced in expression >1.5-fold due to lapatinib, with some known to be downstream of ERK, including c-MYC, FOSL1, ETV4 and ETV5. The transcriptional

regulation of the induced RTKs is largely unknown, so these ERK-regulated transcription factors were tested as candidate mediators of RTK reprogramming. Unfortunately, no induction of RTKs was observed when these kinases were knocked down by siRNA to mimic their loss following EGFR inhibition (Figure 4.3G,H). While the loss of the transcription factors undoubtedly causes significant changes to cell composition and signaling, they do not appear to be mediating RTK induction. The use of expression data may be misleading to the search for transcription factors responsible for RTK reprogramming, as the bortezomib data indicates protein stabilization to be a greater factor. Additionally, more than one transcription factor could regulate RTK reprogramming, and loss of a combination of transcription factors may be necessary for the induced RTK expression.

Targeting lapatinib-induced RTKs

Having defined a core set of RTKs induced by EGFR inhibition in HCC1806 cells, our next goal was to determine whether these RTKs were contributing to growth and survival during lapatinib treatment. Knockdown of individual RTKs in the presence of lapatinib was used to define the contributions of each induced RTK towards preserving ERK phosphorylation after lapatinib treatment (Figure 4.4A). For each RTK knockdown, residual ERK activity was lost to varying degrees, indicating that all induced RTKs provide compensatory signaling through ERK. DDR1 knockdown caused the least ERK loss in the presence of lapatinib, while MET knockdown contributed the most. MET was also the only kinase whose knockdown reduced ERK activity in the absence of lapatinib, suggesting that this is an important growth-promoting RTK in HCC1806 cells. Simultaneous knockdown of all induced RTKs caused the greatest suppression of phosphorylated ERK, to 7% of wildtype levels, indicating that the induced RTKs work in concert to preserve ERK signaling after EGFR inhibition. Consistent with RTK

knockdown reducing ERK phosphorylation, RTK stimulation with cytokines for FGFR2, KIT, or MET enhanced pERK levels under serum-starved and lapatinib-treated conditions in HCC1806-R cells (Figure 4.4B). These experiments confirmed that lapatinib-induced RTKs are important in the survival response to EGFR inhibition, suggesting that combination therapies targeting DDR1, FGFR2, KIT and MET would provide a greater benefit than EGFR inhibition alone.

Four TKIs with distinct targeting profiles were tested for growth inhibition in combination with lapatinib in HCC1806 cells. Foretinib and cabozantinib strongly inhibit MET and KIT, while BGJ398 is specific for FGF receptors and dasatinib is a broader-acting TKI that inhibits DDR1 and KIT. Combination of lapatinib with each of these compounds helped to suppress residual EGFR and ERK phosphorylation in HCC1806 cells (Figure 4.4C). Additionally, cyclin B1 levels were lowered by the drug combinations, suggesting a greater arrest of the cell cycle. Growth assays revealed that lapatinib combinations with foretinib, cabozantinib, BGJ398 or dasatinib synergistically inhibited the growth of HCC1806 cells (Figure 4.4D). SUM229 cell growth was similarly inhibited with lapatinib and MET-targeted inhibitors, validating the importance of activated MET in the intrinsic resistance of this cell line to EGFR inhibition (data not shown). The combination of lapatinib with sorafenib or imatinib, TKIs with targeting profiles not expected to inhibit induced RTKs, produced no additive or synergistic growth inhibition, consistent with induced RTKs selectively driving growth in lapatinib-treated HCC1806 (Figure 4.4E). Importantly, cotreatment of lapatinib with downstream inhibitors to MEK (AZD6244) or AKT (MK2206) matched the benefit of targeting EGFR and induced RTKs, and the AZD6244/MK2206 combination provided a strong growth inhibition in these cells. Taken together, these data suggest that the failure of lapatinib to fully inhibit signaling through ERK and AKT is one reason why HCC1806 cells are not strongly inhibited by EGFR inhibition. Residual ERK and AKT can be inhibited by either

1) targeting induced RTKs that compensate for EGFR loss, or 2) targeting the conserved downstream signaling pathways directly.

Discussion

As a whole, these studies confirm EGFR as a target in basal-like TNBC, identify RTKs induced by EGFR inhibition, and define those RTKs contributing to growth/survival after EGFR inhibitor treatment. An important distinction between TNBC subtypes is made by the discovery of activated EGFR only in basal-like TNBC, despite similar expression levels of EGFR and associated cytokines. The mechanism(s) behind this disparity in EGFR activity remain unclear, however it is known that expression of E-cadherin and increased cell-cell interaction, hallmarks of the epithelial phenotype, can potentiate activation of EGFR[153]. E-cadherin expression has also been linked to gefitinib sensitivity in lung cancer, suggesting that E-cadherin may serve as a biomarker for EGFR activity and susceptibility to EGFR-targeted therapies[154]. Conversely, EMT and loss of E-cadherin expression is proposed to be a mechanism of resistance to EGFR-targeted therapies in lung cancer[155,156]. In light of these studies, the striking dichotomy of EGFR activity suggests the need to stratify patient populations when developing EGFR-targeted therapies in the context of triple-negative breast cancer. Even with careful selection of patients harboring basal-like TNBC, EGFR-inhibitor resistance through EMT, kinome reprogramming, or intrinsic resistance by pre-existing RTK activity are likely to occur. Thus, it is extremely important to understand how basal-like TNBC cells respond to EGFR-targeted therapies in order to anticipate and prevent the onset of resistance.

We have previously defined a signature of kinome reprogramming to MEKi in claudin-low TNBC, with induced expression/activity of PDGFRβ, VEGFR2, DDR1, DDR2 and AXL. Interestingly, the basal-like HCC1806 cell line responds to EGFR inhibitors (through loss of MEK/ERK signaling) with KIT, FGFR2 and DDR1 induction, suggesting

that basal-like TNBC may exhibit a distinct kinome response to MEKi. Though MEKi and EGFR inhibitors target very different kinases, both result is loss of signaling through ERK1/2, leading to the RTK reprogramming response. Any other inhibitors leading to loss of ERK activity would therefore be expected to produce a similar reprogramming response in this context, and likewise, direct or indirect inhibition of AKT would similarly cause activation of MET in these cells. These results impart a global connotation to kinome reprogramming because most therapeutic strategies aim to inhibit growth signaling through the ERK and/or AKT pathways.

The data presented here suggest that targeting either inhibitor-induced RTKs or downstream signaling helps to suppress cell proliferation after EGFR inhibitor treatment. However, without direct inhibition of ERK and/or AKT, there is a very high likelihood that cancer cells will be able to easily surmount targeted inhibition of RTKs through activation of alternative RTKs. The pre-existence of activated MET, as in SUM229 cells, or other RTKs appears to be sufficient to make basal-like TNBC cells completely unresponsive to lapatinib treatment, regardless of baseline EGFR activity. Thus, the high specificity of lapatinib (or other EGFR/HER2 inhibitors) may actually hinder its efficacy for treating TNBC and broader-acting TKIs may preclude some of the RTK redundancy and reprogramming in TNBC cells. In any case, it will be difficult to comprehensively define pre-existing or induced RTK signaling for individual patients, complicating the rational design of combination therapies using TKIs. In contrast, we know that targeting only downstream kinases such as ERK or AKT directly leads to kinome reprogramming and potentiation of upstream signaling. Therefore is seems likely that targeting multiple nodes of growth signaling pathways, as well as inhibitor-induced kinases, will be the best strategy for sustained growth inhibition.

Taken together, these data highlight the resiliency of the kinome against targeted TKIs and reinforce the prevalence of kinome reprogramming as a mechanism of

resistance to kinase inhibitors. Further investigations into subtype-specific kinome reprogramming and alternative strategies to surmount kinome resiliency will help to clarify better therapeutic strategies for TNBC treatment.

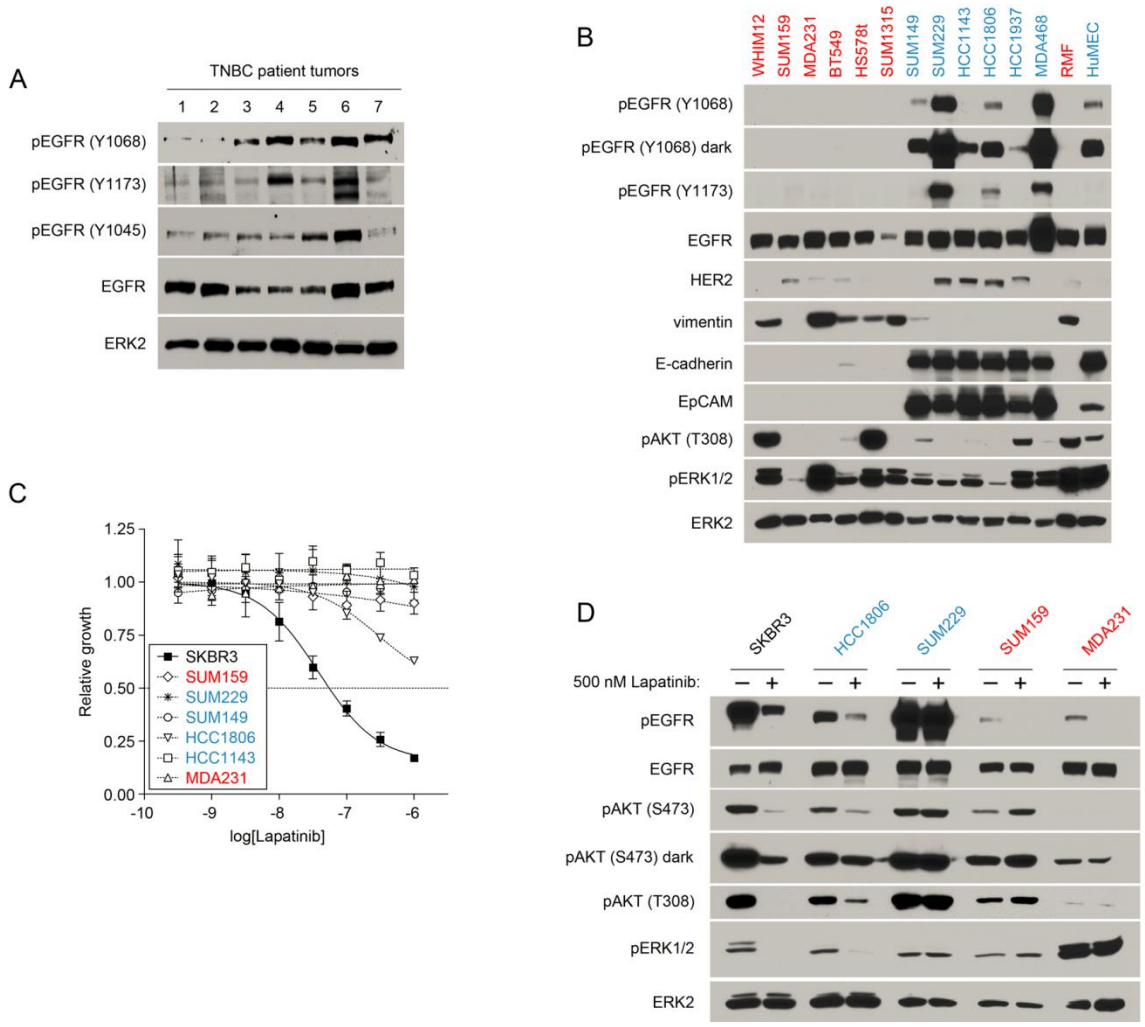

Figure 4.1 Characterization of pEGFR in TNBC. A) Phosphorylated EGFR is observed in TNBC patient tumor samples. B) Basal-like cell lines (shown in blue) exhibit much higher phosphorylated EGFR compared to claudin-low cell lines (shown in red). C) Basal-like and claudin-low cell lines are not growth-inhibited by treatment with lapatinib, whereas HER2-amplified SKBR3 cells are strongly inhibited. D) Inhibition of EGFR does not necessarily lead to loss of downstream signaling through ERK or AKT.

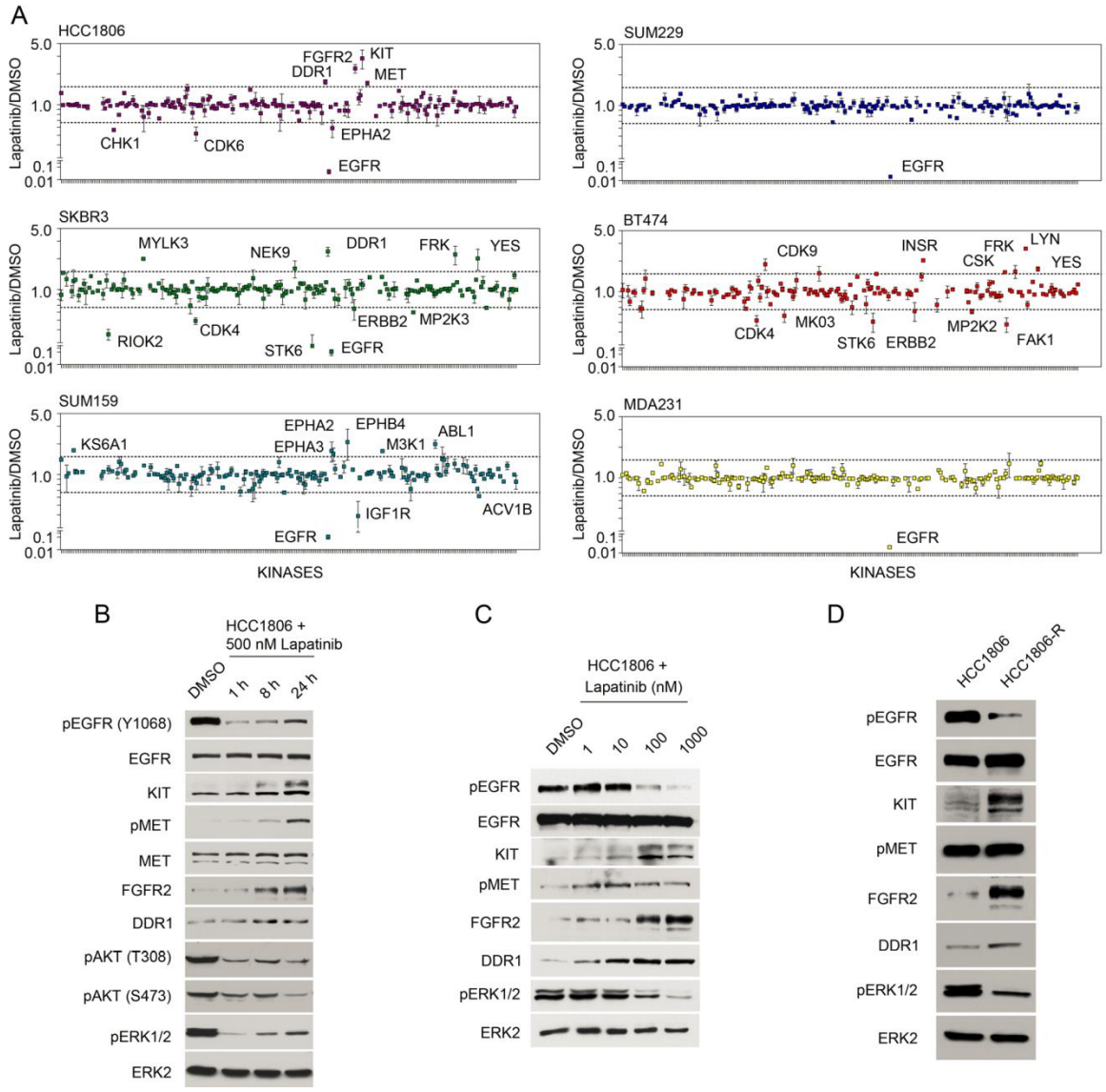

Figure 4.2 MIB/MS defines kinome response to EGFR inhibition. A) EGFR/HER2 inhibition induces distinct kinome reprogramming events in basal-like, HER2+ and claudin-low cell lines. Triplicate MIBs/MS experiments were used to define the 24h lapatinib-responsive kinases in two cell lines from each subtype. B) The timecourse of EGFR inhibition and RTK response in HCC1806 cells was defined by western blot. C) Lapatinib-induced RTKs in HCC1806 are largely dose-responsive, as shown by western blot. D) Lapatinib-resistant HCC806 cells exhibit sustained RTK response after 30 day lapatinib treatment.

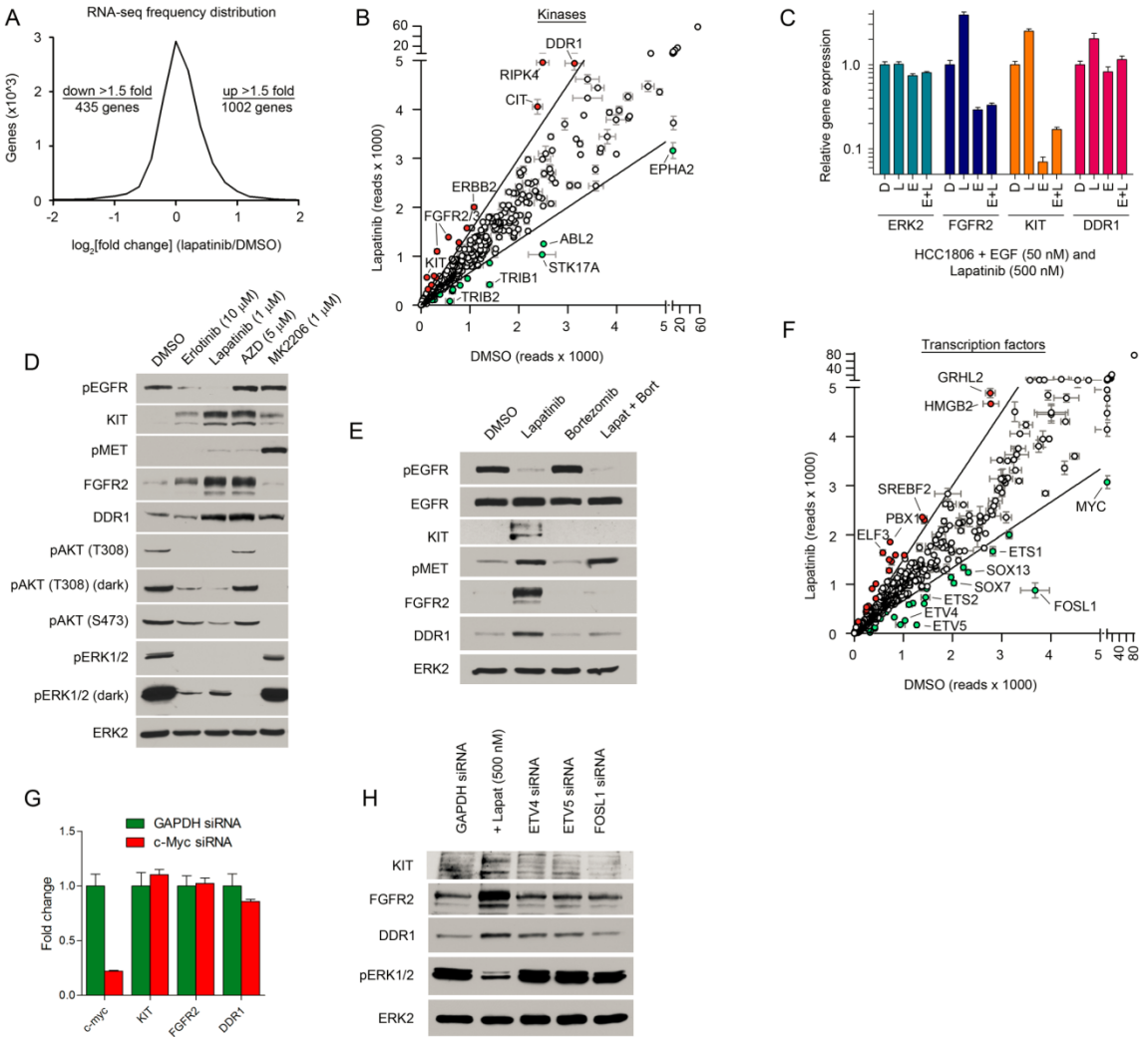

Figure 4.3 Investigating mechanisms of kinome reprogramming in HCC1806. A) Summary of genes transcriptionally altered by lapatinib treatment in HCC1806 cells. B) Transcriptional changes for kinases in HCC1806 cells after lapatinib treatment. Two replicate RNA-seq experiments were performed. Lines represent 1.5-fold change in expression between lapatinib and DMSO. C) qRT-PCR of responsive RTKs with lapatinib and/or EGF treatment in HCC1806 cells. D) Western blot of HCC1806 cells treated with inhibitors targeting EGFR and downstream signaling pathways. E) Western blots showing effect of proteasomal inhibition on RTK induction. F) Transcriptional changes for transcription factors in HCC1806 cells after lapatinib treatment. Two replicate RNA-seq experiments were performed. Lines represent 1.5-fold change in expression between lapatinib and DMSO. G) qRT-PCR testing effects of c-MYC knockdown on RTK expression. H) Western blot testing effects of transcription factor knockdown on RTK expression.

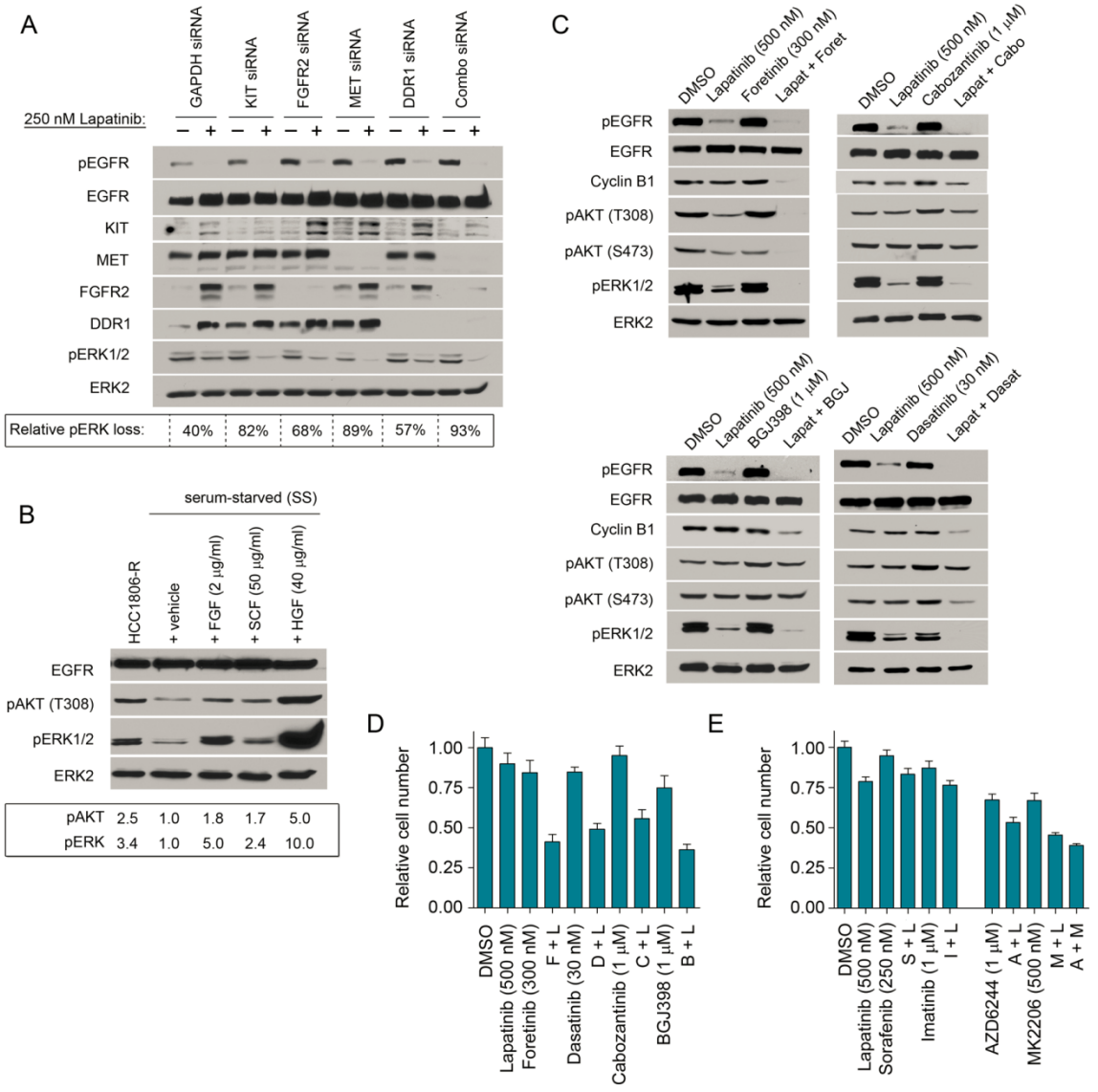

Figure 4.4 Targeting lapatinib-induced RTKs in HCC1806. A) Western blot of HCC1806 cells with 72h RNAi towards induced RTKs with or without lapatinib. Relative phosphorylation of ERK1/2 is quantified by densitometry. B) HCC1806-R cells were treated with cytokines for induced RTKs under serum-starved and lapatinib-treated conditions. C) Western blotting of TKI combinations with lapatinib reveals inhibition of residual ERK and arrest to the cell cycle in HCC1806 cells. D) Combination therapies synergistically inhibit HCC1806 cell growth, as shown by cell counting. E) Combinations with TKIs not targeting induced RTKs do not provide a benefit to growth inhibition, while cotargeting downstream MEK or AKT produces strong growth inhibition. Relative cell growth was assayed by Cell-Titer Glo.

V. TRIPLE-NEGATIVE BREAST CANCER EXHIBITS SUBTYPE-SPECIFIC KINOME REPROGRAMMING TO TARGETED MEK INHIBITION

Introduction

Triple negative breast cancer is clinically treated as a single disease; however, genomic studies have shown that TNBC consists of at least two discrete molecular subtypes, basal-like and claudin-low[8,157]. Differences in incidence, prognosis and response to therapy between these subtypes highlight the heterogeneity of TNBC. BL breast cancer represents the majority of TNBC (70-80%), exhibits high tumor cell proliferation and poor clinical outcome, and lacks approved molecularly targeted therapies. Though CL tumors comprise the minority of TNBC, CL breast cancer has generated great interest because of its correlation with tumor initiating cell features, EMT signature and association with metastasis and drug resistance[10]. Despite elevated MEK-ERK gene signatures in both BL and CL patient tumors, targeting the MEK-ERK pathway with single-agent MEK1/2 inhibitors (MEKi) has shown limited success in clinical trials for TNBC. Previous studies have shown that CL TNBC cell lines develop resistance to MEK inhibitors through acquired dependency on PI3K/mTOR signaling and/or activation of RTKs, suggesting that similar mechanisms of resistance may be at play in BL TNBCs[51,100]. Our goal was to define the response of the kinome to targeted MEK inhibition in both BL and CL breast cancers and design strategies to prevent resistance to MEKi therapies that can be applied globally to all TNBC subtypes.

MIB/MS kinome profiling of BL and CL cell lines and mouse tumors using chemical proteomics showed that each subtype reprograms to MEKi with a distinct

response signature facilitating resistance. These distinct kinome response signatures, including activation of numerous RTKs, were further observed in TNBC patients treated with MEKi in a "window trial" assessing molecular tumor response. Prolonged treatment of a BL/CL heterogeneic cell line or the C3Tag TNBC GEMM with MEKi resulted in the selection of CL reprogrammed tumors, illustrating the differential sensitivity of BL and CL TNBC to MEK inhibition. Combination therapies targeting MEKi-induced RTKs delayed the onset of MEK inhibitor resistance, but the diversity and accumulation of the activated kinome response ultimately overcame the dual agents, leading to eventual resistance. Induced gene expression of RTKs in response to MEKi represents an essential component of kinome reprogramming driving resistance in both BL and CL tumors. Therefore, we targeted the transcriptional activation of the kinome signatures using epigenetic inhibitors against the "epigenetic reader" BRD4. Inhibition of BRD4 with the small molecule inhibitor JQ1 blocked MEKi-mediated kinome reprogramming in both TNBC subtypes, prevented reactivation of MEK-ERK and caused sustained growth arrest. Combination of MEKi and JQ1 abolished the MEKi-mediated selection of CL cells in the dual-population BL/CL SUM229 cell line, suggesting that the novel combination of MEK and BRD4 inhibitors may be an effective approach for TNBC treatment.

Results

Differential kinome reprogramming in response to MEK inhibition defines TNBC subtypes

Active RAF-MEK-ERK signaling was detected in both CL and BL patient tumors, supporting MEK1/2 as a target in both TNBC subtypes (Figure 5.1A). To determine the kinome response to MEKi in both BL and CL TNBC, kinome profiling of BL cell line HCC1806 and CL cell line SUM159 was carried out using MIB/MS (Figure 5.1B).

Treatment of TNBC cell lines with the MEK inhibitor GSK1120212 (GSK212) for 24h resulted in increased MIB-binding of distinct cohorts of TKs and RTKs in BL (FGFR2, IGF1R, DDR1, KIT) and CL (PDGFRβ, AXL, DDR1) cells. Similarly, MIB/MS analysis of MEKi-treated tumors from a BL (2225; p53 null) tumorgraft mouse model showed increased MIB-binding of FGFR2 and FRK, while induction of PDGFRα/β, CSF1R and DDR2 was observed in MEKi-treated CL (T-11; p53 null) mouse tumors (Figure 5.1C). Induction of these distinct RTKs in response to MEKi treatment was further detected at both the protein and RNA level in multiple BL (HCC1806, SUM149, MDA468 and SUM229) and CL (SUM159, MDA231, WHIM12 and HS578T) cell lines, supporting MEKi-mediated RTK reprogramming as a global response in both subtypes, albeit with distinct subtype-specific signatures of RTK induction (Figure 5.1D-H). Western blotting for nduced RTKs in 2225 and T-11 tumors and tumor-derived cell lines further confirmed the distinct RTK responses in tumor cells (Figure 5.1F,G). Increased tyrosine phosphorylation of FGFR2, DDR1 and KIT after GSK212 treatment was observed in HCC1806 by RTK arrays, suggesting that MEKi-induced kinases in BL models are also activated (Figure 5.1I). Furthermore, continuous treatment of either BL HCC1806 or CL MDA231 cells with GSK212 resulted in stable upregulation of RTKs and reactivation of MEK-ERK signaling, consistent with induced RTKs supporting proliferation through ERK reactivation (Figure 5.1J).

Having defined distinct kinome reprogramming in BL and CL models for TNBC, we tested whether the unique RTK responses required distinct combination therapies by cotreating BL or CL cells with MEKi in combination with FGFR inhibitor BGJ398 (to target BL response) or PDGFR, DDR and VEGFR2 inhibitor sorafenib (to target CL response). Synergistic growth inhibition was observed only when BL or CL cells were cotreated with MEKi and the inhibitor targeting induced RTKs for that particular subtype (Figure 5.1K,L). These data show that the distinct BL and CL reprogramming responses

will require separate inhibitor combinations for effective growth inhibition.

We next evaluated the MEKi kinome response of TNBC patient tumors in a "window trial", in which patients received GSK212 for 7 days prior to surgical resection of the tumor. MIB/MS kinome analysis comparing a GSK212-treated patient tumor relative to a pre-treatment core biopsy showed decreased MIB binding of MEK1 but not MEK2, and increased binding of RTKs DDR1 and IGF1-R, similar to our defined BL kinome response signatures in preclinical models (Figure 5.2A). Comparing pre-treatment biopsies to treated tumors, we observed an induction of BL MEKi-responsive RTKs FGFR2, KIT and DDR1 in 3 of 4 BL patients at both protein and transcript levels (Figure 5.2B,C). Partial inhibition of ERK and increased SRC and AKT activity were also detected in tumors post-GSK212 treatment from patients 3 and 4, consistent with induced RTKs driving downstream signaling pathways. Due to sample limitations, the singular CL tumor obtained from patient 2 was suitable only for gene expression analysis, but this was sufficient to confirm our predicted CL-MEKi signature with induced gene expression of PDGFRβ, VEGFR2, CSF1R and DDR2. Interestingly, patient 8 did not show induction of RTKs in response to MEKi treatment, however, evaluation of gene expression of FGFR2, KIT and DDR1 showed strikingly elevated expression of these RTKs, suggesting that the tumor was predisposed to an RTK-reprogrammed state (Figure 5.2D).

Consistent with the MEKi response in our mouse models (Figure 5.2E), MIB/MS analysis showed inhibition of MEK1 but not MEK2 in all of the post MEKi-treated patient tumors analyzed by MIB-MS. This suggested that the dose of GSK212 administered was ineffective at maintaining MEK2 inhibition, particularly in the context of MEKi-induced RTK activation (Figure 5.2F,G). Overall, both BL and CL patient tumors exhibited our predicted MEKi kinome reprogramming signatures identified from cell line and mouse models. Elucidation of distinct kinome responses to MEKi in BL and CL

patient tumors validates the importance of kinome reprogramming in the clinic and highlights the need to understand this mechanism of resistance when treating patients with targeted kinase inhibitors.

MEKi treatment selects for reprogrammed CL cells from heterogeneous cell line

Assessment of kinome reprogramming in BL and CL TNBC after MEKi treatment revealed that each molecular subtype exhibits a distinct inhibitor-induced RTK signature. Histological studies have shown that TNBC tumors have cell populations expressing epithelial (BL) and mesenchymal (CL) markers, supporting the presence of BL and CL subtypes within tumors[158]. Clinically, CL tumors represent only 10% of all breast cancers and 20-30% of TNBC, however, claudin-low characteristics are significantly enriched after chemotherapy, consistent with intratumoral heterogeneity[10]. Our goal was to define the role of differential kinome reprogramming in response to MEKi in heterogeneic TNBC models to determine whether CL cells are enriched by MEKi. Several TNBC BL cell lines, including SUM229, are known to have subpopulations of CL cells, providing a valuable heterogeneic BL/CL model system to evaluate subtype-specific inhibitor responses. Parental SUM229 cells were FACS-sorted into distinct BL (EpCAM+/CD49f+) and CL (EpCAM-/CD49f-) subpopulations (Figure 5.3A) and kinome profiles of each subpopulation analyzed by MIB/MS (Figure 5.3B). Consistent with previously defined BL kinome signatures, the SUM229(+) show elevated DDR1, FRK, LYN and SRC relative to the SUM229(-), whereas, SUM229(-) have strong AXL and PKCα activity characteristic of CL cells[8,159]. We evaluated the response of each FACS-sorted population to MEKi using MIB/MS and found that SUM229(+) cells reprogrammed with induction of FGFR2 and DDR1, while SUM229(-) cells showed increased MIB-binding of PDGFRβ and DDR1 (Figure 5.3C). Subtype-specific RTK responses following MEKi were further observed in the sorted populations at both the protein and

RNA level, with elevated DDR1 common to both populations (Figure 5.3D,E). Importantly, return of ERK activity was detected predominantly in the SUM229(-) cells after MEKi treatment, consistent with RTK reprogramming in the CL population being better able to reactivate MEK-ERK signaling. The distinct kinome responses and ERK reactivation between sorted populations contributes to differential MEKi sensitivity, where SUM229(-) cells are 94-fold less sensitive to MEKi than SUM229(+) cells (Figure 5.4A). We next sought to define whether subtype-specific kinome reprogramming in CL cells provides a survival advantage following MEKi treatment in the parental population containing both BL and CL cells. Following confirmation that both BL (FGFR2 and DDR1) and CL (PDGFRβ and AXL) RTK responses occur simultaneously in parental SUM229 cells (Figure 5.4B), we treated SUM229 parental cells with MEKi over 28 days and monitored the proportion of SUM229(+) and SUM229(-) populations. The CL subpopulation was enriched from 1% to 51.9% after 28 days of MEKi, illustrating the selective advantage of CL reprogramming in response to prolonged MEK inhibition (Figure 5.4C). SUM229 cells after 28 days of MEKi treatment (SUM229-R) were shown to have CL characteristics analogous to sorted SUM229(-), with expression of PDGFRβ, AXL and EMT marker vimentin along with loss of BL markers DDR1, EpCAM and E-cadherin (Figure 5.4D). Removal of MEKi from SUM229-R cells reduced RTK expression, confirming that MEKi-enriched SUM229(-) cells were reprogrammed (Figure 5.4E). Taken together, sustained MEKi treatment of a BL/CL heterogeneic cell line model selects for CL subpopulations that display RTK reprogramming and reactivation of the MEK-ERK pathway.

Enrichment of tumors with CL characteristics in response to targeted kinase inhibition in C3Tag TNBC GEMM

The C3Tag GEMM has been shown to share genetic similarities with patient

TNBC basal-like tumors, providing an *in vivo* BL model to study tumor responses to targeted therapies[160]. Previous studies have demonstrated that single agent MEK inhibitor therapies provide minimal to no effect on C3Tag tumor growth, where tumors rapidly become resistant to MEKi[100]. Intriguingly, although C3Tag tumors cluster tightly with BL TNBC, a rapid induction of the CL MEKi-mediated kinome signature was observed following MEKi treatment, consistent with C3Tag tumors being heterogeneic for both BL and CL TNBC subtypes (Figure 5.5A). To investigate mechanisms of MEKi resistance in C3Tag tumors, we stably treated six tumor-bearing mice with the MEK inhibitor AZD6244 and defined kinome responses using MIB/MS. Following continuous MEKi treatment, tumors T1-T3 gradually increased in tumor volume, whereas tumors T4-T6 were very aggressive with exponential tumor growth (5.5B). Analysis of kinome-wide changes across the six tumors revealed two distinct groups based on MEKi response, with T1-T3 and T4-T6 clustering independently (Figure 5.5C). Consistent with the rapid tumor growth following MEK inhibition, T4-T6 showed increased MIB-binding of cell cycle dependent kinases. Interestingly, comparison of TKs across the six treated tumors revealed increased MIB-binding of the predicted BL MEKi-signature (FRK, DDR1 and KIT) in T3, whereas tumors T4-T6 showed activation of the CL MEKi-signature kinases (PDGFRα, PDGFRβ and DDR2) (Figure 5.5D).

Thus it appears that the tumor response to MEKi can entail both BL and/or CL kinome reprogramming. Enrichment of tumors with CL characteristics following MEKi treatment was further confirmed by blot, where T4-T6 showed elevated PDGFRβ, DDR2 and CL marker vimentin, as well as loss of BL markers KIT, DDR1 and EpCAM (Figure 5.5E). A dramatic induction of cyclin D1, the regulatory component of the cyclin D1-CDK4 complex and a marker of the CL subtype, was also observed consistent with rapid tumor growth and elevated MIB binding of CDK4. These MEKi-resistant C3Tag tumors display striking similarities to CL T-11 tumors in kinase expression and signaling (Figure

5.5F). Overall, these data suggest that CL and BL cells within a heterogeneic *in vivo* model of TNBC reprogram independently to MEKi treatment, and that the robust reprogramming of CL cells contributes to the enrichment of CL tumors following sustained MEKi treatment.

The diversity of kinome reprogramming promotes escape from MEKi/sorafenib combination therapies

The activation of numerous RTKs in the C3Tag tumors following MEKi prompted us to investigate the combination of MEKi with sorafenib. Previous studies in our lab have shown that the combination of MEKi and sorafenib caused tumor regression and apoptosis in a 21-day tumor regression model. Consistent with this observation, inhibition of MEKi-mediated PDGFRβ and induction of apoptotic marker BIM was detected in C3Tag tumors following 7-day cotreatment with MEKi and sorafenib (Figure 5.6A). Overall survival was improved in C3Tag mice treated with the combination of MEKi and sorafenib relative to single agents, though the effect was limited by the development of resistance (Figure 5.6B). Despite an initial tumor regression (tumor 1), the original tumor often returned with a rapid growth rate, along with the development of fast-growing secondary tumors having CL characteristics that were detected 30-40 days post inhibitor treatment (Figure 5.6C-E). Profiling of tyrosine phosphorylation in MEKi/sorafenib resistant tumors using RTK arrays confirmed sustained PDGFRβ inhibition, though persistent tyrosine phosphorylation of sorafenib targets PDGFRα and VEGFR3 were detected, indicating these RTKs evaded inhibition (Figure 5.6F). Tyrosine phosphorylation of non-sorafenib targets RON, FGFR4, MUSK and AXL were also detected in the tumors, demonstrating the diversity of RTK activity in the rapidly growing resistant tumors. Activation of numerous downstream kinases, including PI3K/mTOR, PKC and the RAF-MEK-ERK pathway further revealed that the tumors had

(re)activated alternative survival signaling to evade the initial MEK-ERK inhibition (Figure 5.6G).

To define kinases promoting resistance to the dual agent therapy, we performed a synthetic lethality screen of the kinome with the combination of MEKi/sorafenib or single agents alone in CL MDA231 cells. Knockdown of MEKi-responsive kinases not targeted by sorafenib, including AXL, EGFR, FGFR4, MUSK and RON, as well as downstream signaling kinases AKT, PKC and RAF all enhanced growth inhibition relative to MEKi alone (Figure 5.6H). Knockdown of known sorafenib targets DDR1/2 in the combination therapy displayed enhanced growth inhibition consistent with the MEKi-induced expression and activation of DDR1/2 overcoming the sorafenib inhibition. Combining the EGFR inhibitor lapatinib with both MEKi and sorafenib also enhanced growth inhibition in MDA231 cells, indicating the sorafenib-insensitive EGFR contributes to the kinome reprogramming to promote MEKi/sorafenib resistance (Figure 5.6I). Taken together, cotreatment of the C3Tag mice with MEKi/sorafenib resulted in an initial therapeutic benefit that was ultimately overcome through escape of RTKs and subsequent activation of multiple kinase signaling pathways. Although sorafenib is a broad acting tyrosine kinase inhibitor, the diversity of MEKi/sorafenib kinome reprogramming in C3Tag tumors allowed tumors to exploit sorafenib-insensitive kinases to facilitate dual-agent resistance, demonstrating a substantial challenge in applying effective and stable kinase inhibitor combinations. These data suggest that GSK212 combinations with alternative TKIs would similarly lack the breadth of RTK inhibition to prevent MEK/ERK pathway reactivation (Figure 5.7), and indicate that other strategies to prevent RTK reprogramming may be necessary for sustained growth inhibition.

Targeted BRD4 inhibition blocks kinome reprogramming in BL and CL TNBC cells

Combination therapies directly targeting MEKi-induced RTKs delayed the onset

of MEKi resistance; however, the diversity and accumulation of the activated kinome response ultimately overcame the dual agents. Induced RTK gene expression in response to MEKi represents an essential and global component of kinome reprogramming that drives drug resistance in both BL and CL tumors. Therefore, to address this "kinome reprogramming dilemma", we evaluated strategies to block reprogramming at a transcriptional level, with the goal of preventing the accumulation of kinome activity and subsequent reactivation of the targeted pathways.

Recently, targeted inhibition of bromodomain family member BRD4 has emerged as a potential strategy to interfere with expression of specific oncogenes, such as FOSL1 and c-MYC[161–163]. BRD4 is a multifunctional protein with a kinase domain and acetyl lysine binding activity that recruits transcriptional activators/repressors to specific promoters, regulating gene expression[164,165]. We applied MIB/MS to determine if BRD4 inhibition with small molecule inhibitor JQ1 could alter the activity of specific MEKi-induced kinases in BL and CL cell lines. Following JQ1 treatment, decreased MIB-binding of a number of TKs from different subfamilies including EGFR, DDR1, FGFR4, SRC, CSK and FRK was detected in BL SUM229 cells, while reduced binding of PDGFRα, INSR and DDR1 occurred in SUM159 cells (Figure 5.8A). mRNA of RTKs activated in response to MEKi was reduced in SUM159 cells following 48h JQ1 treatment, consistent with inhibition of BRD4 preventing recruitment of transcriptional activators to RTK promoters (Figure 5.8B).

We next tested whether targeted BRD4 inhibition with JQ1 could block MEKi-mediated RTK reprogramming in both BL and CL cells. Cotreatment of cells with GSK212 and either JQ1 or an analogous BRD4 inhibitor iBET-151 blocked induction of PDGFRβ, DDR1, VEGFR2 and AXL in CL cells and FGFR2, DDR1 and KIT in BL cells at both the RNA and protein levels (Figure 5.8C-H). BRD4 inhibition combined with MEKi treatment also attenuated RTK induction in T-11 and 2225 tumor-derived cell lines,

exemplifying the broad effect of blocking the transcriptional component of reprogramming (Figure 5.8I). siRNA-mediated BRD4 knockdown attenuated BL and CL MEKi reprogramming at the protein and transcript levels, confirming targeted BRD4 inhibition as a mechanism to block kinome reprogramming to MEKi (Figure 5.8J, data not shown).

Combination of JQ1 and GSK212 maintains growth inhibition and blocks MEKi-mediated selection of CL-reprogrammed cells

The combination of MEKi and JQ1 in SUM159 cells blocked reactivation of MEK-ERK signaling, arrested the cell cycle, and caused a strong induction of apoptotic marker BIM (Figure 5.9A). MEKi-activated SRC, STAT, AKT and MEK-ERK pathways were also blocked by the MEKi/JQ1 combination in both SUM159 and SUM229 cells (Figure 5.9B). We next evaluated the ability of JQ1 to block the development of MEKi resistance in both TNBC BL and CL subtypes. Cotreatment of BL and CL cells with GSK212 and JQ1 resulted in a significant growth inhibition over a 30-day period relative to single agents, preventing the development of MEKi resistance (Figure 5.9C). Although HCC1806 cells appear to exhibit some resistance to the dual agent combination, growth inhibition in the combination of GSK212 and JQ1 was significantly enhanced relative to single agents. Previous studies utilizing JQ1 have observed such differential sensitivity of cancer cell lines to JQ1, illustrating the plasticity of cancer cells adapting to targeted therapies[162,163]. The MEKi/JQ1 combination blocked kinome reprogramming in sorted SUM229(+) and SUM229(-) cells, preventing activation of alternative downstream signaling, as well as the RTK-mediated reactivation of MEK-ERK pathway (Figure 5.9D,E). Because JQ1 attenuates MEKi-mediated BL and CL RTK reprogramming, we tested whether selection of CL cells could be prevented by cotreatment with MEKi/JQ1. Importantly, treatment of SUM229 parental cells with the GSK212/JQ1 combination

blocked the selection of CL SUM229(-) cells (Figure 5.9F). These data present BRD4 inhibition as a mechanism for blocking kinome reprogramming in both BL and CL cell lines to prevent adaptive resistance and the selection of CL reprogrammed cells in a heterogeneic model of TNBC.

Discussion

The current paradigm of the clonal evolution of tumors acknowledges that tumors consist of heterogeneous cancer cell populations that harbor different genomic and epigenetic alterations contributing to unique phenotypic characteristics[12]. Our studies highlight the diversity of TNBC cells, revealing distinct kinome activity profiles and responses to MEKi between BL and CL TNBC cells. While these subtypes are treated identically in the clinic, we show that the differences in kinome expression and activity lead to divergent molecular and phenotypic drug responses. Indeed, unique BL and CL kinome responses to MEKi were observed in patient tumors through a window trial assessing kinome reprogramming *in vivo*. While the number of patient tumors was limited and constraints of sample size prevented extensive analysis, these experiments bolster the relevance of kinome reprogramming by showing predicted RTK responses to MEKi in spontaneous, naturally-occurring patient tumors. Importantly, the kinome reprogramming response to MEKi contributes to proliferation/survival in the presence of MEKi for both CL and BL cell lines, through the induction of unique RTK signatures that redrive growth signaling. These signatures of induced RTKs appear to be at least partially aligned with subtype-specific RTK expression profiles, where highly-expressed subtype-specific RTKs (such as PDGFRβ in CL or FGFR2 in BL) are often responsive to MEKi. It is interesting to note, however, that the CL reprogramming response to MEKi allows for a more consistent and robust reactivation of ERK1/2, suggesting that CL MEKi-responsive RTKs may be more potent activators of RAF-MEK-ERK signaling. In

general, CL cells seem to exhibit greater plasticity and a more uniform signature of responsive RTKs, possibly due to broader heterogeneity within the BL subtype[166].

Where heterogeneous populations of BL and CL cells coexist, such as in split-population cell lines or tumor models, the diversity in cell composition contributes to tumor plasticity and the acquisition of drug resistance via the selection of cancer cells equipped to evade drug action. Previous studies have shown that chemotherapy enriches the CL phenotype from heterogeneous breast tumors, consistent with this subtype exhibiting greater plasticity and drug resistance[10]. Here we show that selection of the CL phenotype also occurs in heterogeneic cell line and tumor model systems after MEK inhibitor treatment. While the mechanism for the enrichment of CL cells is poorly understood, there are indications that the relatively robust kinome reprogramming in CL cells contributes to decreased drug sensitivity (though other factors undoubtedly also influence MEKi sensitivity)[43]. In the heterogeneic SUM229 cell line, sorted CL cells reactivate ERK after MEKi treatment whereas sorted BL cells do not. Consideration of kinome reprogramming as a mechanism for selection of resistant subpopulations adds to the complexity of drug response in the context of heterogeneic models. Ultimately, the diversity of cell populations within a tumor and the target-specific reprogramming responses among these populations will determine how tumors will evolve after a given treatment. With the prevalence of acquired resistance to targeted therapies coinciding with an apparent selection for the CL phenotype, there is a clear need to tailor therapeutic strategies to account for these mechanisms of resistance.

Small, albeit synergistic, gains in growth inhibition and apoptosis can be achieved by small molecule inhibition of MEKi-induced RTKs in combination with MEKi. Unfortunately these responses are not durable, due to the dynamic nature of kinome reprogramming (‘the reprogramming dilemma’) and the diversity of cell populations within heterogeneic model systems. Thus, we identify kinome reprogramming as a

mechanism of resistance and selection, but also as a vulnerability that can be exploited. Our goal was to develop an effective targeted therapy for TNBC that accounts for divergent kinome responses and prevents the selection of CL tumors, which are highly aggressive and refractory to conventional treatments. We propose epigenetic inhibition in combination with kinase inhibitors as a global strategy to prevent kinome reprogramming and block CL selection. Whereas combination therapies targeting induced RTKs or parallel growth signaling pathways are reactionary and allow the accumulation of induced kinase activity, the use of epigenetic inhibitors (such as JQ1) to block the ability of cancer cells to respond to targeted kinase inhibition prevents kinome reprogramming and selection of CL cells (Figure 5.10). Blocking the ability of cells to reprogram in response to targeted kinase inhibitors may transform their capacity for sustained tumor responses, as evidenced by the long-term inhibition of both BL and CL cells after cotreatment with MEKi and JQ1. The mechanism by which BRD4 inhibition prevents kinome reprogramming is not completely understood, but likely lies in the critical role of BRD4 in supporting gene transcription at promoters, enhancers and super enhancers for highly expressed oncogenic kinases[165,167]. Preliminary experiments with panobinostat suggest that HDAC inhibition and other alternative strategies (HSP90 inhibition?) may also be employed to block kinome reprogramming.

Despite our optimism for this epigenetic/kinase inhibitor strategy, it is prudent to be wary of a reprogramming response to epigenetic inhibitors that may eventually lead to resistant populations. Indeed, intrinsic and acquired resistance to JQ1 has been observed in a variety of cell lines[162,163,168]. Additionally, using MIB/MS we have identified a small subset of TKs and other kinases that respond to JQ1 treatment with increased expression/activity, raising the possibility that these may contribute to an eventual resistance. However, the advantage of BRD4 inhibitors is that they cripple the ability of the cell to reprogram to MEKi (and likely other cytostatic/cytotoxic inhibitors), opening

the door for inhibitor combinations that would otherwise fail due to kinome plasticity. Our data indicate that BRD4 inhibitor combinations present a promising therapeutic strategy for the sustained inhibition of TNBC cells, and future studies should define the mechanisms by which BRD4 inhibition prevents kinome reprogramming and the *in vivo* efficacy of these combinations.

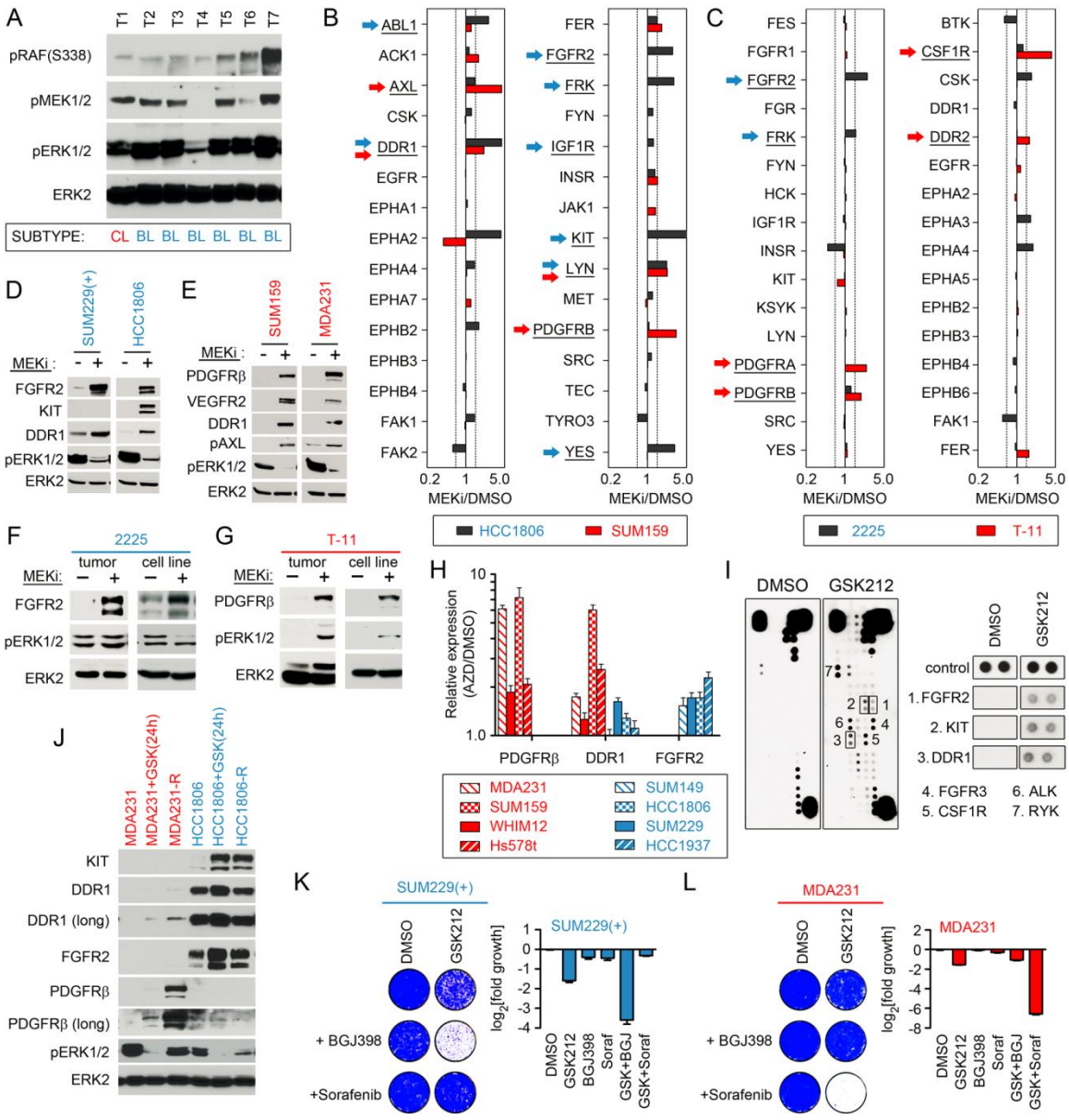

Figure 5.1 Differential kinome reprogramming in BL and CL TNBC following MEKi. A) Activated MEK-ERK signaling in CL and BL patient tumors, shown by western blot. B) Tyrosine kinase response to 24h GSK212 (500 nM) in BL (blue) HCC1806 and CL (red) SUM159 TNBC cell lines. Bar graph shows iTRAQ-determined quantitative MIB binding. C) MIB/MS profile of BL (blue) 2225 and CL (red) T-11 tumors in response to 35 mg/kg AZD6244 for 2 days. Differential induction of RTKs in response to 24h GSK212 treatment in D) BL and E) CL TNBC cell lines as shown by western blot. Distinct kinome response in F) 2225 and G) T-11 tumor and tumor-derived cell lines treated with 35 mg/kg AZD6244 or 10 nM GSK212 for 2d, as shown by western blot. H) qRT-PCR for RTK expression in BL and CL cell lines after 24h AZD6244 (5 μM). I) RTK arrays of HCC1806 cells after 24h DMSO or GSK212 (100 nM). J) RTK expression after continuous 30d treatment of BL HCC1806 or CL MDA231 cell lines with 10 nM GSK212. K,L) Colony formation in BL and CL cells following cotreatment with GSK212 and 1 μM BGJ398 or 250 nM sorafenib. Quantification of staining is plotted.

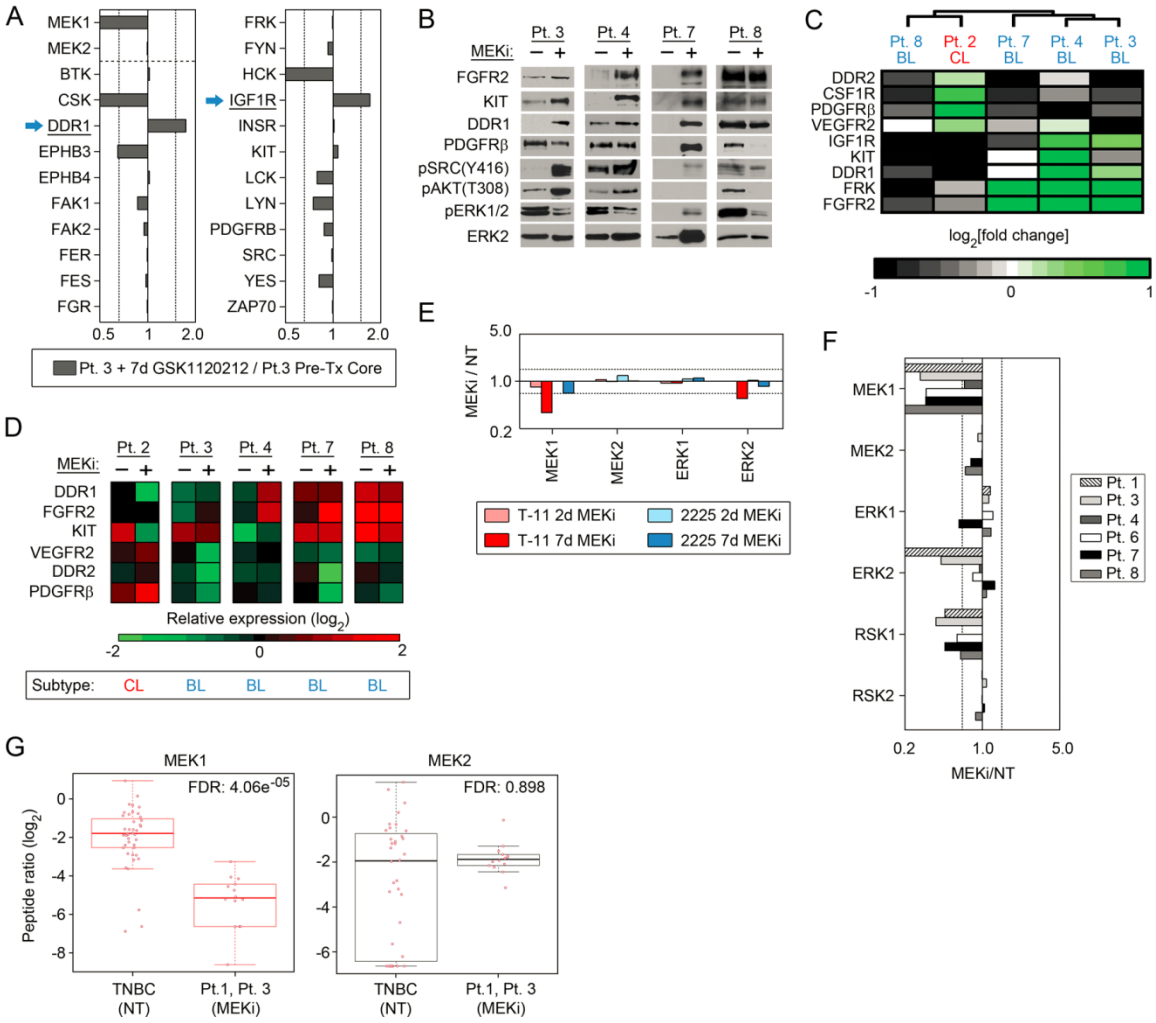

Figure 5.2 Kinome reprogramming in patient window trial for TNBC. A) MIB-MS analysis of 7 day GSK212 (1.5 mg/day) response in TNBC patient (Pt.3). Bar graph shows iTRAQ-determined quantitative MIB binding as a ratio of GSK212- treated tumor to untreated core biopsy. B) Inhibition of ERK activity (Pt.3, 4 and 8) and induction of RTKs (Pt.3 and Pt.4), in response to 7 day GSK212 treatment as shown by western blot. Matched untreated core biopsies were used as controls. C) Gene expression changes of BL and CL MEKi response signature in TNBC patients, comparing pretreatment core versus GSK212-treated tumor by gene arrays. D) Relative gene expression of core MEKi response signature of TNBC patients treated with GSK212 for 7 days, as determined by gene array. Untreated core biopsy was used as a control for each patient. E) MIB/MS binding profile of MEK-ERK pathway kinases from AZD6244-treated 2225 and T-11 tumors. F) MIB/MS-derived peptide ratios of MEK1 and MEK2 in Pt.1 and 3 GSK212-treated tumors relative to untreated BL tumors. G) MIB/MS binding profile of MEK-ERK pathway kinases from GSK212-treated patient tumors. The bar graphs show iTRAQ-determined quantitative changes in MIB binding as a ratio of GSK212/untreated patient tumor.

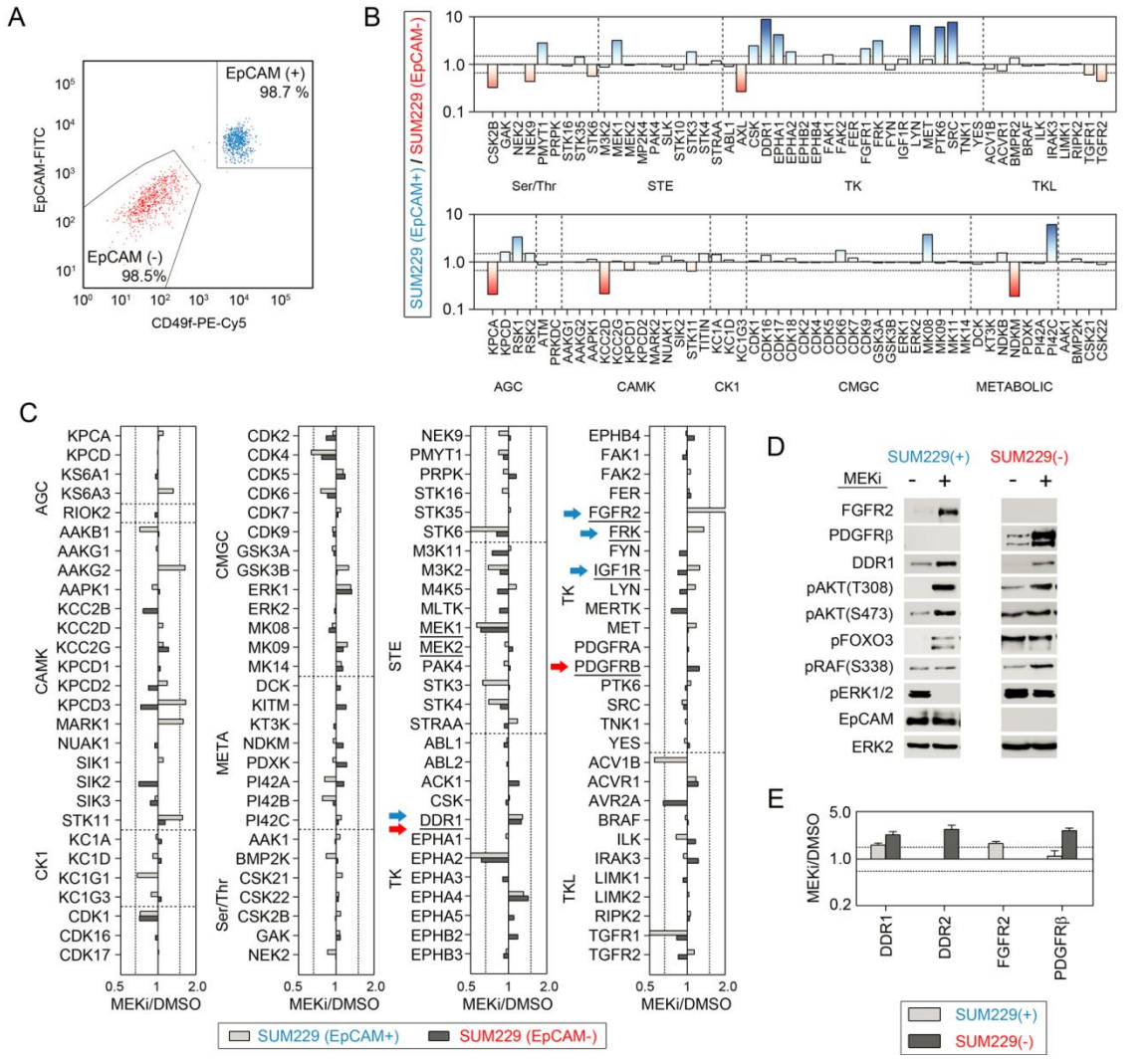

Figure 5.3 Distinct responses within heterogeneous cell populations. A) Purity of sorting SUM229 parental cells into distinct EpCAM+/CD49f+ and EpCAM-/CD49f- populations using flow cytometry. B) Quantitative comparison of SUM229 subpopulations using MIB/MS, where line graph denotes iTRAQ-determined quantitative changes in MIB binding as a ratio of SUM229(EpCAM-)/SUM229(EpCAM+). C) Distinct kinome reprogramming in SUM229(EpCAM+) and SUM229(EpCAM-) cells in response to 24h AZD6244 (5 μM) treatment, as shown by MIB/MS analysis. Line graph shows iTRAQ-determined quantitative MIB binding as a ratio of AZD6244/DMSO. D) Differential induction of RTK and downstream signaling in sorted SUM229(+) and SUM229(-) cells in response to 24h AZD6244 (5 μM) treatment, as shown by western blot. E) Increased gene expression of RTKs in sorted SUM229 cells in response to 24h AZD6244 (5 μM), determined by qRT-PCR.

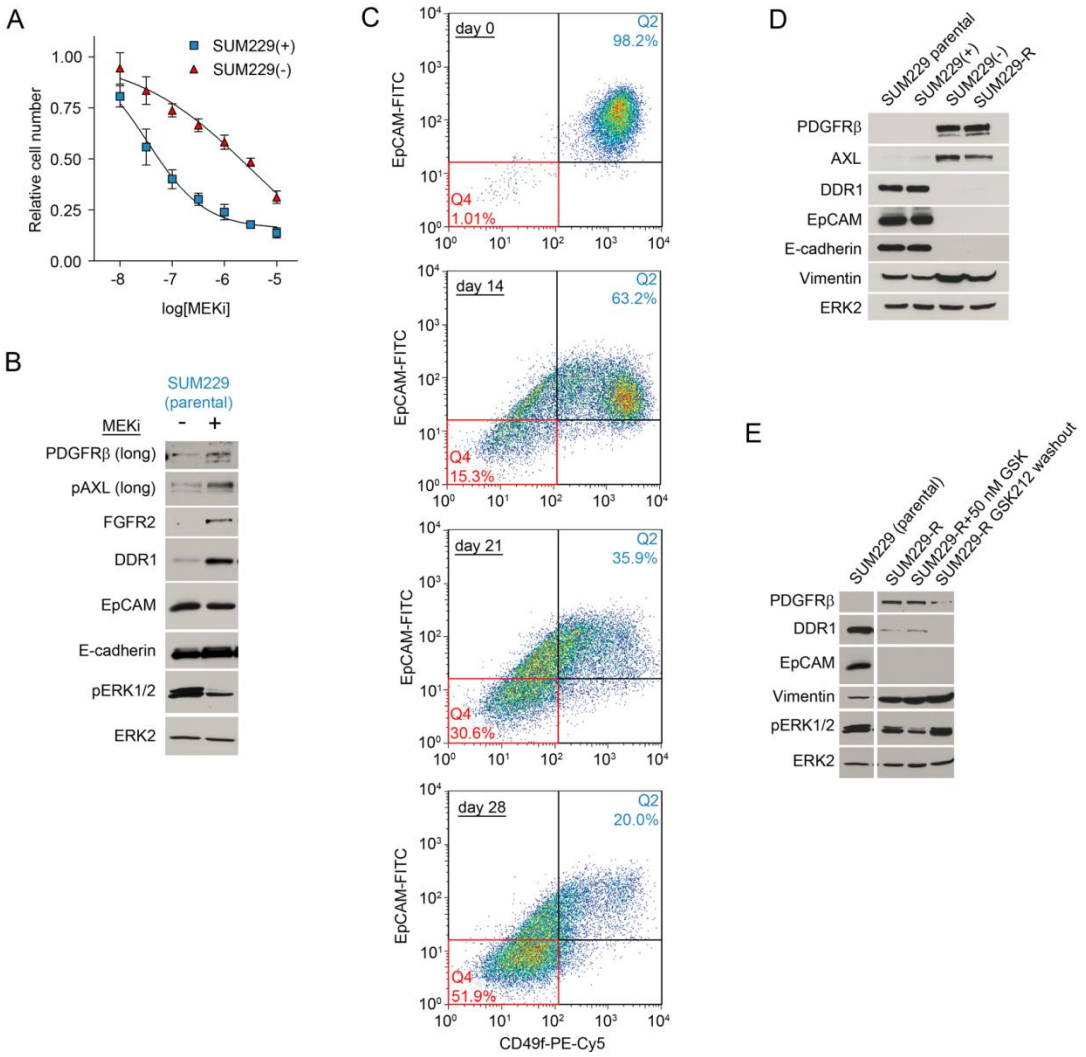

Figure 5.4 Prolonged MEKi treatment of BL/CL heterogeneous cell line selects for CL reprogrammed cells. A) Differential MEKi sensitivity in SUM229 subpopulations, determined by cell counting. B) RTK induction in SUM229 parental cells in response to 24h GSK212 treatment. C) FACS of SUM229 parental population continuously treated with 10 nM GSK212 over a 28 day period. SUM229(+) sort into quadrant Q2, while SUM229(-) occupy Q4. D) Western blot comparison of parental, sorted, and 30 day GSK212-treated SUM229 cells. E) Western blot of 30 day GSK212-treated SUM229 cells (SUM229-R) with increased GSK212 or GSK212 washout.

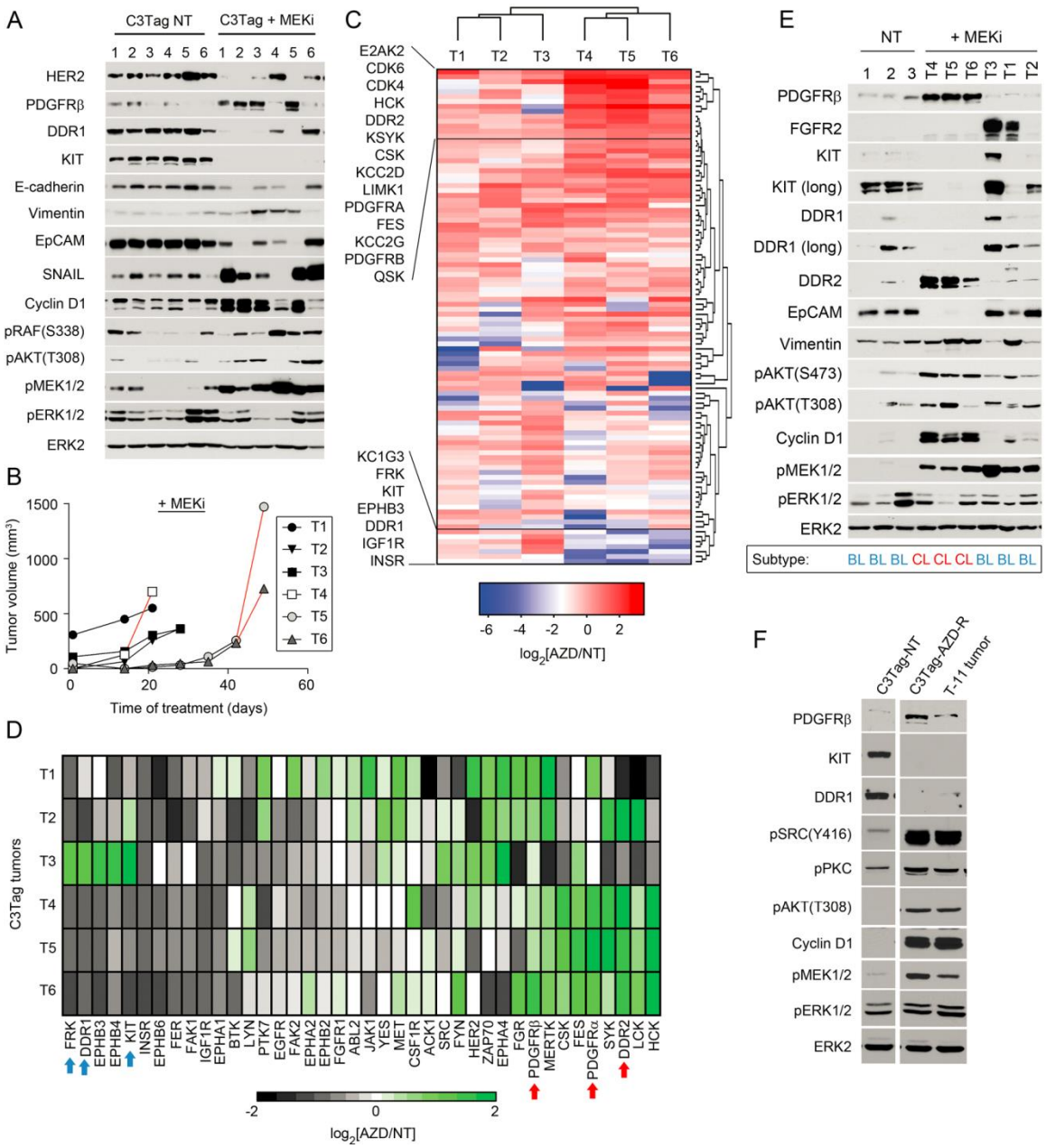

Figure 5.5 Treatment of C3Tag mice with MEK inhibitor enriches tumors with claudin-low characteristics. A) Western blot of untreated and AZD6244-treated C3Tag tumors showing enrichment of CL markers and loss of BL markers after sustained AZD6244 treatment. B) C3Tag tumor growth during 20 mg/kg AZD6244 treatment. C) MIB/MS analysis of kinases in AZD6244-treated C3Tag tumors T1-T6 relative to untreated control tumor, showing T1-T3 and T4-T6 clustering independently. D) Comparison of tyrosine kinase activity in AZD6244-treated C3Tag tumors relative to untreated control by MIB/MS. E) Western blot comparison of RTK response in untreated and AZD6244-treated C3Tag tumors. F) C3Tag AZD6244-resistant tumors display kinase signaling similarities to CL T-11 mouse model by western blot.

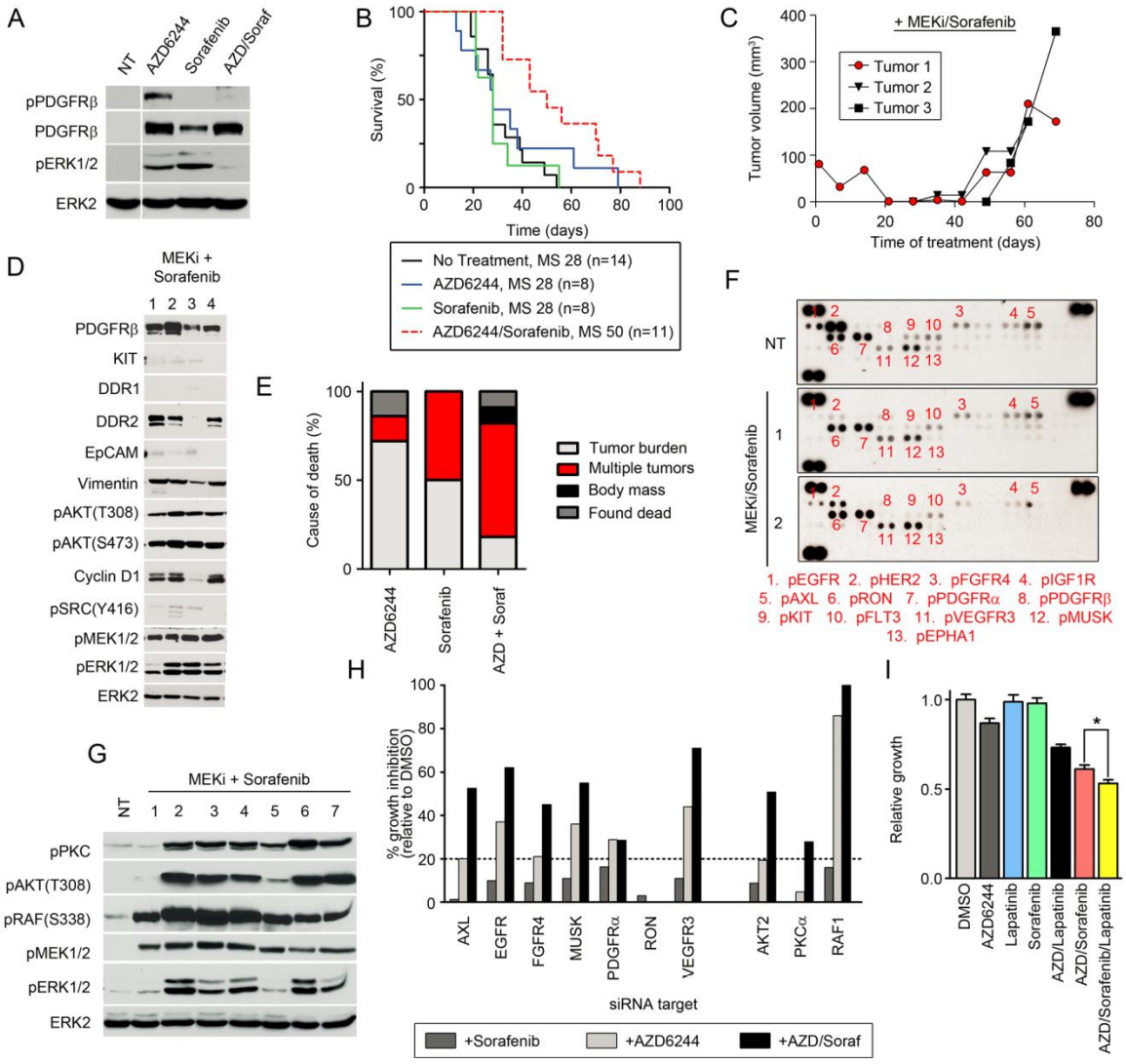

Figure 5.6 Diversity of kinase activation in response to MEKi protects C3Tag tumors from dual agent combination therapies. A) Western blot of C3Tag tumors treated with AZD6244 (20 mg/kg) and/or sorafenib (35 mg/kg) for 7d. B) C3Tag survival after cotreatment with AZD6244 (20 mg/kg) and sorafenib (35 mg/kg). C) C3Tag tumor growth during AZD6244 and sorafenib treatment. D) Activation of kinase signaling pathways in AZD6244/sorafenib resistant tumors, as shown by western blot. E) Quantitation of causes of death in C3Tag mice treated with AZD6244 and/or sorafenib. F) RTK arrays showing tyrosine phosphorylation of sorafenib-insensitive kinases in AZD6244/sorafenib resistant C3Tag tumors. G) Activation of kinase signaling pathways in AZD6244/sorafenib resistant tumors, as shown by western blot. H) MDA231 growth was measured by Cell-Titer Glo after 96h RNAi knockdown of RTKs, AKT, PKC or RAF1 in the presence or absence of 1.25 µM AZD6244. I) Growth assays of MDA231 cells treated with MEKi and TK inhibitor combinations. Cell growth was monitored using Cell-Titer Glo.

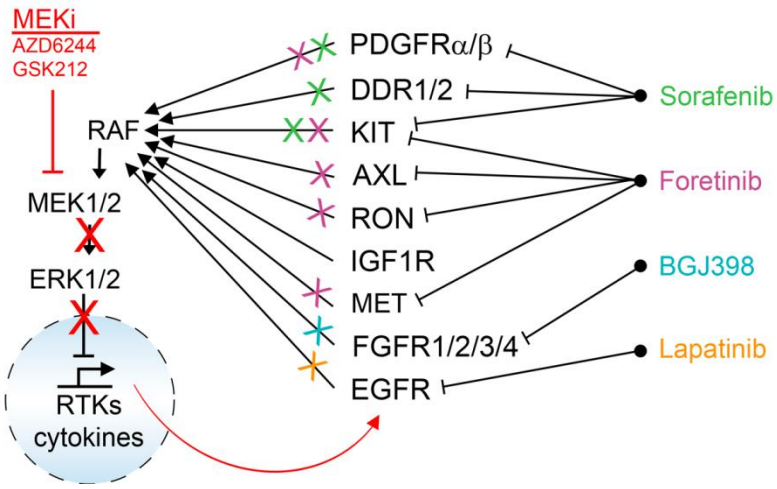

Figure 5.7 Inability of TKIs to prevent MEK/ERK reactivation. Schematic of TKIs targeting GSK212-induced RTKs, revealing inability of TKIs to completely inhibit RTK activity and MEK/ERK pathway reactivation.

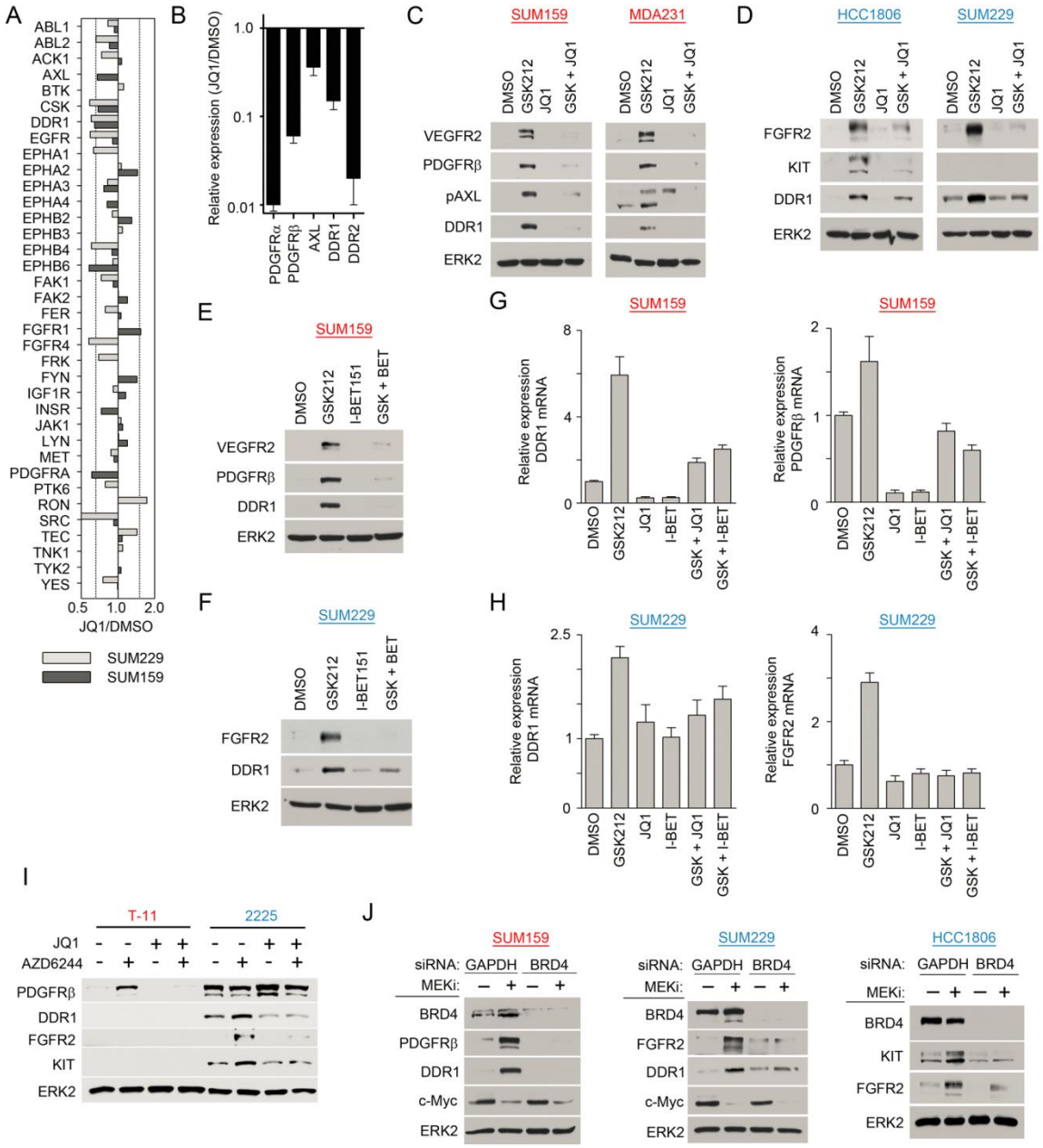

Figure 5.8 Targeted BRD4 inhibition prevents MEKi mediated kinome reprogramming in BL and CL TNBC. A) Inhibition of BL and CL MEKi-response kinases in SUM229 and SUM159 cells following 300 nM JQ1 treatment, as determined by MIB/MS analysis. Line graph shows iTRAQ-determined quantitative MIB binding as a ratio of JQ1/DMSO. B) Decreased RNA expression of CL MEKi-response kinases following JQ1 treatment, quantitated by qRT-PCR. C-F) Western blot of GSK212 (10 nM) and JQ1 (300 nM) or I-BET151 (1 μM) combination in CL (red) and BL (blue) cell lines. qRT-PCR of GSK212 and JQ1 or I-BET151 combinations in G) CL and H) BL cell lines. I) Western blot of CL T-11 and BL 2225 cell lines after 48h treatment with GSK212 (10 nM) and JQ1 (300 nM). J) BRD4 knockdown in CL SUM159 and BL SUM229 cells prevents RTK induction after 48h GSK212 (10 nM) treatment, as shown by western blotting.

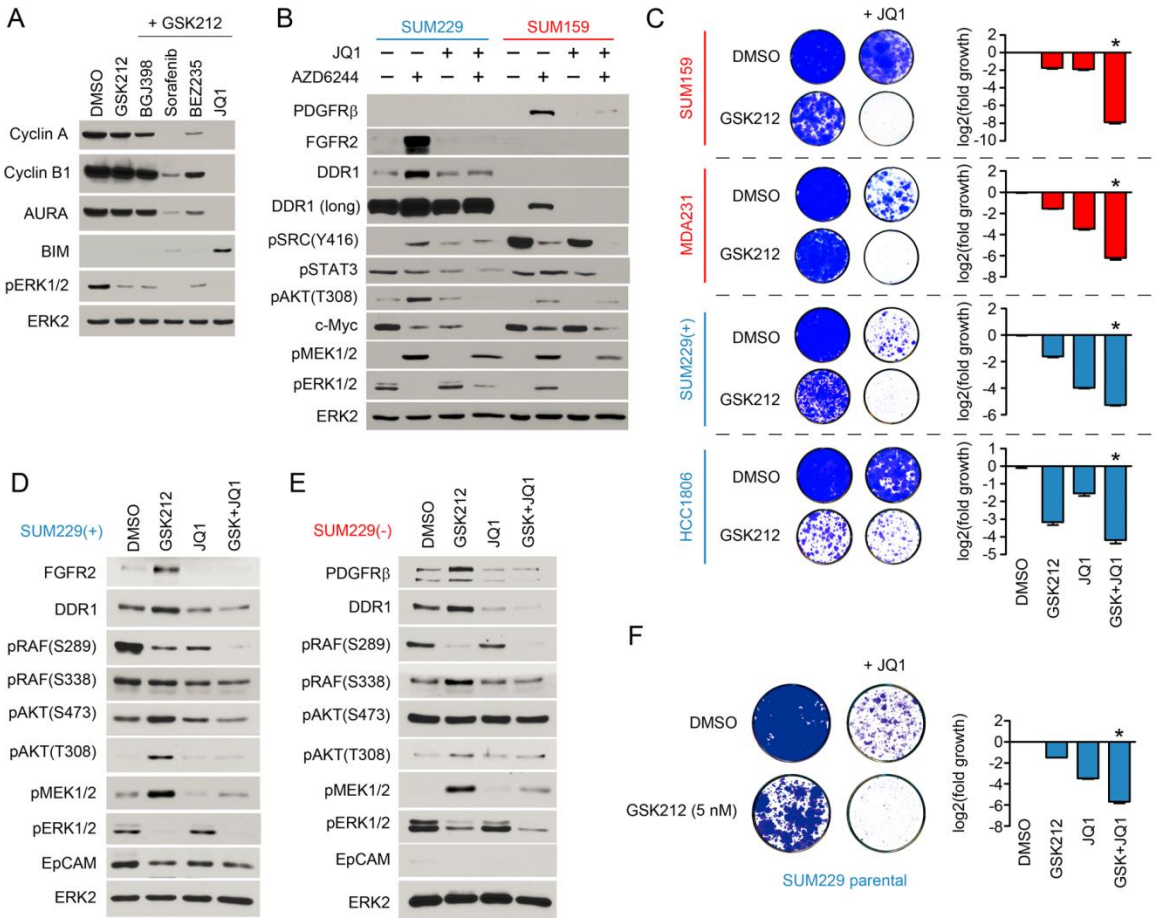

Figure 5.9 Combination of GSK212 and JQ1 promotes stable growth inhibition and prevents selection of CL cells. A) Western blot comparison of GSK212 combinations in SUM159 cells. B) Activation of downstream SRC, AKT, STAT and MEK-ERK signaling after 48h treatment with 10nM GSK212 and/or 300 nM JQ1 in SUM159 and SUM229 cells, as determined by western blot. C) Colony formation in CL (red) and BL (blue) cell lines following cotreatment with GSK212 and JQ1 (200-300 nM). Quantification of crystal violet staining is plotted. D,E) Attenuation of RTK responses to GSK212 by cotreatment with JQ1 in sorted SUM229(+) and SUM229(-) populations, as shown by western blot. F) Crystal violet staining of SUM229 parental cells treated with GSK212 and 300 nM JQ1 shows inhibited selection of CL SUM229(-) cells.

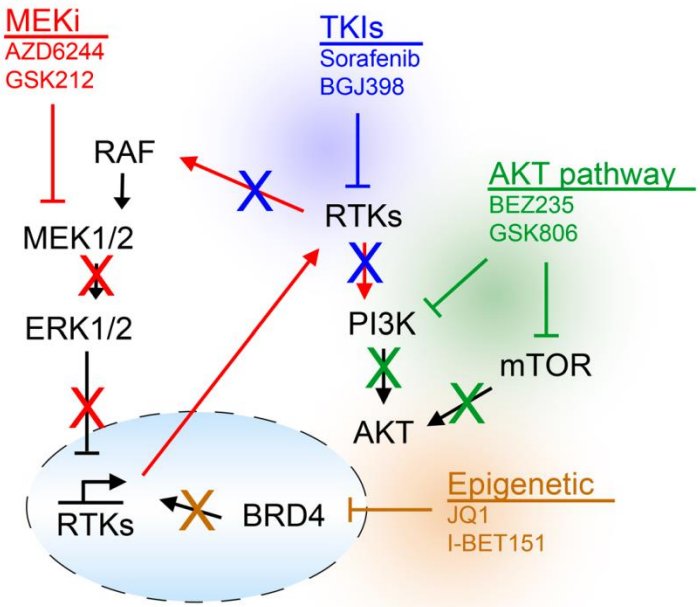

Figure 5.10 Strategies to target kinome reprogramming. Schematic of combination strategies targeting MEKi-induced kinome reprogramming in CL and BL TNBC.

VI. SIGNIFICANCE AND FUTURE DIRECTIONS

The innovation of these studies lies partly in the development of technologies and protocols that facilitate quantitative assessment of expression and activity dynamics of the endogenous kinome. The development of such proteomic methods to allow investigation of kinome reprogramming represents a major milestone in understanding kinome network signaling. MIB/MS can be used for any non-denatured protein sample to capture endogenous kinases, allowing for wide applicability to study diverse model systems. Using our MIB/MS technique, robust kinome responses have been observed in a variety of models (i.e. to drug treatment in diverse cancer types, to viral infection of fibroblasts, and to gene knockdown in an endothelial cell model for cerebral cavernous malformations), illustrating the plasticity of kinome network signaling to disparate perturbations. MIB/MS has provided an unbiased method to discover kinase dysregulation in such diverse model systems, and will certainly yield further insight into the mechanisms behind these and other diseases. Importantly, MIB/MS also functions as a tool to investigate activity of kinase paralogs where individual reagents are lacking. For instance, our studies have highlighted the unique ability of MEK2 to escape inhibition by MEK1/2-targeted inhibitors, whereas antibody-based techniques would be unable to distinguish between MEK1 and MEK2 activity.

Continual efforts are being made to improve the scalability of MIB/MS to accommodate small (<1mg) protein samples and increase the breadth of kinase capture. The addition of newly-developed pan-kinase inhibitors to the modular MIB columns could substantially improve the capture of expressed kinases[169]. Furthermore, work is under

way to combine MIB enrichment with multiple reaction monitoring (MRM) to improve sensitivity in small samples for signature kinases[170]. MRM peptides against most (or all) of the RTKs (or kinome?) could be developed to facilitate enhanced detection of underrepresented or signature kinases in patient-derived samples and other instances where sample size is limiting. Successful implementation of these strategies will allow greater applicability of MIBs to translational samples, such as needle biopsies of tumors from patients participating in clinical window trials.

There is still a great potential for MIB/MS to advance the understanding of kinome signaling dynamics in cancer models. Application of these techniques to study kinome response to drug treatment is a novel approach to rationally design small molecule inhibitor combinations for the effective treatment of breast and other cancers. Our work has shown that cancer cells exhibit a rapid initial response to drug treatment that leads to kinome reprogramming and cancer cell adaptation, presenting a new mode of rapidly acquired drug resistance. Specifically, we discovered that breast cancer cells evade growth inhibition from MEK1/2 and EGFR inhibitors by upregulating specific signatures of RTKs, ultimately leading to the reactivation of downstream growth signaling. Kinome reprogramming is a new paradigm for drug response that highlights the immediate consequences of targeted inhibition in the development of drug resistance (Figure 6.1). Responses to MEKi were specific to particular subtypes of TNBC, with CL and BL cells responding distinctly. Our “window trial” for GSK212 confirms that kinome reprogramming to MEK inhibition occurs in patient tumors, underscoring the relevance of kinome reprogramming *in vivo*. Targeting drug-induced kinases suppressed persistent growth signaling and substantially inhibited proliferation of cancer cells in long-term growth assays and tumor models. Slight alterations to MIB/MS experimental design could further define kinome signaling differences by the regimen of drugs (i.e. drug order, dose scheduling, etc), kinase signaling at distinct subcellular localizations, or

subtle mechanistic difference between similar drugs. Taken together, these studies will significantly impact the concept of drug resistance in cancer, and will inform scientists and clinicians about viable strategies for the development of effective cancer therapies. Future applications of MIBs could help to define other modes of kinome reprogramming to diverse therapeutics and in other cancer types. For instance, our lab is now interested in exploring the kinome response to chemotherapeutics in TNBC, and we have many collaborations applying MIBs to define drug response in other cancers (CML, pancreatic, melanoma, etc.).

This work has advanced our understanding of compensatory kinase signaling after targeted kinase inhibitor treatment to the point where we now know that different strategies for effectively targeting oncogenic driver kinases are needed. Adaptive resistance via kinome reprogramming compels the targeting of diverse drug-induced kinases to prevent growth pathway hyperactivity. Highly induced expression and activity of kinases can prevent full inhibition of target kinases to bypass targeted inhibitors. Furthermore, subtype-specific reprogramming events facilitate the selection of drug-resistant, kinome-reprogrammed cells from heterogeneous tumor cell populations. Thus, broadly targeting compensatory kinases to block induced kinase signaling will be extremely difficult with the current compendium of biologically active kinase inhibitors. We have proposed preventing kinome reprogramming as a method to preempt this form of adaptive resistance, aiming to exploit the transcriptional component of kinome reprogramming. A variety of strategies can be envisioned to block the ability of cancer cells to rewire kinase growth signaling pathways, including BRD4 inhibition (exemplified here), HDAC inhibition through panobinostat or vorinostat, or HSP90 inhibition. We have shown that this strategy works to broadly prevent reprogramming of the kinome in response to MEKi and gives long-term inhibition of cell proliferation, providing a proof-of-principle and strong foundation for further preclinical studies on kinome resistance.

Finally, although we have focused our work on defining induced kinases that support growth/survival in the presence of targeted inhibitors, a bioinformatic assessment of reprogramming signatures could provide information on the network behavior of the kinome. A significant number of kinases exhibit reduced MIB binding after targeted drug treatment; while drug targets may simply be competed off the column by free drug, the loss of non-target kinases (as defined by in vitro assessment of the inhibitors ability to inhibit kinase activity) suggests pervasive network regulation of the kinome. For instance, loss of cell-cycle regulating CDKs are often seen after MEKi treatment, indicative of slowed cell cycle progression caused by MEK/ERK loss. Computational analysis of kinome behavior may elucidate other unknown regulatory interactions within the kinome, where loss of activity for a single kinase instigates cascading effects to reorient the activity equilibrium of the kinome. MIB/MS provides a platform for such computational analysis, where the kinome activity after specific perturbations can be measured and used to define the extent of kinases increasing and decreasing in activity. By mapping patterns of kinase changes, undiscovered relationships between distinct kinases may be discovered. Greater appreciation of how the kinome is “wired” could then provide more precise models of kinase signaling, facilitating more accurate prediction of cell signaling responses and viable kinase targets. Using these methods of analysis, we can begin to unravel the dynamic nature of the kinome and use this information to understand and target dysregulated kinase signaling in cancer and other diseases.

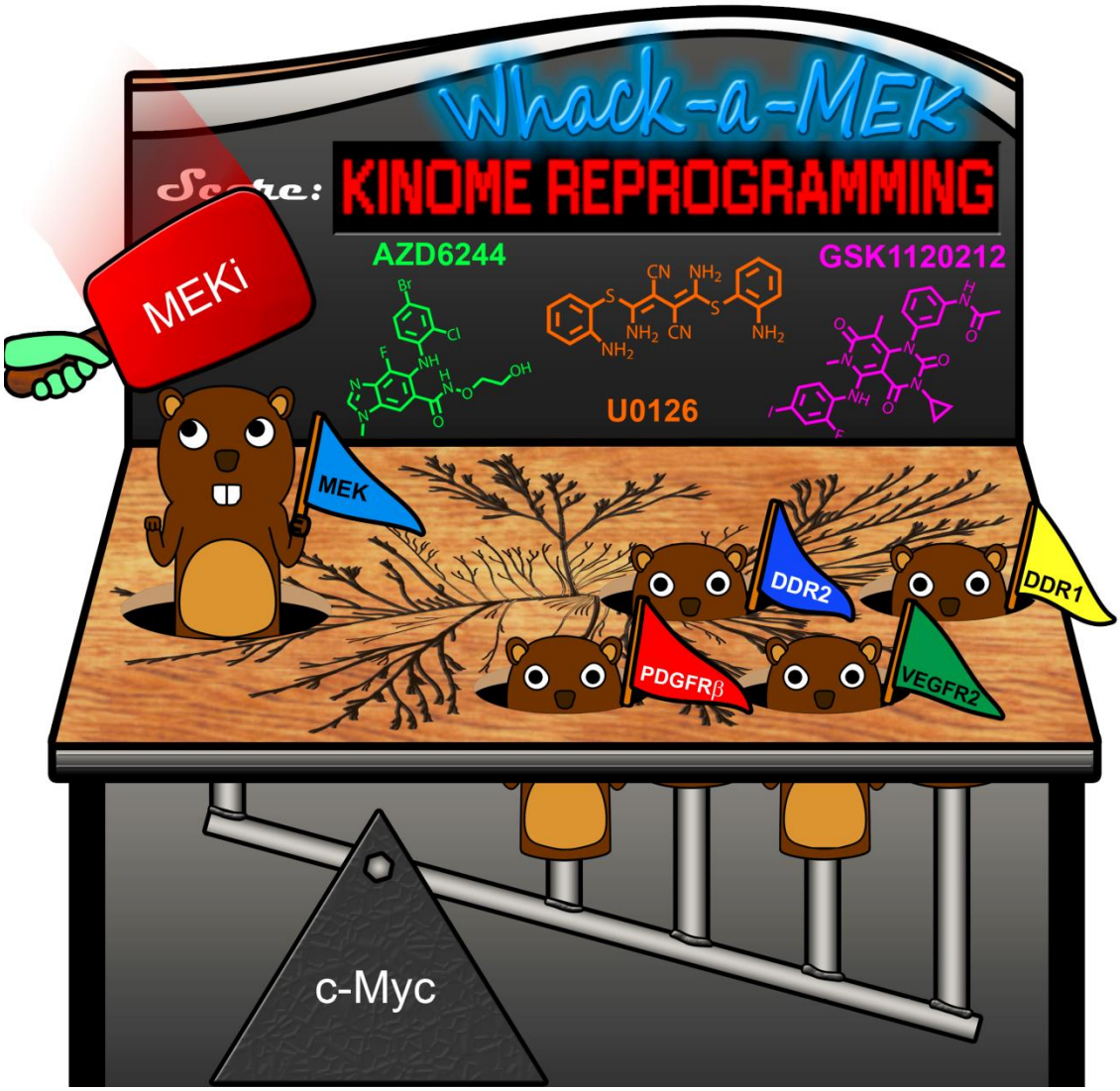

Figure 6.1 The dilemma of kinome reprogramming. This cartoon illustrates the adaptive response of claudin-low TNBC cells where targeted MEKi led to compensatory upregulation of receptor tyrosine kinases through a mechanism involving c-Myc. This concept of kinome reprogramming provides a new paradigm in kinase network signaling and drug response.

REFERENCES

1. American Cancer Society. *Cancer Facts & Figures*. *American Cancer Society* (2013).

2. American Cancer Society. *Breast Cancer Facts & Figures 2011-2012*. *American Cancer Society* (2012).

3. Siegel, R. *et al.* Cancer Treatment and Survivorship Statistics , 2012. *CA Cancer J Clin* **62,** 220–241 (2012).

4. Bauer, K. R., Brown, M., Cress, R. D., Parise, C. A. & Caggiano, V. Descriptive analysis of estrogen receptor (ER)-negative, progesterone receptor (PR)-negative, and HER2-negative invasive breast cancer, the so-called triple-negative phenotype: a population-based study from the California cancer Registry. *Cancer* **109,** 1721–8 (2007).

5. Onitilo, A. A., Engel, J. M., Greenlee, R. T. & Mukesh, B. N. Breast cancer subtypes based on ER/PR and Her2 expression: comparison of clinicopathologic features and survival. *Clin Med Res* **7,** 4–13 (2009).

6. Dent, R. *et al.* Triple-negative breast cancer: clinical features and patterns of recurrence. *Clin Cancer Res* **13,** 4429–34 (2007).

7. Liedtke, C. *et al.* Response to neoadjuvant therapy and long-term survival in patients with triple-negative breast cancer. *J Clin Oncol* **26,** 1275–81 (2008).

8. Prat, A. *et al.* Phenotypic and molecular characterization of the claudin-low intrinsic subtype of breast cancer. *Breast Cancer Res* **12,** R68 (2010).

9. Prat, A. & Perou, C. M. Mammary development meets cancer genomics. *Nat Med* **15,** 842–4 (2009).

10. Creighton, C. J. *et al.* Residual breast cancers after conventional therapy display mesenchymal as well as tumor-initiating features. *Proc Natl Acad Sci* **106,** 13820–5 (2009).

11. Singh, A. & Settleman, J. EMT, cancer stem cells and drug resistance: an emerging axis of evil in the war on cancer. *Oncogene* **29,** 4741–51 (2010).

12. Gerlinger, M. *et al.* Intratumor heterogeneity and branched evolution revealed by multiregion sequencing. *N Engl J Med* **366,** 883–892 (2012).

13. Zhang, J., Yang, P. L. & Gray, N. S. Targeting cancer with small molecule kinase inhibitors. *Nat Rev Cancer* **9,** 28–39 (2009).

14. Manning, G., Whyte, D. B., Martinez, R., Hunter, T. & Sudarsanam, S. The protein kinase complement of the human genome. *Science* **298,** 1912–1934 (2010).

15. Cohen, P. The role of protein phosphorylation in human health and disease. *Eur J Biochem* **5010,** 5001–5010 (2001).

16. Huse, M. & Kuriyan, J. The conformational plasticity of protein kinases. *Cell* **109,** 275–82 (2002).

17. Nolen, B., Taylor, S. & Ghosh, G. Regulation of protein kinases: controlling activity through activation segment conformation. *Mol Cell* **15,** 661–675 (2004).

18. Kendall, R. L. *et al.* Vascular endothelial growth factor receptor KDR tyrosine kinase activity Is increased by autophosphorylation of two activation loop tyrosine residues. *J Biol Chem* **274,** 6453–6460 (1999).

19. Jauch, R. *et al.* Mitogen-activated protein kinases interacting kinases are autoinhibited by a reprogrammed activation segment. *EMBO J* **25,** 4020–32 (2006).

20. Brown, N. R. *et al.* Effects of phosphorylation of threonine 160 on cyclin-dependent kinase 2 structure and activity. *J Biol Chem* **274,** 8746–56 (1999).

21. Liu, Y. & Gray, N. S. Rational design of inhibitors that bind to inactive kinase conformations. *Nat Chem Biol* **2,** 358–64 (2006).

22. Druker, B. J. *et al.* Efficacy and safety of a specific inhibitor of the BCR-Abl tyrosine kinase in chronic myeloid leukemia. *N Engl J Med* **344,** 1031–1037 (2001).

23. Arteaga, C. L. *et al.* Treatment of HER2-positive breast cancer: current status and future perspectives. *Nature Rev Clin Oncol* **9,** 16–32 (2012).

24. Fedorov, O., Müller, S. & Knapp, S. The (un)targeted cancer kinome. *Nat Chem Biol* **6,** 166–169 (2010).

25. Songyang, Z. *et al.* Specific Motifs Recognized by the SH2 Domains of Csk, 3BP2, fps/fes, GRB-2, HCP, SHC, Syk, and Vav. *Mol Cell Biol* **14,** 2777–85 (1994).

26. Casar, B., Pinto, A. & Crespo, P. Essential role of ERK dimers in the activation of cytoplasmic but not nuclear substrates by ERK-scaffold complexes. *Mol Cell* **31,** 708–21 (2008).

27. Yoon, S. & Seger, R. The extracellular signal-regulated kinase: multiple substrates regulate diverse cellular functions. *Growth Factors* **24,** 21–44 (2006).

28. Wang, W. *et al.* Sequential activation of the MEK–Extracellular Signal-Regulated Kinase and MKK3/6–p38 mitogen-activated protein kinase pathways mediates oncogenic Ras-induced premature senescence. *Mol Cell Biol* **22,** 3389–3403 (2002).

29. Hauschild, A. *et al.* Dabrafenib in BRAF-mutated metastatic melanoma: a multicentre, open-label, phase 3 randomised controlled trial. *Lancet* **380,** 358–65 (2012).

30. Flaherty, K. T. *et al.* Inhibition of mutated, activated BRAF in metastatic melanoma. *N Engl J Med* **363,** 809–819 (2010).

31. Sullivan, R. J. & Flaherty, K. T. Resistance to BRAF-targeted therapy in melanoma. *Eur J Cancer* **49,** 1297–1304 (2013).

32. Fischmann, T. O. *et al.* Crystal structures of MEK1 binary and ternary complexes with nucleotides and inhibitors. *Biochemistry* **48,** 2661–74 (2009).

33. Gilmartin, A. G. *et al.* GSK1120212 (JTP-74057) is an inhibitor of MEK activity and activation with favorable pharmacokinetic properties for sustained in vivo pathway inhibition. *Clin Cancer Res* **17,** 989–1000 (2011).

34. Sheth, P. R. *et al.* Fully activated MEK1 exhibits compromised affinity for binding of allosteric inhibitors U0126 and PD0325901. *Biochemistry* **50,** 7964–76 (2011).

35. Morris, E. J. *et al.* Discovery of a novel ERK inhibitor with activity in models of acquired resistance to BRAF and MEK inhibitors. *Cancer Discov* **3,** 742–750 (2013).

36. Hatzivassiliou, G. *et al.* ERK inhibition overcomes acquired resistance to MEK inhibitors. *Mol Cancer Ther* **11,** 1143–54 (2012).

37. Salh B *et al.* Investigation of the Mek-MAP kinase-Rsk pathway in human breast cancer. *Anticancer Res* **19,** 731–740 (1999).

38. Sivaraman, V. S., Wang, H., Nuovo, G. J. & Malbon, C. C. Hyperexpression of mitogen-activated protein kinase in human breast cancer. *J Clin Invest* **99,** 1478–1483 (1997).

39. Xing, C. & Imagawa, W. Altered MAP kinase (ERK1,2) regulation in primary cultures of mammary tumor cells: elevated basal activity and sustained response to EGF. *Carcinogenesis* **20,** 1201–8 (1999).

40. Ripple, M. O., Kalmadi, S. & Eastman, A. Inhibition of either phosphatidylinositol 3-kinase/Akt or the mitogen/extracellular-regulated kinase, MEK/ERK, signaling pathways suppress growth of breast cancer cell lines, but MEK/ERK signaling is critical for cell survival. *Breast Cancer Res Treat* **93,** 177–88 (2005).

41. Fukazawa, H., Noguchi, K. & Murakami, Y. Mitogen-activated protein/extracellular signal-regulated kinase kinase (MEK) inhibitors restore anoikis sensitivity in human breast cancer cell lines with a constitutively activated extracellular-regulated kinase (ERK) pathway. *Mol Cancer Ther* **1,** 303–309 (2002).

42. Hoeflich, K. P. *et al.* In vivo antitumor activity of MEK and phosphatidylinositol 3-kinase inhibitors in basal-like breast cancer models. *Clin Cancer Res* **15,** 4649–64 (2009).

43. Jing, J. *et al.* Comprehensive predictive biomarker analysis for MEK inhibitor GSK1120212. *Mol Cancer Ther* **11,** 720–9 (2009).

44. Mirzoeva, O. K. *et al.* Basal subtype and MAPK/ERK kinase (MEK)-phosphoinositide 3-kinase feedback signaling determine susceptibility of breast cancer cells to MEK inhibition. *Cancer Res* **69,** 565–72 (2009).

45. Balko, J. M. *et al.* Profiling of residual breast cancers after neoadjuvant chemotherapy identifies DUSP4 deficiency as a mechanism of drug resistance. *Nat Med* **18,** 1052–9 (2012).

46. MacKeigan, J. P., Collins, T. S. & Ting, J. P. MEK inhibition enhances paclitaxel-induced tumor apoptosis. *J Biol Chem* **275,** 38953–6 (2000).

47. Adjei, A. a *et al.* Phase I pharmacokinetic and pharmacodynamic study of the oral, small-molecule mitogen-activated protein kinase kinase 1/2 inhibitor AZD6244 (ARRY-142886) in patients with advanced cancers. *J Clin Oncol* **26,** 2139–46 (2008).

48. Rinehart, J. *et al.* Multicenter phase II study of the oral MEK inhibitor, CI-1040, in patients with advanced non-small-cell lung, breast, colon, and pancreatic cancer. *J Clin Oncol* **22,** 4456–62 (2004).

49. Emery, C. M. *et al.* MEK1 mutations confer resistance to MEK and B-RAF inhibition. *Proc Natl Acad Sci* **106,** 20411–6 (2009).

50. Wang, H. *et al.* Identification of the MEK1(F129L) activating mutation as a potential mechanism of acquired resistance to MEK inhibition in human cancers carrying the B-RafV600E mutation. *Cancer Res* **71,** 5535–45 (2011).

51. Roberts, P. J. *et al.* Combined PI3K/mTOR and MEK Inhibition Provides Broad Antitumor Activity in Faithful Murine Cancer Models. *Clin Cancer Res* **18,** 5290–303 (2012).

52. Blencke, S. *et al.* Characterization of a conserved structural determinant controlling protein kinase sensitivity to selective inhibitors. *Chem Biol* **11,** 691–701 (2004).

53. Knight, Z. A., Lin, H. & Shokat, K. M. Targeting the cancer kinome through polypharmacology. *Nat Rev Cancer* **10,** 130–137 (2010).

54. Nazarian, R. *et al.* Melanomas acquire resistance to B-RAF(V600E) inhibition by RTK or N-RAS upregulation. *Nature* **468,** 973–7 (2010).

55. Bollag, G. *et al.* Clinical efficacy of a RAF inhibitor needs broad target blockade in BRAF-mutant melanoma. *Nature* **467,** 596–9 (2010).

56. Heidorn, S. J. *et al.* Kinase-dead BRAF and oncogenic RAS cooperate to drive tumor progression through CRAF. *Cell* **140,** 209–21 (2010).

57. Poulikakos, P. I., Zhang, C., Bollag, G., Shokat, K. M. & Rosen, N. RAF inhibitors transactivate RAF dimers and ERK signalling in cells with wild-type BRAF. *Nature* **464,** 427–30 (2010).

58. Hatzivassiliou, G. *et al.* RAF inhibitors prime wild-type RAF to activate the MAPK pathway and enhance growth. *Nature* **464,** 431–5 (2010).

59. Su, F. *et al.* Resistance to selective BRAF inhibition can be mediated by modest upstream pathway activation. *Cancer Res* **72,** 969–78 (2012).

60. Smalley, K. S. M. & Flaherty, K. T. Integrating BRAF/MEK inhibitors into combination therapy for melanoma. *Br J Cancer* **100,** 431–5 (2009).

61. Flaherty, K. T. *et al.* Combined BRAF and MEK inhibition in melanoma with BRAF V600 mutations. *N Engl J Med* **367,** 1694–703 (2012).

62. Greger, J. G. *et al.* Combinations of BRAF, MEK, and PI3K/mTOR inhibitors overcome acquired resistance to the BRAF inhibitor GSK2118436 dabrafenib, mediated by NRAS or MEK mutations. *Mol Cancer Ther* **11,** 909–20 (2012).

63. Villanueva, J. *et al.* Acquired resistance to BRAF inhibitors mediated by a RAF kinase switch in melanoma can be overcome by cotargeting MEK and IGF-1R/PI3K. *Cancer Cell* **18,** 683–95 (2010).

64. Laplante, M. & Sabatini, D. M. mTOR signaling in growth control and disease. *Cell* **149,** 274–93 (2012).

65. Haruta, T. *et al.* A rapamycin-sensitive pathway down-regulates insulin signaling via phosphorylation and proteasomal degradation of insulin receptor substrate-1. *Mol Endocrinol* **14,** 783–94 (2000).

66. O'Reilly, K. E. *et al.* mTOR inhibition induces upstream receptor tyrosine kinase signaling and activates Akt. *Cancer Res* **66,** 1500–8 (2006).

67. Chandarlapaty, S. *et al.* AKT inhibition relieves feedback suppression of receptor tyrosine kinase expression and activity. *Cancer Cell* **19,** 58–71 (2011).

68. Chakrabarty, A., Sánchez, V., Kuba, M. G., Rinehart, C. & Arteaga, C. L. Feedback upregulation of HER3 (ErbB3) expression and activity attenuates antitumor effect of PI3K inhibitors. *Proc Natl Acad Sci* **109,** 2718–2723 (2012).

69. Hynes, N. E. & MacDonald, G. ErbB receptors and signaling pathways in cancer. *Curr Opin Cell Biol* **21,** 177–84 (2009).

70. Ciardiello, F. & Tortora, G. EGFR Antagonists in Cancer Treatment. *N Engl J Med* **358,** 1160–1174 (2008).

71. Vivanco, I. & Mellinghoff, I. K. Epidermal growth factor receptor inhibitors in oncology. *Curr Opin Oncol* **22,** 573–8 (2010).

72. Engelman, J. a *et al.* MET amplification leads to gefitinib resistance in lung cancer by activating ERBB3 signaling. *Science* **316,** 1039–43 (2007).

73. Turke, A. B. *et al.* Preexistence and clonal selection of MET amplification in EGFR mutant NSCLC. *Cancer Cell* **17,** 77–88 (2010).

74. Mueller, K. L., Yang, Z.-Q., Haddad, R., Ethier, S. P. & Boerner, J. L. EGFR/Met association regulates EGFR TKI resistance in breast cancer. *J Mol Signal* **5,** 8 (2010).

75. Pillay, V. *et al.* The plasticity of oncogene addiction : implications for targeted therapies directed to receptor tyrosine kinases. *Neoplasia* **11,** 448–458 (2009).

76. Jun, H. J. *et al.* Acquired MET expression confers resistance to EGFR inhibition in a mouse model of glioblastoma multiforme. *Oncogene* **31,** 3039–50 (2012).

77. Ware, K. E. *et al.* Rapidly acquired resistance to EGFR tyrosine kinase inhibitors in NSCLC cell lines through de-repression of FGFR2 and FGFR3 expression. *PloS One* **5,** e14117 (2010).

78. Wheeler, D. L. *et al.* Epidermal Growth Factor Receptor cooperates with Src Family Kinases in acquired resistance to cetuximab. *Cancer Biol Ther* **8,** 696–703 (2009).

79. Zhang, S. *et al.* Combating trastuzumab resistance by targeting SRC, a common node downstream of multiple resistance pathways. *Nat Med* **17,** 461–9 (2011).

80. Gianni, L. *et al.* Treatment with trastuzumab for 1 year after adjuvant chemotherapy in patients with HER2-positive early breast cancer: a 4-year follow-up of a randomised controlled trial. *Lancet Oncol* **12,** 236–244 (2011).

81. Goss, P. E. *et al.* Adjuvant lapatinib for women with early-stage HER2-positive breast cancer: a randomised, controlled, phase 3 trial. *Lancet Oncol* **14,** 88–96 (2013).

82. Verma, S. *et al.* Trastuzumab emtansine for HER2-positive advanced breast cancer. *N Engl J Med* **367,** 1783–1791 (2012).

83. Baselga, J. *et al.* Lapatinib with trastuzumab for HER2-positive early breast cancer (NeoALTTO): a randomised, open-label, multicentre, phase 3 trial. *Lancet* **379,** 633–640 (2012).

84. Blackwell, K. L. *et al.* Overall survival benefit with lapatinib in combination with trastuzumab for patients with human epidermal growth factor receptor 2-positive metastatic breast cancer: final results from the EGF104900 Study. *J Clin Oncol* **30,** 2585–92 (2012).

85. Sergina, N. V *et al.* Escape from HER-family tyrosine kinase inhibitor therapy by the kinase-inactive HER3. *Nature* **445,** 437–41 (2007).

86. Kong, A. *et al.* HER2 oncogenic function escapes EGFR tyrosine kinase inhibitors via activation of alternative HER receptors in breast cancer cells. *PloS One* **3,** e2881 (2008).

87. Amin, D. N. *et al.* Resiliency and vulnerability in the HER2-HER3 tumorigenic driver. *Sci Transl Med* **2,** 16ra7 (2010).

88. Nahta, R., Hung, M. & Esteva, F. J. The HER-2-Targeting Antibodies Trastuzumab and Pertuzumab Synergistically Inhibit the Survival of Breast Cancer Cells. *Cancer Res* **64,** 2343–2346 (2004).

89. Swain, S. M. *et al.* Pertuzumab, trastuzumab, and docetaxel for HER2-positive metastatic breast cancer (CLEOPATRA study): overall survival results from a randomised, double-blind, placebo-controlled, phase 3 study. *Lancet Oncol* **14,** 461–71 (2013).

90. Nahta, R., Yuan, L. X. H., Zhang, B., Kobayashi, R. & Esteva, F. J. Insulin-like growth factor-I receptor/human epidermal growth factor receptor 2 heterodimerization contributes to trastuzumab resistance of breast cancer cells. *Cancer Res* **65,** 11118–28 (2005).

91. Shattuck, D. L., Miller, J. K., Carraway, K. L. & Sweeney, C. Met receptor contributes to trastuzumab resistance of Her2-overexpressing breast cancer cells. *Cancer Res* **68,** 1471–7 (2008).

92. Liu, L. *et al.* Novel mechanism of lapatinib resistance in HER2-positive breast tumor cells: activation of AXL. *Cancer Res* **69,** 6871–8 (2009).

93. Zhuang, G. *et al.* Elevation of receptor tyrosine kinase EphA2 mediates resistance to trastuzumab therapy. *Cancer Res* **70,** 299–308 (2010).

94. Gossage, L. & Eisen, T. Targeting multiple kinase pathways: a change in paradigm. *Clin Cancer Res* **16,** 1973–8 (2010).

95. Gillies, R. J., Verduzco, D. & Gatenby, R. A. Evolutionary dynamics of carcinogenesis and why targeted therapy does not work. *Nat Rev Cancer* **12,** 487–93 (2012).

96. Johnson, S. A. & Hunter, T. Kinomics: methods for deciphering the kinome. *Nat Methods* **2,** 17–25 (2005).

97. Olsen, J. V *et al.* Global, in vivo, and site-specific phosphorylation dynamics in signaling networks. *Cell* **127,** 635–48 (2006).

98. Del Rosario, A. M. & White, F. M. Quantifying oncogenic phosphotyrosine signaling networks through systems biology. *Curr Opin Gen Dev* **20,** 23–30 (2010).

99. Anastassiadis, T., Deacon, S. W., Devarajan, K., Ma, H. & Peterson, J. R. Comprehensive assay of kinase catalytic activity reveals features of kinase inhibitor selectivity. *Nat Biotech* **29,** 1039–45 (2011).

100. Duncan, J. S. *et al.* Dynamic reprogramming of the kinome in response to targeted MEK inhibition in triple-negative breast cancer. *Cell* **149,** 307–21 (2012).

101. Midland, A. *et al.* Defining the expressed breast cancer kinome. *Cell Res* **22,** 620–3 (2012).

102. Zang, Z. J. *et al.* Genetic and structural variation in the gastric cancer kinome revealed through targeted deep sequencing. *Cancer Res* **71,** 29–39 (2011).

103. Kilpinen, S., Ojala, K. & Kallioniemi, O. Analysis of kinase gene expression patterns across 5681 human tissue samples reveals functional genomic taxonomy of the kinome. *PloS One* **5,** e15068 (2010).

104. Sutton, C. W. The role of targeted chemical proteomics in pharmacology. *Br J Pharmacol* **166,** 457–75 (2012).

105. Knockaert, M. *et al.* Intracellular Targets of Paullones. *J Biol Chem* **277,** 25493–501 (2002).

106. Knockaert, M. *et al.* Intracellular targets of cyclin-dependent kinase inhibitors: identification by affinity chromatography using immobilised inhibitors. *Chem Biol* **7,** 411–22 (2000).

107. Haystead, C., Gregory, P., Sturgill, T. & Haystead, T. Gamma-phosphate-linked ATP-sepharose for the affinity purification of protein kinases. *Eur J Biochem* **214,** 459–67 (1993).

108. Godl, K. *et al.* An efficient proteomics method to identify the cellular targets of protein kinase inhibitors. *Proc Natl Acad Sci* **100,** 15434–9 (2003).

109. Fabian, M. a *et al.* A small molecule-kinase interaction map for clinical kinase inhibitors. *Nat Biotech* **23,** 329–36 (2005).

110. Godl, K. *et al.* Proteomic characterization of the angiogenesis inhibitor SU6668 reveals multiple impacts on cellular kinase signaling. *Cancer Res* **65,** 6919–6926 (2005).

111. Brehmer, D. *et al.* Cellular targets of gefitinib. *Cancer Res* **65,** 379–382 (2005).

112. MacKay, V. L. *et al.* Gene expression analyzed by high-resolution state array analysis and quantitative proteomics: response of yeast to mating pheromone. *Mol Cell Proteomics* **3,** 478–89 (2004).

113. Wissing, J. *et al.* Chemical proteomic analysis reveals alternative modes of action for pyrido[2,3-d]pyrimidine kinase inhibitors. *Mol Cell Proteomics* **3,** 1181–93 (2004).

114. Rix, U. & Superti-Furga, G. Target profiling of small molecules by chemical proteomics. *Nat Chem Biol* **5,** 616–24 (2009).

115. Oppermann, F. S. *et al.* Large-scale proteomics analysis of the human kinome. *Mol Cell Proteomics* **8,** 1751–64 (2009).

116. Bantscheff, M. *et al.* Quantitative chemical proteomics reveals mechanisms of action of clinical ABL kinase inhibitors. *Nat Biotech* **25,** 1035–44 (2007).

117. Karaman, M. W. *et al.* A quantitative analysis of kinase inhibitor selectivity. *NatBiotech* **26,** 127–32 (2008).

118. Rix, U. *et al.* A comprehensive target selectivity survey of the BCR-ABL kinase inhibitor INNO-406 by kinase profiling and chemical proteomics in chronic myeloid leukemia cells. *Leukemia* **24,** 44–50 (2010).

119. Rix, U. *et al.* Chemical proteomic profiles of the BCR-ABL inhibitors imatinib, nilotinib, and dasatinib reveal novel kinase and nonkinase targets. *Blood* **110,** 4055–63 (2007).

120. Li, J. *et al.* A chemical and phosphoproteomic characterization of dasatinib action in lung cancer. *Nat Chem Biol* **6,** 291–9 (2010).

121. Pan, C., Olsen, J. V, Daub, H. & Mann, M. Global effects of kinase inhibitors on signaling networks revealed by quantitative phosphoproteomics. *Mol Cell Proteomics* **8,** 2796–808 (2009).

122. Wissing, J. *et al.* Proteomics analysis of protein kinases by target class-selective prefractionation and tandem mass spectrometry. *Mol Cell Proteomics* **6,** 537–47 (2007).

123. Daub, H. *et al.* Kinase-selective enrichment enables quantitative phosphoproteomics of the kinome across the cell cycle. *Mol Cell* **31,** 438–48 (2008).

124. Stommel, J. M. *et al.* Coactivation of receptor tyrosine kinases affects the response of tumor cells to targeted therapies. *Science* **318,** 287–90 (2007).

125. Klutchko, S. R. *et al.* 2-Substituted aminopyrido[2,3-d]pyrimidin-7(8H)-ones. Structure-activity relationships against selected tyrosine kinases and in vitro and in vivo anticancer activity. *J Med Chem* **41,** 3276–3292 (1998).

126. Das, J. *et al.* 2-Aminothiazole as a Novel Kinase Inhibitor Template. Structure-Activity relationship studies (Dasatinib, BMS-354825) as a potent pan-Src kinase inhibitor. *J Med Chem* **49,** 6819–6832 (2006).

127. Barker, a J. *et al.* Studies leading to the identification of ZD1839 (IRESSA): an orally active, selective epidermal growth factor receptor tyrosine kinase inhibitor targeted to the treatment of cancer. *Bioorg Med Chem Lett* **11,** 1911–4 (2001).

128. Gallagher, T. F. *et al.* Regulation of stress-induced cytokine production by pyridinylimidazoles; inhibition of CSBP kinase. *Bioorg Med Chem* **5,** 49–64 (1997).

129. Langmead, B., Trapnell, C., Pop, M. & Salzberg, S. L. Ultrafast and memory-efficient alignment of short DNA sequences to the human genome. *Genome Biol* **10,** R25 (2009).

130. Mortazavi, A., Williams, B. A., Mccue, K., Schaeffer, L. & Wold, B. Mapping and quantifying mammalian transcriptomes by RNA-Seq. *Nat Methods* **5,** 621–628 (2008).

131. Thingholm, T. E., Jørgensen, T. J. D., Jensen, O. N. & Larsen, M. R. Highly selective enrichment of phosphorylated peptides using titanium dioxide. *Nat Protoc* **1,** 1929–35 (2006).

132. Shteynberg, D. *et al.* iProphet: multi-level integrative analysis of shotgun proteomic data improves peptide and protein identification rates and error estimates. *Mol Cell Proteomics* **10,** M111.007690 (2011).

133. Parker, J. S. *et al.* Supervised risk predictor of breast cancer based on intrinsic subtypes. *J Clin Oncol* **27,** 1160–7 (2009).

134. Johannessen, C. M. *et al.* COT drives resistance to RAF inhibition through MAP kinase pathway reactivation. *Nature* **468,** 968–72 (2010).

135. Sun, T. *et al.* Activation of multiple proto-oncogenic tyrosine kinases in breast cancer via loss of the PTPN12 phosphatase. *Cell* **144,** 703–18 (2011).

136. Cooper, M. J. *et al.* Application of multiplexed kinase inhibitor beads to study kinome adaptations in drug-resistant leukemia. *PloS One* **8,** e66755 (2013).

137. Bianchi, G. *et al.* Phase II multicenter, uncontrolled trial of sorafenib in patients with metastatic breast cancer. *Anticancer Drugs* **20,** 616–624 (2009).

138. Finn, R. S. *et al.* Estrogen receptor, progesterone receptor, human epidermal growth factor receptor 2 (HER2), and epidermal growth factor receptor expression and benefit from lapatinib in a randomized trial of paclitaxel with lapatinib or placebo as first-line treatment in. *J Clin Oncol* **27,** 3908–15 (2009).

139. Ritt, D. a, Monson, D. M., Specht, S. I. & Morrison, D. K. Impact of feedback phosphorylation and Raf heterodimerization on normal and mutant B-Raf signaling. *Mol Cell Biol* **30,** 806–19 (2010).

140. Marchetti, S., Gimond, C., Touboul, T., Roux, D. & Pagès, G. Extracellular signal-regulated kinases phosphorylate mitogen-activated protein kinase phosphatase 3 / DUSP6 at serines 159 and 197 , two sites critical for its proteasomal degradation. *Mol Cell Biol* **25,** 854–864 (2005).

141. Sears, R. *et al.* Multiple Ras-dependent phosphorylation pathways regulate Myc protein stability. *Genes Dev* **14,** 2501–2514 (2000).

142. Marampon, F., Ciccarelli, C. & Zani, B. M. Down-regulation of c-Myc following MEK/ERK inhibition halts the expression of malignant phenotype in rhabdomyosarcoma and in non muscle-derived human tumors. *Mol Cancer* **5,** 31 (2006).

143. Wierstra, I. & Alves, J. The c-myc promoter: still MysterY and challenge. *Adv Cancer Res* **99,** 113–333 (2008).

144. Oster, S. K. *et al.* Myc is an essential negative regulator of platelet-derived growth factor beta receptor expression. *Mol Cell Biol* **20,** 6768–6778 (2000).

145. Rodrik-Outmezguine, V. S. *et al.* mTOR kinase inhibition causes feedback-dependent biphasic regulation of AKT signaling. *Cancer Discov* **1,** 248–59 (2011).

146. Garrett, J. T. *et al.* Transcriptional and posttranslational up-regulation of HER3 (ErbB3) compensates for inhibition of the HER2 tyrosine kinase. *Proc Natl Acad Sci* **108,** 5021–6 (2011).

147. Corkery, B., Crown, J., Clynes, M. & O'Donovan, N. Epidermal growth factor receptor as a potential therapeutic target in triple-negative breast cancer. *Annals Oncol* **20,** 862–7 (2009).

148. Viale, G. *et al.* Invasive ductal carcinoma of the breast with the "triple-negative" phenotype: prognostic implications of EGFR immunoreactivity. *Breast Cancer Res Treat* **116,** 317–328 (2009).

149. Liu, D. *et al.* EGFR expression correlates with decreased disease-free survival in triple-negative breast cancer: a retrospective analysis based on a tissue microarray. *Med Oncol* **29,** 401–405 (2012).

150. Carey, L. a *et al.* TBCRC 001: randomized phase II study of cetuximab in combination with carboplatin in stage IV triple-negative breast cancer. *J Clin Oncol* **30,** 2615–23 (2012).

151. Mueller, K. L., Hunter, L. A., Ethier, S. P. & Boerner, J. L. Met and c-Src cooperate to compensate for loss of epidermal growth factor receptor kinase activity in breast cancer cells. *Cancer Res* **68,** 3314–22 (2008).

152. Rexer, B. *et al.* Phosphoproteomic mass spectrometry profiling links Src family kinases to escape from HER2 tyrosine kinase inhibition. *Oncogene* **30,** 4163–74 (2011).

153. Fedor-Chaiken, M., Hein, P. W., Stewart, J. C., Brackenbury, R. & Kinch, M. S. E-Cadherin Binding Modulates EGF Receptor Activation. *Cell Commun Adhes* **10,** 105–118 (2003).

154. Witta, S. E. *et al.* Restoring E-cadherin expression increases sensitivity to epidermal growth factor receptor inhibitors in lung cancer cell lines. *Cancer Res* **66,** 944–50 (2006).

155. Maseki, S. *et al.* Acquisition of EMT phenotype in the gefitinib-resistant cells of a head and neck squamous cell carcinoma cell line through Akt/GSK-3β/snail signalling pathway. *Br J Cancer* **106,** 1196–204 (2012).

156. Suda, K. *et al.* Epithelial to mesenchymal transition in an epidermal growth factor receptor-mutant lung cancer cell line with acquired resistance to erlotinib. *J Thorac Oncol* **6,** 1152–61 (2011).

157. Lehmann, B. D. *et al.* Identification of human triple-negative breast cancer subtypes and preclinical models for selection of targeted therapies. *J Clin Invest* **121,** 2750–2767 (2011).

158. Keller, P. J. *et al.* Mapping the cellular and molecular heterogeneity of normal and malignant breast tissues and cultured cell lines. *Breast Cancer Res* **12,** R87 (2010).

159. Neve, R. M. *et al.* A collection of breast cancer cell lines for the study of functionally distinct cancer subtypes. *Cancer Cell* **10,** 515–27 (2006).

160. Green, J. *et al.* The C3(1)/SV40 T-antigen transgenic mouse model of mammary cancer: ductal epithelial cell targeting with multistage progression to carcinoma. *Oncogene* **19,** 1020–7 (2000).

161. Filippakopoulos, P. *et al.* Selective inhibition of BET bromodomains. *Nature* **468,** 1067–73 (2010).

162. Mertz, J. A. *et al.* Targeting MYC dependence in cancer by inhibiting BET bromodomains. *Proc Natl Acad Sci* **108,** 16669–16674 (2011).

163. Lockwood, W. W., Zejnullahu, K., Bradner, J. E. & Varmus, H. Sensitivity of human lung adenocarcinoma cell lines to targeted inhibition of BET epigenetic signaling proteins. *Proc Natl Acad Sci* **109,** 19408–13 (2012).

164. Wu, S. & Chiang, C. The double bromodomain-containing chromatin adaptor Brd4 and transcriptional regulation. *J Biol Chem* **282,** 13141–5 (2007).

165. Zhang, W. *et al.* Bromodomain-containing protein 4 (BRD4) regulates RNA polymerase II serine 2 phosphorylation in human CD4+ T cells. *J Biol Chem* **287,** 43137–43155 (2012).

166. Lehmann, B. D. *et al.* Identification of human triple-negative breast cancer subtypes and preclinical models for selection of targeted therapies. *J Clin Invest* **121,** 2750–67 (2011).

167. Lovén, J. *et al.* Selective inhibition of tumor oncogenes by disruption of super-enhancers. *Cell* **153,** 320–34 (2013).

168. Ott, C. J. *et al.* BET bromodomain inhibition targets both c-Myc and IL7R in high-risk acute lymphoblastic leukemia. *Blood* **120,** 2843–52 (2012).

169. Zhang, L. *et al.* Characterization of the novel broad-spectrum kinase inhibitor CTx-0294885 as an affinity reagent for mass spectrometry-based kinome profiling. *J Proteome Res* **12,** 3104–3116 (2013).

170. Chen, Y.-T. *et al.* Multiplexed quantification of 63 proteins in human urine by multiple reaction monitoring-based mass spectrometry for discovery of potential bladder cancer biomarkers. *J Proteomics* **75,** 3529–45 (2012).